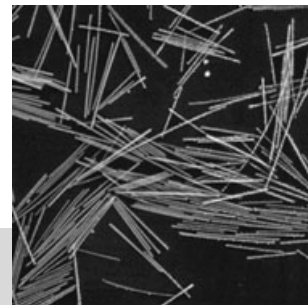# One-Dimensional Nanostructures: Synthesis, Characterization, and Applications**

By *Younan Xia,* *Peidong Yang,* *Yugang Sun,*
Yiying Wu, Brian Mayers, Byron Gates,
Yadong Yin, Franklin Kim, and *Haoquan Yan*

This article provides a comprehensive review of current research activities that concentrate on one-dimensional (1D) nanostructures—wires, rods, belts, and tubes— whose lateral dimensions fall anywhere in the range of 1 to 100 nm. We devote the most attention to 1D nanostructures that have been synthesized in relatively copious quantities using chemical methods. We begin this article with an overview of synthetic strategies that have been exploited to achieve 1D growth. We then elaborate on these approaches in the following four sections: i) anisotropic growth dictated by the crystallographic structure of a solid material; ii) anisotropic growth confined and directed by various templates; iii) anisotropic growth kinetically controlled by supersaturation or through the use of an appropriate capping reagent; and iv) new concepts not yet fully demonstrated, but with long-term potential in generating 1D nanostructures. Following is a discussion of techniques for generating various types of important heterostructured nanowires. By the end of this article, we highlight a range of unique properties (e.g., thermal, mechanical, electronic, optoelectronic, optical, nonlinear optical, and field emission) associated with different types of 1D nanostructures. We also briefly discuss a number of methods potentially useful for assembling 1D nanostructures into functional devices based on crossbar junctions, and complex architectures such as 2D and 3D periodic lattices. We conclude this review with personal perspectives on the directions towards which future research on this new class of nanostructured materials might be directed.

1. Introduction

Nanostructures—structures that are defined as having at least one dimension between 1 and 100 nm—have received steadily growing interests as a result of their peculiar and fascinating properties, and applications superior to their bulk counterparts.[1–3] The ability to generate such minuscule structures is essential to much of modern science and technology. There are a large number of opportunities that might be realized by making new types of nanostructures, or simply by down-sizing existing microstructures into the 1–100 nm regime. The most successful example is provided by microelectronics, where "smaller" has meant greater performance ever since the invention of integrated circuits: more components per chip, faster operation, lower cost, and less power consumption.[4] Miniaturization may also represent the trend in a range of other technologies. In information storage, for example, there are many active efforts to develop magnetic and optical storage components with critical dimensions as small as tens of nanometers.[5] It is also clear that a wealth of interesting and new phenomena are associated with nanometer-sized structures, with the best established examples including size-dependent excitation or emission,[6] quantized (or ballistic) conductance,[7] Coulomb blockade (or single-electron tunneling, SET),[8] and metal–insulator transition.[9] It is generally accepted that quantum confinement of electrons by the potential wells of nanometer-sized structures may provide one of the most powerful (and yet versatile) means to control the electrical, optical, magnetic, and thermoelectric properties of a solid-state functional material.

[*] Prof. Y. Xia, Dr. Y. Sun, B. Mayers, Dr. B. Gates, Dr. Y. Yin
Department of Chemistry, University of Washington
Seattle, WA 98195 (USA)
E-mail: xia@chem.washington.edu

Prof. P. Yang, Dr. Y. Wu, F. Kim, H. Yan
Department of Chemistry, University of California
Berkeley, CA 94720 (USA)
E-mail: p_yang@uclink.berkeley.edu

REVIEW

Two-dimensional (2D) nanostructures (or quantum wells)[10] have been extensively studied by the semiconductor community because they can be conveniently prepared using techniques such as molecular beam epitaxy (MBE).[11] Thanks to the efforts from many research groups, significant progress has also been made with regard to zero-dimensional (0D) nanostructures (or quantum dots)[12] in the past two decades. For example, a rich variety of chemical methods have already been developed for generating quantum dots with well-controlled dimensions and from a broad range of materials.[13] With quantum dots as a model system, a lot of interesting chemistry and physics has been learned by studying the evolution of their fundamental properties with size.[14] Using quantum dots as active components, various types of nanoscale devices have also been fabricated as prototypes in many research laboratories. Notable examples include quantum-dot lasers,[15] single-electron transistors,[16] memory units,[17] sensors,[18] optical detectors,[19] and light-emitting diodes (LEDs).[20] For most of these applications, it is believed that the dimension of an individual quantum dot may represent the ultimate limit to the miniaturization of currently existing functional devices.

Recently, one-dimensional (1D) nanostructures such as wires, rods, belts, and tubes have also become the focus of intensive research owing to their unique applications in mesoscopic physics and fabrication of nanoscale devices.[21] It is generally accepted that 1D nanostructures provide a good system to investigate the dependence of electrical and thermal transport or mechanical properties on dimensionality and size

reduction (or quantum confinement). They are also expected to play an important role as both interconnects and functional units in fabricating electronic, optoelectronic, electrochemical, and electromechanical devices with nanoscale dimensions. In comparison with quantum dots and wells, the advancement of 1D nanostructures has been slow until very recently, as hindered by the difficulties associated with the synthesis and fabrication of these nanostructures with well-controlled dimensions, morphology, phase purity, and chemical composition. Although 1D nanostructures can now be fabricated (in the setting of a research laboratory) using a number of advanced nanolithographic techniques,[22] such as electron-beam (e-beam) or focused-ion-beam (FIB) writing,[23] proximal-probe patterning,[24] and X-ray or extreme-UV lithography,[25] further development of these techniques into practical routes to large quantities of 1D nanostructures from a diversified range of materials, rapidly, and at reasonably low costs, still requires great ingenuity. In contrast, unconventional methods based on chemical synthesis might provide an alternative and intriguing strategy for generating 1D nanostructures in terms of material diversity, cost, throughput, and the potential for high-volume production.[26]

This article reviews current research activities that center on nanometer-sized wires, rods, belts, and tubes. Since carbon nanotubes (CNTs) have already been reviewed by a number of authors,[27] we intend to exclude them from the scope of this article. The main text of this article is organized into eight sections: The next section (Section 2) explicitly discusses several concepts related to the growth of nanowires, as well as

Younan Xia was born in Jiangsu, China, in 1965. He received a B.S. degree in chemical physics from the University of Science and Technology of China (USTC) in 1987, and then worked as a graduate student for four years at the Fujian Institute of Research on the Structure of Matter, Academia Sinica. He came to the United States in 1991, received a M.S. degree in inorganic chemistry from the University of Pennsylvania (with Prof. A. G. MacDiarmid) in 1993, and a Ph.D. degree in physical chemistry from Harvard University (with Prof. G. M. Whitesides) in 1996. He has been an Assistant Professor of Chemistry at the University of Washington in Seattle since 1997, and was promoted to the rank of tenured Associate Professor in 2001. His research interests include nanostructured materials, self-assembly, microfabrication, surface modification, conducting polymers, microfluidic and microanalytical systems, and novel devices for optics, optoelectronics, and display.
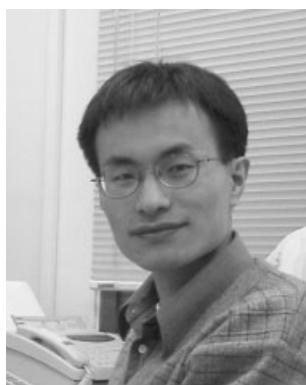
Peidong Yang was born in Jiangsu, China, in 1971. He received a B.S. degree in chemistry from the University of Science and Technology of China (USTC) in 1993. He came to the United States in 1993, received a Ph.D. degree in inorganic chemistry from Harvard University (with Prof. Charles Lieber) in 1997. He then spent two years as a postdoctoral fellow in Prof. Galen Stucky's lab at University of California, Santa Barbara. He has been an Assistant Professor of Chemistry at the University of California, Berkeley since 1999. His research interests include nanostructured materials, self-assembly and optoelectronic, thermoelectric, and electromechanical properties of nanostructures.

synthetic strategies that have been developed for achieving 1D morphologies. The following four sections fully illustrate these strategies using specific examples, including new ones whose potentials remain to be fully demonstrated. Section 7 evaluates the use of several methods for generating hetero-structured nanowires such as superlattices. Section 8 highlights a range of unique properties associated with 1D nanostructures, as well as their potential applications in various areas. The final section concludes with personal remarks on the directions towards which future research on this new class of materials might be directed.

The objectives of this article are the following: i) to provide a brief account on the chemical methods that have been demonstrated for generating various types of 1D nanostructures; ii) to illustrate the intriguing properties associated with 1D nanostructures; iii) to address experimental issues related to the assembly of 1D nanostructures into complex architectures; and iv) to evaluate the potential of 1D nanostructures as functional components in device fabrication. As we proceed, we will address most of the barriers that we believe must be overcome before 1D nanostructures can reach their ultimate potential as a new class of industrial materials. At the end of this review, we will also briefly mention some impacts that 1D nanostructures might potentially have on the environment and health.

2. Strategies for Achieving 1D Growth

The essence of 1D nanostructure formation is about crystallization,[28] a process that has already been investigated for hundreds of years. The evolution of a solid from a vapor, liquid, or solid phase involves two fundamental steps: nucleation and growth. As the concentration of the building blocks (atoms, ions, or molecules) of a solid becomes sufficiently high, they aggregate into small clusters (or nuclei) through homogeneous nucleation. With a continuous supply of the building blocks, these nuclei can serve as seeds for further growth to form larger structures. Although crystallization has been studied for hundreds of years, very little is quantitatively known about this process. Neither is it trivial to achieve a complete control over this process. It is generally accepted that the formation of a perfect crystal requires a reversible pathway between the building blocks on the solid surface and those in a fluid phase (i.e., vapor, solution, or melt). These conditions allow the building blocks to easily adopt correct positions in developing the long-range-ordered, crystalline lattice. In addition, the building blocks also need to be supplied at a well-controlled rate in order to obtain crystals having a homogeneous composition and uniform morphology.

When developing a synthetic method for generating nanostructures, the most important issue that one needs to address is the simultaneous control over dimensions, morphology (or shape), and monodispersity (or uniformity). In the past several years, a variety of chemical methods have been reexamined or demonstrated as the "bottom–up" approach for generating

1D nanostructures with different levels of control over these parameters. Figure 1 schematically illustrates some of these synthetic strategies that include: i) use of the intrinsically an-
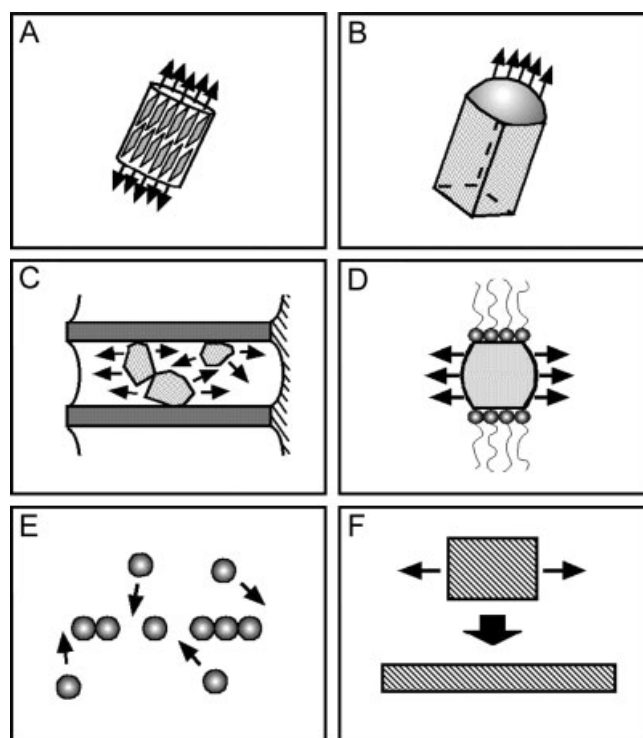

Fig. 1. Schematic illustrations of six different strategies that have been demonstrated for achieving 1D growth: a) dictation by the anisotropic crystallographic structure of a solid; B) confinement by a liquid droplet as in the vapor–liquid–solid process; C) direction through the use of a template; D) kinetic control provided by a capping reagent; E) self-assembly of 0D nanostructures; and F) size reduction of a 1D microstructure.

isotropic crystallographic structure of a solid to accomplish 1D growth (Fig. 1A); ii) introduction of a liquid–solid interface to reduce the symmetry of a seed (Fig. 1B); iii) use of various templates with 1D morphologies to direct the formation of 1D nanostructures (Fig. 1C); iv) use of supersaturation control to modify the growth habit of a seed ; v) use of appropriate capping reagent(s) to kinetically control the growth rates of various facets of a seed (Fig. 1D); vi) self-assembly of 0D nanostructures (Fig. 1E); and vii) size reduction of 1D microstructures (Fig. 1F). Because many of these methods were not demonstrated until very recently, most of their characteristics (such as reproducibility, product uniformity and purity, potential for scaling up, cost effectiveness, and in some cases, mechanism) are only vaguely known. We therefore emphasize their demonstrated performance (e.g., control of size range and flexibility in materials that can be synthesized) and their intrinsic limits (i.e., limits that originate from the physics and chemistry upon which they are based), rather than comment on their current level of technological development. In some cases, we also highlight approaches that may extend the scope of materials or circumvent shortcomings associated with the current procedures of these synthetic methods.

3. Materials with Highly Anisotropic Crystal Structures

Many solid materials naturally grow into 1D nanostructures, and this habit is determined by the highly anisotropic bonding in the crystallographic structure. One of the best-known examples is probably poly(sulphur nitride), $(SN)_x$, an inorganic polymer that was extensively studied in the 1970s due to its metallic and superconducting properties.[29] Uniform nanowires ~20 nm in diameter and hundreds of micrometers in length could be easily grown from vapor phase $(SN)_x$, and some of them might also aggregate into bundles. Ironically, the focus at that time was placed on the growth of single crystals with dimensions as large as possible for conductivity measurements, and most people were trying (extremely hard!) to avoid the whisker morphology. Many inorganic minerals such as asbestos and chrysolite are also known to exhibit a fibrous growth habit,[30] which is a manifestation of their chain structures, or some other anisotropic arrangements between atoms or ion groups within their crystal lattices. Directed and confined by the anisotropic conformation of their building blocks, these materials could be processed into nanowires with diameters being kept essentially the same as the dimensions of the seeds perpendicular to the growth direction. In addition, many polymeric and biological systems have also been known to exist preferentially in the fibrous form, and typical examples include cellulose,[31] and collagen.[32] As limited by space, here we only discuss two inorganic systems—molybdenum chalcogenides and chalcogens—for their interesting electronic and optical properties.

3.1. Molybdenum Chalcogenide Molecular Wires

Molybdenum chalcogenides, with the general formula $M_2Mo_6X_6$ (M = Li, Na; X = Se, Te), are a family of compounds that contain hexagonal close-packed linear chains in the formula of Mo_6X_6. The Mo_6X_6 chain can be considered as a prismatic column (Fig. 2A) formed by staggered stacking the Mo_3X_3 triangular units, with a repeating distance of 0.45 nm. When dissolved in a highly polar solvent such as dimethylsulfoxide or *N*-methylformamide, they mainly exist as chains ~2 nm in diameter.[33] Some chains might also aggregate into bundles (or fibers) with cross-sections of ~1 μm diameter and lengths up to ~20 μm. DiSalvo, Fréchet, and co-workers demonstrated that it was possible to fabricate a polymeric matrix containing mostly $(Mo_3Se_3^-)_n$ mono- and biwires by polymerizing in situ a dilute solution of $LiMo_3Se_3$ in vinylene carbonate.[34] These molecular wires were 0.6–2 nm in diameter and 5–10 nm in length. Lieber and co-workers have prepared molybdenum selenide molecular wires and used scanning tunneling microscopy (STM) to investigate their structural and electronic properties.[35] Their tunneling spectroscopic measurements indicated the existence of sharp peaks in the local density of states. This observation was consistent with the Van Hove singularities characteristic of 1D conductors. No evi-
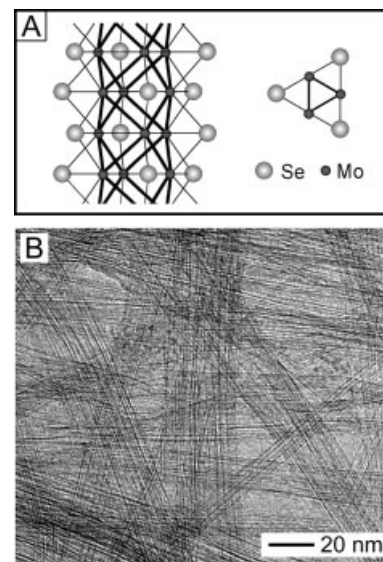

Fig. 2. A) Structural model of the linear chain contained in $LiMo_6Se_6$ molecular wires that is formed by staggered stacking the triangular planar $(Mo_3Se_3)^-$ units. B) A TEM image of bundles assembled from $(Mo_6Se_6)^-$ molecular wires in the presence of polymerizable cationic surfactants such as ω-undecenyltrimethylammonium bromide (ω-UTAB) [36].

dence for the opening of an energy gap (or the metal-to-insulator transition) was found in their conductance measurements with temperatures down to 5 K. Yang and co-workers studied the self-organization of these molecular wires into mesoscopic bundles (Fig. 2B) in the presence of organic surfactants of opposite charges.[36] Their transmission electron microscopy (TEM) and low-angle X-ray diffraction (XRD) studies indicated that the crystallinity along each individual molecular wire could be well maintained while the spacing between these inorganic wires could be varied in the range of 2–4 nm by changing the length of surfactant molecules. It was further found that the counter cations within the $Li_2Mo_6Se_6$ nanowires can be readily exchanged to form $[Mo_3Se_3^-]$ nanowires with different counter cations, and hence electrical properties tunable from semiconducting to superconducting. These demonstrations suggest that this simple and unique system of 1D nanostructures deserves systematic study to fully examine its potential in device fabrication.

3.2. Chalcogens: Selenium and Tellurium

Chalcogens (or more specifically, Se and Te) represent another ideal system for generating nanostructures with 1D morphologies. The trigonal (t-) phase of these two solids is interesting because of its unique crystal structure. Unlike oxygen, Se and Te atoms tend to form polymeric, helical chains through covalent bonding while oxygen exists primarily as O_2 molecules.[37] As shown in Figure 3A, the helical chains can be readily packed into a hexagonal lattice through van der Waals interactions. As dictated by this highly anisotropic structure, crystallization tends to occur along the *c*-axis, favoring the stronger covalent bonds over the relatively weak van

der Waals forces among chains. As a result, these two solids have a strong tendency to become 1D structures even when they are crystallized from an isotropic medium. In addition to their natural anisotropy, Se and Te have a range of other intriguing properties.[38] Not least among these is their intrinsic chirality. In principle, each individual nanostructure should be composed entirely of either *R*- or *L*-helices. These two materials are also interesting for their photoconductivity ($\sim 0.8 \times 10^5$ S cm^{-1} for t-Se), piezoelectricity, and high reactivity to generate a wealth of important functional materials (e.g., optoelectronic materials such as CdSe and ZnTe, and thermoelectric materials such as PbTe and Bi$_2$Te$_3$). In the past, chalcogens and chalcogenides have been exploited in an array of applications that include light or temperature sensors; rectifiers; photocopying machines; inorganic pigments; and piezoelectric actuators.[39] The ability to process these two solid materials into 1D nanostructures may improve the performance of existing devices or lead to new applications.

3.2.1. Selenium Nanowires

Xia and co-workers have recently demonstrated a generic, solution-phase approach to the large-scale synthesis of uniform nanowires of t-Se with lateral dimensions controllable in the range of 10 to 100 nm, and lengths up to several hundred micrometers.[40] The first step of this approach involved the formation of solid selenium in an aqueous solution through the reduction of selenious acid with excess hydrazine by refluxing this reaction mixture at an elevated temperature:[41]

$$H_2SeO_3 + N_2H_4 \longrightarrow Se\ (\downarrow) + N_2\ (\uparrow) + 3H_2O \qquad (1)$$
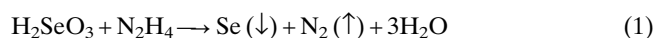
The initial product was brick-red-colored, spherical colloids of amorphous (a-) selenium with diameters of ~ 300 nm. When this solution was cooled to room temperature, the small amount of selenium dissolved in the hot solution precipitated out as nanocrystallites of t-Se. When this dispersion containing a mixture of a-Se colloids and t-Se nanocrystallites was aged in the dark, it underwent the Ostwald ripening process,[42] in which the a-Se colloids slowly dissolved into the solution as a result of their higher free energy as compared to the t-Se phase. The dissolved selenium subsequently grew as crystalline nanowires of t-Se on the seeds (Fig. 3B). In this transformation, the linear morphology of the final product was determined by the intrinsic anisotropy of the building blocks—that is, the extended, helical chains of Se atoms in the trigonal phase. Each nanowire was essentially a single crystal (see Fig. 3C for a high-resolution (HR)TEM image and the inset of Figure 3D for an electron diffraction pattern), characterized by a uniform diameter along its longitudinal axis (Fig. 3D). The diameters of these nanowires could be easily varied in a controllable fashion from 10 to 100 nm by changing the temperature at which the redox reaction was refluxed. An increase in the aging time merely led to the formation of longer nanowires with essentially no variation in the wire thickness. Note that no exotic seeding materials and surfac-
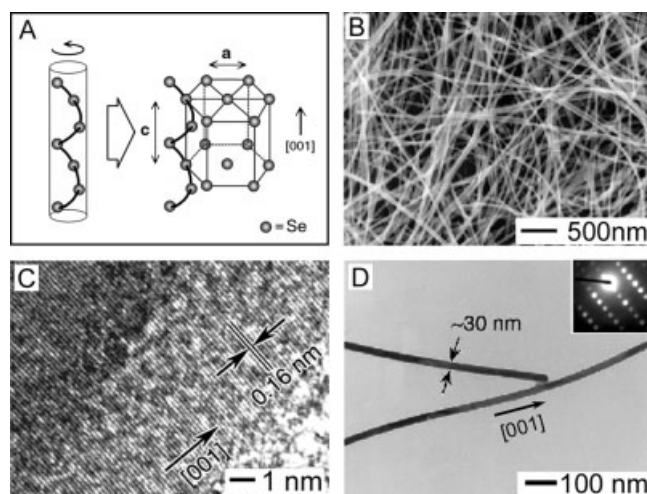

Fig. 3. A) An illustration of the crystal structure of t-Se composed of hexagonally packed, helical chains of Se atoms parallel to each other along the *c*-axis. B) A scanning electron microscopy (SEM) image of t-Se nanowires with a mean diameter of 32 nm. C) A high-resolution TEM image recorded from the edge of an individual nanowire showing well-resolved interference fringe spacing of 0.16 nm that agrees well with the interplanar distance between the {003} lattice planes. D) A TEM image of two t-Se nanowires, indicating the dimensional uniformity along each wire. The inset shows an electron diffraction pattern obtained from the middle portion of an individual nanowire, confirming that the growth direction was along the <001> axis [40].

tants were used in this synthesis, and both byproducts of the reaction (nitrogen gas and water) should not cause contamination problems for the t-Se nanowires. The absence of kinks and other types of defects should also make these nanowires particularly useful in fabricating nanoscale electronic and optoelectronic devices.

Formation of t-Se seeds could also be induced at room temperature using other means such as sonication.[43] Figure 4A illustrates the schematic mechanism of such a process. In this case, spherical a-Se colloids were also prepared as an aqueous suspension by reducing selenious acid with an excess amount of hydrazine. This reaction was carried out at room temperature to prevent any homogeneous nucleation events as induced by a drop in temperature. The colloids were initially characterized by diameters in the range of 0.1 to 2 μm. They were subsequently dried and redispersed in an alcohol such as ethanol. When a short pulse of sonication was applied, these colloids underwent disruption and aggregation. In addition, small nanocrystallites of t-Se were generated on the surfaces of the colloids as a result of cavitation effects.[44] In the following step, Se atoms were transferred from the less stable, amorphous colloids to the trigonal seeds until all a-Se colloids had been consumed. Note that this mechanism differs from the one discussed in the previous paragraph in a number of aspects: for example, the seeds are formed primarily on the surfaces of the colloids (rather than in the dispersing medium); wire growth mainly originates from the surfaces of a-Se colloids; and the growth occurs in a mater of hours (rather than days) due to the higher solubility/mobility of selenium in an alcohol. Figure 4B shows t-Se nanowires that were synthesized using the sonochemical route with a yield approaching
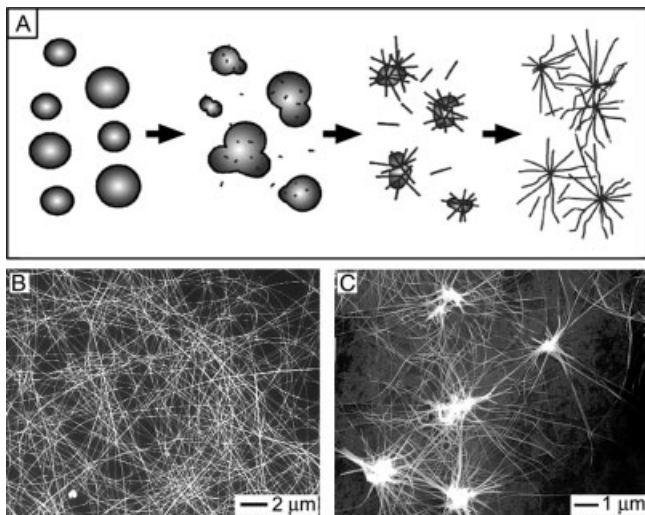
ADVANCED MATERIALS

Fig. 4. A) Schematic illustration of major steps involved in the sonochemical approach to the synthesis of t-Se nanowires: formation of t-Se seeds on the surfaces of a-Se colloids through cavitation; growth of t-Se nanowires at the expense of a-Se colloids; and continuous growth of t-Se nanowires until all a-Se colloids have been consumed. B) An SEM image of t-Se nanowires formed in an ethanol solution after they had grown for ~5 h. C) An SEM image of t-Se nanowires that were directly grown into an interconnected 2D network by supporting the sonicated a-Se colloids on the surface of a silicon substrate [43].

100 %. Note that complete transformation of a-Se colloids to t-Se wires was often observed after growth was allowed to proceed for ~5 h. Uniform nanowires with lengths up to several hundred micrometers and controllable diameters in the range of 25 to 120 nm could be routinely achieved. Since both redox reaction and wire growth were carried out at ambient temperature and pressure, this procedure can be conveniently scaled up for high-volume production.

There is another interesting feature associated with this sonochemical approach: Once the colloidal suspension had been sonicated, the disrupted a-Se colloids (whose surfaces were decorated with newly formed t-Se seeds) could be deposited onto a surface and dried there. This substrate could then be submersed in an alcohol (e.g., by placing a drop of ethanol on the surface in a closed, airtight container to prevent evaporation) to allow the growth of nanowires to proceed across the surface of the substrate. Figure 4C shows nanowires that were grown on a silicon substrate using this new procedure. Here one can clearly see the nanowires radiating out from what were initially a-Se colloids in a conformal 2D network. Varying the concentration of a-Se colloids in the initial dispersion could control the wire density in the network. It is believed that the conformal growth of nanowires supported on solid substrates represents an important step toward self-guided growth of interconnects between nanoelectronic devices.

3.2.2. Tellurium Nanowires, -Rods, -Tubes, and -Belts

Furuta and co-workers have extensively studied the growth of Te whiskers in the vapor phase.[45] It was found that Te whiskers of various morphologies could be grown on solid substrates by controlling the temperature. Xia and co-workers recently demonstrated that t-Te nanowires could also be synthesized using a procedure similar to the one demonstrated for the Se nanowires, in which the reduction of precursor acid by hydrazine generated tellurium, nitrogen gas, and water:[46]

$$2Te(OH)_6 + 3N_2H_4 \longrightarrow 2Te\,(\downarrow) + 3N_2\,(\uparrow) + 12H_2O \qquad (2)$$
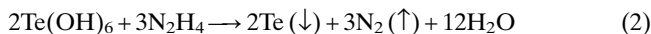
The primary difference between Se and Te systems is that Te atoms can form nuclei without the need for cooling of the solution. As a result, there are two types of Te product formed at the outset of this redox reaction: a-Te colloids and t-Te seeds (in the form of nanocrystallites). The transfer of material from the amorphous to the crystalline phase is essentially the same for both Se and Te. Because nucleation events might continuously occur in the reduction of orthotelluric acid, it was harder to control the monodispersity of the tellurium nanowires. Nevertheless, the t-Te nanowires prepared using this reaction were characterized by a relatively narrow distribution in size, with a typical standard deviation of < 10 % (Fig. 5A).
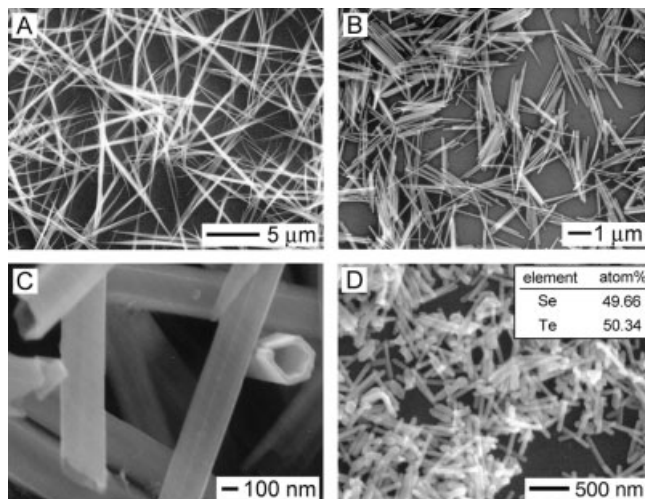

Fig. 5. A,B) SEM images of t-Te nanowires and nanorods synthesized using a solution-phase method similar to that demonstrated for selenium [46]. C) An SEM image of t-Te nanotubes that were synthesized by reducing orthotelluric acid with ethylene glycol at 197 °C [48]. D) An SEM image of $Se_{0.5}Te_{0.5}$ nanorods that were synthesized by reducing a mixture (1:1) of selenious acid and orthotelluric acid with hydrazine [49].

Similar to the vapor-phase experiments done by Furuta and co-workers,[45] various morphologies were observed over different temperature ranges: wires formed at 20–100 °C (with water as the solvent) developed a spine-like morphology having slight taper and equilateral triangular cross-sections. Wires formed at 100–196 °C in ethylene glycol displayed filamentary structures with pronounced taper and isosceles triangular cross-sections. Synthesis carried out at 178 °C in a water/ethylene glycol mixture yielded nanorods with hexagonal cross-sections and no tapering (Fig. 5B). In this case, the product was highly monodispersed in dimensions, with a mean diameter of

98 ± 3 nm and length of 1.80 ± 0.16 μm. Electron diffraction studies confirmed single crystallinity and growth direction along the <001> axis. It is believed that these nanorods were formed because of an increased solubility and mobility for Te in ethylene glycol solution (with the addition of a small amount of water) and at high temperatures. This change ensured a higher supersaturation of Te atoms at the growing tips, and thus allowed for the formation of defect-free nanowires with uniform hexagonal cross-sections (instead of filamentary nanowires).

A new morphology was also observed when telluric acid was reduced not by hydrazine, but by the ethylene glycol solvent itself at 198 °C via the so-called polyol process.[47] In this case, the growth mechanism does not include the formation of amorphous colloids, although it can still be described in terms of discrete nucleation and growth steps. The reaction seems to begin with the decomposition of orthotelluric acid into tellurium dioxide, followed by the formation of t-Te hexagonally shaped seeds. The subsequent growth along the circumferential edges of these seeds leads to the evolution of a nanotube morphology.[48] The solid walls of these nanotubes had a reasonably uniform thickness of ~30 nm, as determined by the diffusion of Te atom across the surfaces of the seeds. The lengths of these inorganic nanotubes could be varied by controlling the growth time. Figure 5C shows the SEM image of a typical example of Te nanotubes crystallized in the trigonal phase. It is believed that the formation of hollow structures was most likely a manifestation of Te concentration profiles on the surfaces of their solid seeds. Immediately after the nucleation step, further addition of tellurium atoms to the seed surface seemed to occur preferentially at the circumferential edges of each cylindrical seed because these sites had relatively higher free energies than other sites on the surface. As soon as crystal growth began, mass transport to the growing regions led to undersaturation (or complete depletion of tellurium) in the central portions of the growing faces, the {001} planes on each seed, and eventually resulted in the formation of nanotubes having well-defined hollow interiors. In addition to nanotubes, Qian and co-workers recently demonstrated a hydrothermal route to the synthesis of single-crystalline Te nanobelts.[49]

3.2.3. Nanorods of Se/Te Alloys

Because trigonal-phase Se and Te solids crystallize in the same structure and the reaction conditions are also essentially the same for the generation of pure Se and Te nanowires, it was a natural step to combine these two reactions to generate 1D nanostructures made of their alloys. Xia and co-workers found that it was possible to generate single-crystalline nanorods made of Se/Te alloys by reducing selenious and orthotelluric acids with hydrazine in one pot.[50] These nanorods were found to retain the elemental ratio as that of the acids used as the precursors. Each helical chain is believed to consist of domains of Se and Te atoms, as in a random organic block copolymers. The individual Se and Te domains, however, could

not be resolved with TEM or electron diffraction, indicating that these two elements were blended on the atomic scale. Figure 5D displays an SEM image of nanorods that were obtained in a reaction that involved a 1:1 molar ratio of selenious and orthotelluric acids and excess hydrazine. In this case, the mean diameter and length of these nanorods were ~50 nm and ~250 nm, respectively. Energy-dispersive X-ray (EDX) analysis of these nanorods was also done, and characteristic peaks for selenium and tellurium were observed and confirmed an elemental ratio of 1:1 (inset of Figure 5D) for Se and Te in the nanorods. The lattice parameters calculated from the XRD diffraction pattern also fell in between those values for trigonal tellurium and selenium, indicating the formation of a solid solution between these two elements in the alloy.[51] By fine-tuning the elemental composition of these nanorods, it should be possible to control their properties such as piezoelectricity (greater for Te) or photoconductivity (greater for Se) while still maintaining their dimensionality and single crystallinity.

3.3. Other Solids with Anisotropic Structures

In principle, the synthetic approach described in the above two sections can also be extended to a range of other solid materials whose crystallographic structures are characterized by chain-like building blocks.[52] Many of these solids have already been extensively studied in the context of low-dimensional semiconductors or conductors, and some of them have often been observed to crystallize in the form of fine needles or whiskers (the macroscopic and microscopic counterparts of nanorods). Typical examples include SbSI, a ferroelectric and optoelectronic material;[53] $K_2[Pt(CN)_4]$, a narrow-bandgap semiconductor;[54] and MX_3 (M = transition metal, X = S, Se, and Te), a host of semiconductors and thermoelectric materials;[55] metallophthalocyanines, M(Pc) with M = H_2, Ni, and $[M(Pc)O]_n$ with M = Si, Ge, Sn, a group of organometallic polymers with metallic conductive and photoconductive properties.[56] By modifying the experimental procedures that have been developed for chalcogens and molybdenum chalcogenides, one should be able to obtain uniform nanowires from the reaction solutions of these solid materials.

4. Template-Directed Synthesis

Template-directed synthesis represents a straightforward route to 1D nanostructures. In this approach, the template simply serves as a scaffold within (or around) which a different material is generated in situ and shaped into a nanostructure with its morphology complementary to that of the template. A wealth of templates have been successfully demonstrated by various research groups, with notable examples including step edges present on the surfaces of a solid substrate; channels within a porous material; mesoscale structures self-assembled from organic surfactants or block copolymers;

biological macromolecules such as DNA strains or rod-shaped viruses; and existing nanostructures synthesized using other approaches. When the template is only involved physically, it is often necessary to selectively remove the template using post-synthesis treatment (such as chemical etching and calcination) in order to harvest the resultant nanostructures. In a chemical process, the template is usually consumed as the reaction proceeds and it is possible to directly obtain the nanostructures as a pure product. It is generally accepted that template-directed synthesis provides a simple, high-throughput, and cost-effective procedure that also allows the complex topology present on the surface of a template to be duplicated in a single step. As a major drawback, nanostructures synthesized using template-directed methods are often polycrystalline, and the quantity of structures that can be produced in each run of synthesis is relatively limited. Here, we only briefly discuss four templating methods, with a focus on their capability, feasibility, and potential extension.

4.1. Templating Against Features on Solid Substrates

Relief structures present on the surface of a solid substrate can serve as a class of natural templates for generating supported 1D nanostructures. In this regard, microstructures that could be conveniently patterned on the surface of a solid substrate using lithography and etching could be exploited as templates to fabricate nanowires made of various materials.[57] Decoration of these templates (usually their edges) with a different material, for example, provides a powerful route to the formation of nanowires from various metals and semiconductors.[58] As shown by Jorritsma and co-workers, metal nanowires as thin as 15 nm could be prepared by shadow sputtering (Fig. 6A) a metal source against an array of V-grooves etched on the surface of a Si(100) wafer.[59] In another procedure, metal or semiconductor was applied at normal incidence

Fig. 6. Schematic illustrations of procedures that generated 1D nanostructures by A) shadow evaporation [58]; B) reconstruction at the bottom of V-grooves [60]; C) cleaved-edge overgrowth on the cross-section of a multilayer film [64]; and D) templating against step edges on the surface of a solid substrate [68].

using techniques based on vapor-phase deposition (e.g., MBE) or solution-phase electrochemical plating, and then allowed to reconstruct into 1D nanostructures at the bottom of each V-groove (Fig. 6B).[60] Using this simple approach, continuous thin nanowires with lengths up to hundreds of micrometers could be routinely prepared as parallel arrays on the surfaces of solid supports that could be subsequently released into the free-standing form or be transferred onto the surfaces of other substrates. As demonstrated by Müller and co-workers, it was possible to fabricate large parallel arrays of Ge nanowires by templating against V-grooves etched in the surfaces of Si(100) substrates.[61] It is also worth mentioning that Sugawara and co-workers have fabricated 3D arrays of iron nanowires by templating against relief features present on the (110) surfaces of NaCl crystals.[62]

The cross-sections of multilayer films prepared using MBE[63] have also been exploited as templates to grow simple patterns of quantum structures from many kinds of metals and semiconductors (Fig. 6C).[64] This technique is commonly known as cleaved-edge overgrowth (CEO), and it takes advantage of the high accuracy of MBE in controlling the layer thickness of a superlattice. In this technique, a superlattice consisting of alternating layers (made of, e.g., AlGaAs and GaAs) is fabricated by MBE, and then cleaved in situ through the thickness of the multilayer structure to produce an atomically clean surface. In the following step, MBE or electrochemical deposition is used to grow epitaxial layers on selected regions of the exposed surface. This approach has enabled the formation of intersecting quantum wells with atomic or angstrom-level control over the thickness in two directions.[65] Prototype devices such as quantum-wire lasers formed from the intersection of ~7 nm wide quantum wells have also been fabricated using this technique.[66] For most fabrication tasks, CEO provides quantum structures with more uniform morphologies than e-beam or optical lithography, because CEO inherits the atomic uniformity and precision of MBE. This technique is, however, limited to those structures that can be fabricated along the natural cleavage directions of a substrate and along lattice planes on which MBE growth occurs preferentially. In addition, the structures must be built up from intersecting planes of a material. Although this technique is most commonly used and has the highest resolution when combined with MBE, the same basic approach should be suitable for use with multilayer films grown using many other deposition techniques.[67]

Penner and co-workers have demonstrated the growth of metal nanowires by templating against the steps present on a highly oriented, pyrolytic graphite using electrodeposition (Fig. 6D).[68] Two different types of materials have been employed in their studies: noble metals (e.g., Pd, Cu, Ag, and Au) and electronically conductive metal oxides (MoO_x, MnO_2, Cu_2O, and Fe_2O_3) that could be subsequently reduced to the corresponding metals (Mo, Mn, Cu, and Fe) by hydrogen gas at elevated temperatures. The nanowires were found to preferentially nucleate and grow along the step edges pres-
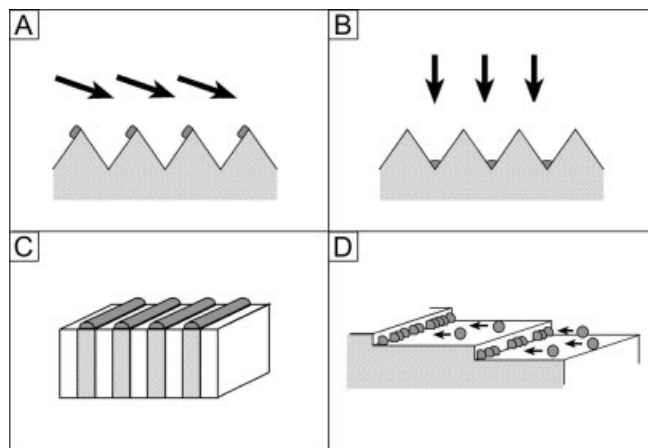
ent on a graphite surface into a 2D parallel array that could be transferred onto the surface of a cyanoacrylate film supported on a glass slide. For the formation of metal nanowires through an oxide precursor, the dimensional uniformity and hemicylindrical shape of the parent oxide wires could be retained in the H_2 reduction process, although the diameter was often reduced by as much as ~35 %. In addition to physical features present on the surface of a solid substrate, strains generated during film deposition have also been exploited as physical templates to direct the organization of a deposited material into arrayed 1D nanostructures.[69]

4.2. Channels in Porous Materials

Channels in porous membranes provide another class of templates for use in the synthesis of 1D nanostructures (Fig. 7). This method was pioneered by Martin and several others.[70] Two types of porous membranes are commonly used in such syntheses: polymer films containing track-etched
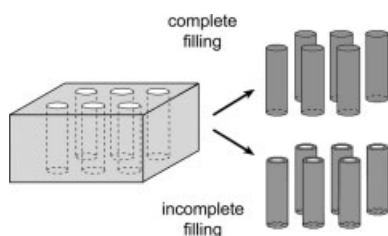
Fig. 7. Schematic drawings illustrating the formation of nanowires and nanotubes by filling and partial filling the pores within a porous membrane with the desired material or a precursor to this material [70,79].

channels and alumina films containing anodically etched pores. Both of them can be obtained commercially from a number of venders that include Nuclepore, Poretics, and Whatman. For track-etching, a polymer film (6–20 μm thick) is irradiated with heavy ions (from nuclear fission) to generate damaged spots in the surface of this film. These spots are then amplified through chemical etching to generate uniform, cylindrical pores penetrating the membrane film.[71] The pores fabricated using this method are often randomly scattered across the membrane surface; and their orientation may also be tilted by as much as 34° with respect to the surface normal. Porous alumina membranes are often prepared using anodization of aluminum foils in an acidic medium,[72] and they usually contain a hexagonally packed 2D array of cylindrical pores with a relatively uniform size. Unlike the polymer membranes fabricated by track-etching, the pores in alumina membranes have little or no tilting with respect to the surface normal and the pore density is also much higher.

A variety of materials have been examined for use with this class of templates, with typical examples as diverse as metals,[73] semiconductors,[74] ceramics,[75] and organic polymers.[76] The only requirement seems to be that the material can be loaded into the pores using a method based on vapor-phase sputtering, liquid-phase injection, or solution-phase

chemical or electrochemical deposition. In addition to vapor-phase evaporation and solution-phase deposition, metals (such as Bi) with relatively low melting points could be directly injected as liquids into the pores of an anodic alumina membrane and subsequently solidified into highly crystalline nanowires.[77] Most recently, Cao and co-workers also demonstrated the use of electrophoretic deposition to fill the pores of a polymeric or alumina membrane with charged sols generated in situ from a sol–gel precursor.[78] Subsequent firing at elevated temperatures led to the formation of uniform, ceramic nanorods with compositions such as titania and $Pb(Zr,Ti)O_3$ (PZT). It is worth mentioning that, in the early stage of this process, the material might be preferentially deposited as uniform layers on the walls of these pores to form tubular nanostructures instead of solid rods (Fig. 7).[79] In both cases, the resultant nanostructures could exist as well-aligned arrays within the pores, or be released from the templates and collected as an ensemble in the free-standing form.

Although the nanowires synthesized using this method are usually polycrystalline, single crystals have also been obtained under carefully controlled conditions. For example, Barbic and co-workers have demonstrated the use of electroless deposition in generating single-crystalline nanowires of silver in the channels of a polycarbonate membrane via a self-catalyzed process.[80] Neumann and co-workers have also shown that pulse electrodeposition could be exploited to selectively grow either single-crystalline or polycrystalline copper nanowires.[81] It was also observed that formation of single-crystalline wires of Pb required a significant departure from the equilibrium conditions (e.g., with a greater overpotential) than those required for the formation of polycrystalline samples.[82] In a recent study, Guo and co-workers discovered that titania nanowires synthesized using the electrophoretic deposition method became single crystals once their diameters had been reduced below 15 nm.[83] The major advantage associated with membrane-based templates is that both the dimensions and compositions of nanowires can be easily controlled by varying experimental conditions. In a set of publications, Mallouk, Keating, and co-workers have demonstrated that this method could be exploited to generate nanowires containing bands of different metals with well-defined dimensions.[84]

In addition to macroporous membranes, mesoporous materials containing much smaller, 1D channels (1.5–30 nm in diameter) have been actively explored as physical templates to generate ultrafine nanostructures.[85] Two types of mesoporous silica have been examined as the templates: the MCM series (e.g., MCM-41) and the SBA family (e.g., SBA-15). Both of them contained hexagonal arrays of mesopores. Preparation of 1D nanostructures in these mesoporous materials also involves three steps: infiltration of the pores with an appropriate precursor via a vapor- or solution-based approach, conversion of this precursor to the desired material, and recovery of the 1D nanostructures by selectively removing the template. Materials that have been incorporated into this process include noble metals (e.g., Ag, Au, Pt, and Pd), and bimetallic

alloys (e.g., Au/Pt). Each individual 1D nanostructure obtained from these templates was a polycrystal. Most of them were characterized by relatively low aspect ratios, and some of them might even exist as discrete nanoparticles as a result of a high volume shrinkage involved in the thermal conversion of the precursor.

Similar to mesoporous materials, CNTs with at least one open end could also be filled with liquids (molten metals or salt solutions) through capillary action.[86] Due to the small diameter of CNTs, it has been difficult to achieve complete filling with high yields. The length of filling is usually limited to a few hundred nanometers. As reported by Green and co-workers, the yield of filling single-wall CNTs with Ru by wet chemistry was only 2 %.[87] More recently, they also put forward a more efficient liquid-phase method that could increase the yield of the filling process with silver to 50 % by employing eutectic melting system composed of KCl and UCl$_4$ or a solid-solution system formed from AgCl and AgBr.[88] In addition to metals, metal oxides have also been demonstrated for use with this type of template.[89] In comparison with porous membranes and mesoporous materials, it is much harder to remove CNT templates when naked nanowires are needed for electronic applications.

4.3. Templating Against Self-Assembled Molecular Structures

Mesophase structures self-assembled from surfactants provide another class of useful and versatile templates for generating 1D nanostructures in relatively large quantities (Fig. 8). It is well known that surfactant molecules spontaneously organize into rod-shaped micelles (or inverse micelles) when their concentration reaches a critical value.[90] These anisotropic structures can be immediately used as soft templates to promote the formation of nanorods when coupled with an appropriate chemical or electrochemical reaction. The surfactant molecules need to be selectively removed to collect the nano-
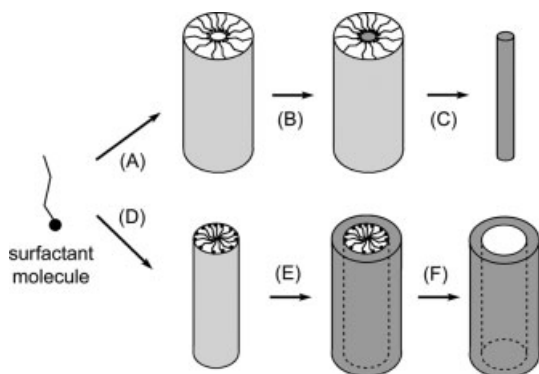

Fig. 8. Schematic illustrations showing the formation of nanowires by templating against mesostructures self-assembled from surfactant molecules: A) formation of a cylindrical micelle; B) formation of the desired material in the aqueous phase encapsulated by the cylindrical micelle; C) removal of the surfactant molecules with an appropriate solvent (or by calcination) to obtain an individual nanowire. D–F) Similar to the processes illustrated in (A–C), except that the exterior surface of an inverted micelle serves as the physical template.

rods as a relatively pure sample. Based on this principle, Mann and co-workers and Yang and co-workers have demonstrated the synthesis of BaCrO$_4$, BaSO$_4$, and BaWO$_4$ nanorods with monodispersed dimensions.[91] Wang and co-workers also demonstrated the synthesis of gold nanorods by templating against rod-like micelles assembled from cetyltri-methylammonium bromide (CTAB) and another much more hydrophobic cationic surfactant (e.g., tetraoctylammonium bromide (TOAB)).[92] The gold was generated in situ through electrochemical dissolution within a cell that contained a gold anode and a platinum cathode. This method was later exploited by El-Sayed and co-workers to synthesize gold and silver nanorods with well-controlled aspect ratios and plasmon properties.[93] More recently, a photochemical route was developed by Esumi, Yang, and co-workers for the preparation of uniform gold nanorods with similar aspect ratio.[94] Another useful route to gold nanorods was demonstrated by Murphy and co-workers, in which seed-mediated growth was used to generate metal nanorods with a controllable thicknesses and aspect ratios.[95] In a typical synthesis, gold or silver nanoparticles of 3–5 nm diameter were added as seeds to a solution that contained rod-like micelles (assembled from CTAB) and a metal precursor such as HAuCl$_4$ or AgNO$_3$. When a weak reducing agent (e.g., ascorbic acid) was added, the seeds served as nucleation sites for the growth of nanorods within the confinement of micelle structures. The lateral dimensions and aspect ratios of these nanorods could be controlled by varying the ratio of seeds relative to the metal precursors. In another demonstration, arrayed crystalline nanowires of Ag with a relatively high aspect ratio have been fabricated by Yan and co-workers when electrodeposition was performed in a micellar phase composed of sodium bis(2-ethylhexyl)sulfosuccinate (AOT), *p*-xylene, and water.[96] In this case, the rod-shaped micelles were further assembled into a hexagonal liquid-crystalline phase (normal or reverse) by increasing the concentration of surfactants. The major advantage of this method is that metal nanowires could be synthesized as regular arrays rather than randomly oriented samples. Most recently, Li and co-workers synthesized single-crystalline W nanowires by templating WO$_4$$^{2-}$ ions against the lamellar phase of CTAB, followed by pyrolysis in vacuo.[97] Metal nanowires have been synthesized in large quantities by using this class of templates, however the preparation and removal of the micellar phase is often difficult and tedious.

Block copolymers[98]—polymers formed by connecting two or more chemically distinct segments (or blocks) end-to-end with a covalent bond—can also be exploited as soft templates to generate 1D nanostructures. When the chemically distinct polymers are immiscible, a large collection of these chains will separate into different phases. Under appropriate conditions (e.g., with a proper ratio between the molecular weights of different segments), regular arrays of cylinders can be formed, with a structure similar to that of self-assembled surfactants. Different regions in such an arrayed structure can be selectively decorated with the precursor to a metal (or semiconductor) through physical adsorption or chemical coordination,

ADVANCED MATERIALS

making block copolymers a powerful system of templates for the synthesis of 1D nanostructures. A range of different block copolymers have been tested for the synthesis of silver nanowires, with notable examples including those made of carbosilane dendrimers and polyisocyanopeptides,[99] and the double-hydrophilic, poly(ethylene oxide)-*block*-poly(methacrylic acid).[100] Because the blocks can be easily designed with functional groups to selectively interact with any specific metal ion or compound, the range of materials that can be incorporated into this templating procedure is potentially very broad. Similar to the nanowires synthesized using other soft templates, the product obtained in this case is often polycrystalline and may aggregate into bundles.

4.4. Templating Against Existing Nanostructures

Currently existing nanowires are immediately useful as templates (physical or chemical) to generate nanowires and other types of 1D nanostructures from various materials, some of which might be difficult (or impossible) to directly synthesize as uniform samples. In one approach, the surfaces of these nanowires could be directly coated with conformal sheaths made of a different material to form coaxial nanocables. Subsequent dissolution of the original nanowires would lead to the formation of nanotubes. For instance, Murphy and co-workers have directly coated gold nanorods with polystyrene or silica (5–10 nm in thickness) to form cable-like nanostructures.[101] Layer-by-layer (LBL) deposition of oppositely charged species on nickel nanorods has also been adopted by Caruso and co-workers to prepare nanocables and composite nanotubes.[102] In addition, the sol–gel coating method has been examined as a generic route to coaxial nanocables that may contain electrically conductive cores (made of metals) and insulating sheaths (in the form of amorphous silica or other dielectric materials).[103] Figure 9A shows the TEM image of a typical sample of Ag@SiO$_2$ coaxial nanocables obtained by coating silver nanowires with silica derived from a sol–gel precursor. The thickness of sheath could be controlled in the range from 2 to 100 nm by varying the concentration of the precursor and/or the deposition time. Selective removal of the silver cores (by etching in an ammonia solution) yielded silica nanotubes with well-controlled dimensions and uniform wall structures (Fig. 9B). As discussed in Section 9, these coaxial nanocables might find use as ideal building blocks to generate 2D and 3D periodic structures through Langmuir–Blodgett self-assembly.

Yang and co-workers recently demonstrated that single-crystalline nanowires (pre-synthesized using methods such as thermal evaporation or laser ablation) could serve as substrates for the epitaxial growth of another solid to generate coaxial, bilayer nanotapes having sharp structural and compositional interfaces.[104] As an example, they have synthesized TiO$_2$/SnO$_2$ (Fig. 10) and Co$_{0.05}$Ti$_{0.95}$O$_2$/SnO$_2$ nanotapes. The latter structures were shown to be ferromagnetic at room temperature. In a related study, Lieber and co-workers synthesized semiconductor core–shell and multishell nanowire het-
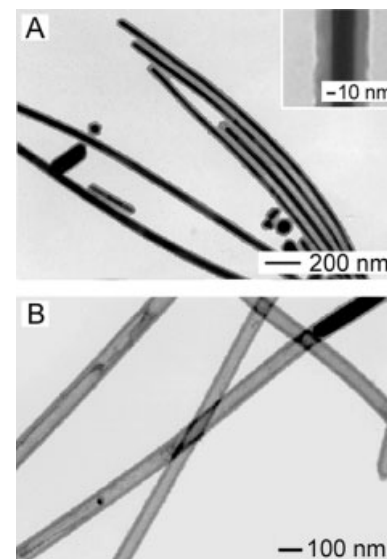

Fig. 9. A) TEM images of Ag/SiO$_2$ coaxial nanocables that were prepared by directly coating silver nanowires with an amorphous silica sheath using the sol–gel method. B) A TEM image of silica nanotubes prepared by selectively dissolving the silver cores of Ag/SiO$_2$ nanocables in an ammonia solution with ~pH 11 [103].
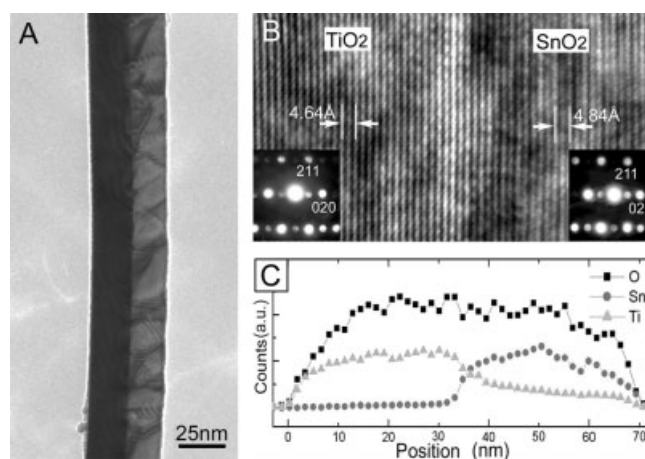

Fig. 10. A) TEM image of a TiO$_2$/SnO$_2$ nanotape obtained through epitaxial growth of TiO$_2$ on a single-crystalline SnO$_2$ nanobelt. B) A high-resolution TEM image of the atomically sharp TiO$_2$/SnO$_2$ interface. The fringe spacings of 4.64 and 4.84 Å correspond to the interplanar distances between the (010) planes of TiO$_2$ and SnO$_2$ (in the rutile structure), respectively. The insets show electron diffraction patterns taken from each side of the interface along the same zone axes of [$\bar{1}$02]. C) Compositional line profile across the TiO$_2$/SnO$_2$ interface in the direction perpendicular to the long axis of the nanotape [104].

erostructures via epitaxial growth by modulating the composition of reactant gases in sequential steps.[105] These studies clearly demonstrate the possibility to incorporate many functions (e.g., luminescent, ferromagnetic, ferroelectric, piezoelectric, and superconducting) into an individual nanowire that will find new applications in various areas.

In addition to nanowires, CNTs have been exploited as another type of physical template to generate nanorods or tubes from many materials.[106] For example, CNTs have been explored by Dai and co-workers to fabricate metal nanowires

through direct vapor evaporation.[106a] The pre-deposition of a thin layer of Ti was found to be critical to the formation of continuous nanostructures from metals such as Au, Pd, Fe, Al, and Pb, because Ti was able to improve the wettability of nanotube surfaces. Otherwise, direct deposition of these metals only led to the formation of discrete particles as a result of dewetting. Since CNTs as long as half a centimeter have already been synthesized, this approach can be, in principle, adopted to fabricate relatively long nanowires from a rich variety of materials. In another demonstration, chain-like biomolecules have also been exploited to guide the assembly of metal ions into linear arrays through the interaction between their functional side groups and the metal ions. These metal ions could be subsequently reduced to form a string of nanoparticles along the backbone of each biomolecule. If a reservoir of the metal ions were also present, these nanoparticles could be further connected to generate continuous nanowires. For instance, electrically conductive nanowires of Ag and Pt have been successfully produced using this approach by templating against DNA strands.[107] These metal nanowires could serve as interconnects to fabricate simple electronic circuits in the prototype form. One of the major advantages associated with this type of template is that it might be possible to generate complex patterns with arbitrary designs using many tools that have been well developed in biochemistry.

Some nanostructures can be converted to other materials without changing their morphology when they react with appropriate reagents under carefully controlled conditions. The concept of this method is evident from the thermal oxidation of silicon nanostructures, by which method silicon can be transformed into various silicon oxides. This templating effect provides another promising route to 1D nanostructures that may, otherwise, be difficult to directly synthesize or fabricate. The concept of this method was originally demonstrated by Lieber and co-workers, and it was found that highly crystalline nanorods of metal carbides could be formed by reacting CNTs with vapors of metal oxides or halides at elevated temperatures.[108] A similar templating procedure was later exploited by Fan and co-workers to produce crystalline nanorods of GaN, GaP, and SiC.[109] In addition to CNTs, boron nanowires have been used as templates by Yang and co-workers to form highly crystalline nanowires of MgB_2, a material that exhibits interesting superconductive properties.[110]

A number of solution-phase reactions have also been demonstrated to transform currently existing nanowires into 1D nanostructures with other chemical compositions. For example, Yang and co-workers demonstrated that free-standing nanowires of noble metals (e.g., Au, Ag, Pd, and Pt) could be prepared through a redox reaction that involved $LiMo_3Se_3$ molecular wires (serving as the reducing agent) and aqueous solution containing metal ions (e.g., $AuCl_4^-$, Ag^+, $PdCl_4^{2-}$, and $PtCl_4^{2-}$).[111] Using a similar approach, Xia and co-workers have synthesized highly crystalline nanotubes (Fig. 11) of noble metals such as Au, Pd, and Pt via galvanic displacement reactions between Ag nanowires and appropriate precursors of these metals in the aqueous medium.[112] For example,
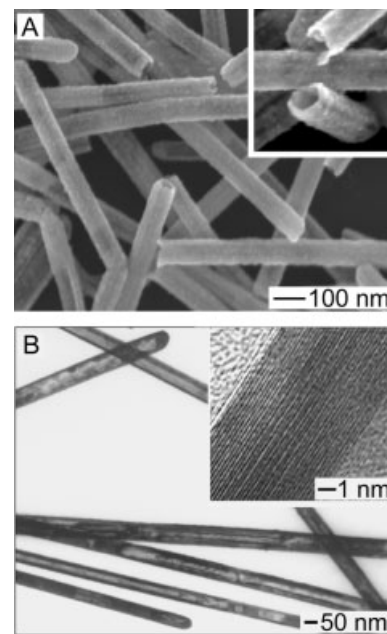

Fig. 11. A) SEM images of Pd nanotubes generated by reacting silver nanowires with an aqueous $Pd(NO_3)_2$ solution. The nanotubes were broken via sonication for a few minutes to expose their cross-sections. B) A TEM image of Au nanotubes prepared by reacting silver nanowires with an aqueous $HAuCl_4$ solution. The inset shows a high-resolution TEM image of the edge of an individual gold nanotube, indicating its highly crystalline structure and uniformity in wall thickness [112].

when silver nanowires are dispersed into an aqueous $HAuCl_4$ solution, they will be immediately oxidized to silver ions. The resultant Au atoms will be mainly confined to the vicinity of the template surface. Once their concentration has reached a critical value, the Au atoms will nucleate and grow into small clusters, and eventually evolve into a sheath-like structure around the silver template. This reaction is believed to be initiated on the facets with the highest surface energy and then proceed to those with lower energies. As a result, the thin sheath formed in the early stage is incomplete, and therefore it is possible for both reactants and products to diffuse across this layer until the silver template has been completely consumed. If the reaction is continued with refluxing at an elevated temperature, the wall of each gold tube will be reconstructed into a highly crystalline structure via processes such as Ostwald ripening. At the same time, the openings in the wall will also be closed to form a seamless gold nanotube bounded by smooth surfaces. Based on the stoichiometry of the reaction, the thickness of the gold nanotube is approximately one ninth of the lateral dimension of the corresponding silver template.

It is worth noting that single-crystalline nanowires of Ag_2Se (Fig. 12) have been synthesized through a room-temperature, topotactic reaction between single-crystalline nanowires of t-Se and aqueous $AgNO_3$ solutions.[113] In this template-engaged process, the silver ions diffused into the lattice of t-Se and formed Ag_2Se without involving significant reorganization of the Se atoms. An interesting, diameter-dependent phase transition was also observed in this new nanowire sys-
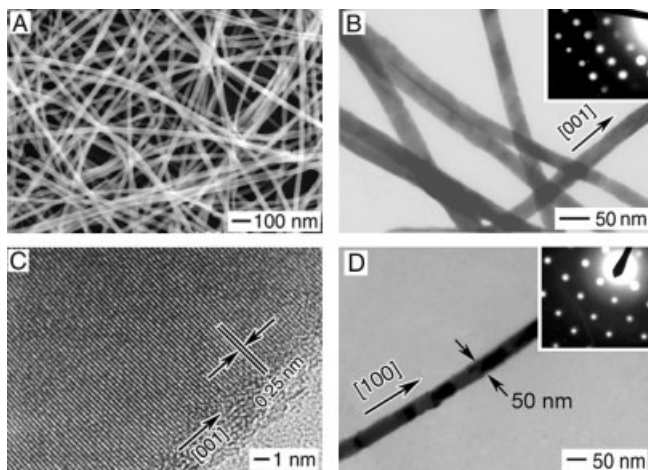
Fig. 12. A) An SEM image of α-Ag$_2$Se nanowires obtained by reacting t-Se nanowires with an aqueous AgNO$_3$ solution. B) A TEM image of α-Ag$_2$Se nanowires and the electron diffraction pattern (inset) taken from the middle portion of an individual nanowire. The diffraction spots can be indexed to the orthorhombic structure. C) A high-resolution TEM image obtained from the edge of an individual wire, indicating its single crystallinity. The fringe spacing of 0.35 nm corresponds to the interplanar distance of {200} planes, implying that the growth direction of this nanowire was <100>. D) A TEM image of an α-Ag$_2$Se nanowire of ~50 nm in diameter. This wire was crystallized in the tetragonal structure, as revealed by its electron diffraction pattern (inset) [113].

tem: The Ag$_2$Se nanowires were found to crystallize in the tetragonal structure when their diameters were less than ~40 nm (Figs. 12A–C). As the lateral dimensions of these nanowires increased beyond ~40 nm, the orthorhombic structure became the more stable one (Fig. 12D). This work seems to represent the first demonstration of a template-directed synthesis that is able to generate single-crystalline nanowires in a solution phase and at room temperature. These uniform Ag$_2$Se nanowires are interesting for their applications as a superionic conductor and thermoelectric material.

Templating against nanowires pre-synthesized using other methods provides a generic and powerful approach to greatly expand the diversity of materials that can be processed as uniform 1D nanostructures. One of the major problems associated with the nanowire-templated process is the difficulty in achieving a tight control over the composition and crystallinity of the final product. Nanowires synthesized using these methods were often polycrystalline in structure, and only a few schemes have led to the formation of single-crystalline products. For a templating process that involves chemical reactions on the surfaces of nanowires, if the product has a larger molar volume than the initial template, the reaction may automatically stop after a certain period of time when the stress accumulated around the template has reached the paramount value.[114] In general, the mechanisms of most template-directed reactions still need to be investigated in order to fully understand how these solid–vapor or solid–liquid reactions proceed at the atomic scale. A deeper understanding on this fundamental issue will certainly allow us to achieve a better control over the product, including its composition, phase purity, crystallinity, and morphology.

5. Generic Methods Suitable for All Solid Materials

The growth of nanowires from an isotropic medium is relatively simple and straightforward if the solid material has a highly anisotropic crystal structure. As illustrated in Section 3, uniform nanowires can be easily grown from an anisotropic solid (such as trigonal phase chalcogens) with lengths up to hundreds of micrometers, no matter whether the synthesis is carried out in a vapor or solution phase. For many solids that are characterized by isotropic crystal structures (e.g., almost all metals are crystallized in the face-centered cubic (fcc) lattice), symmetry breaking is required in the nucleation step to induce anisotropic growth. To this end, a large number of approaches have been explored to lower the symmetry of a seed (or the environment around a seed) to produce nanostructures with 1D morphologies. The template-directed methods described in Section 4 provide some good examples. The vapor–liquid–solid (VLS) process represents another elegant method, in which the symmetry is broken through the introduction of a flat solid–liquid interface. Furthermore, the supersaturation of a system can also be controlled below a certain level to effectively induce and maintain 1D growth, as has been demonstrated by many vapor-phase and solvothermal processes. Capping reagents have also been examined to kinetically control the growth rates of various faces of a solid and thus to achieve anisotropic growth. The objective of this section is to provide a brief account on all these chemical methods, with an emphasis on their mechanisms, capabilities, limitations, and possible extensions. In principle, these methods are suitable for use with all types of solid materials, no matter if they have an isotropic or anisotropic crystallographic structure.

5.1. Growth of Nanowires from the Vapor Phase

Vapor-phase synthesis is probably the most extensively explored approach to the formation of 1D nanostructures such as whiskers, nanorods, and nanowires.[115] In principle, it is possible to process any solid material into 1D nanostructures by controlling the supersaturation at a relatively low level. As early as 1921, Volmer and Estermann observed the formation of Hg nanofibers of 20 nm in diameter (determined by measuring the Brownian motion under an optical microscope) and up to 1 mm in length when mercury vapor was condensed on a glass surface cooled below the melting point of mercury.[116] In a series of studies, Sears extended this method to many other metals, and proposed a mechanism based on axial screw dislocation to explain the 1D growth.[117] In this mechanism, the driving force for 1D growth was determined by an axial screw dislocation, and incoming atoms could adsorb onto the entire surface of a nanowire and then migrate towards the growing tip. Although this model could explain the growth kinetics, no one has been able to observe the proposed screw dislocation in the final product. Now it is generally accepted

ADVANCED MATERIALS

that the control of supersaturation is a prime consideration in obtaining 1D nanostructures, because there is strong evidence that the degree of supersaturation determines the prevailing growth morphology. The relative supersaturation factors associated with the principal growth forms (whiskers, bulk crystal, and powders) have also been documented extensively: A low supersaturation is required for whisker growth whereas a medium supersaturation supports bulk crystal growth. At high supersaturation, powders are formed by homogeneous nucleation in the vapor phase. The lateral dimensions of the whiskers can be varied by controlling a number of parameters that include the supersaturation factor, nucleation size, and growth time.

Fig. 13. A) An SEM image of SnO_2 nanobelts synthesized by heating its commercial powders at 1000 °C. B) A cross-sectional transmission electron microscopy image of these nanobelts, confirming their quasi-rectangular cross-sections [104,120].

5.1.1. Direct Vapor-Phase Methods

Although the exact mechanism responsible for 1D growth in the vapor phase is still not clear, this approach has been explored by many research groups to synthesize whiskers and derivatives from a variety of materials. Most of the products were oxides because oxidation seemed to be inevitable due to the inclusion of trace amounts of O_2 in the reaction systems. The major advantage of a vapor-phase method is its simplicity and accessibility. In a typical process, the vapor species is first generated by evaporation, chemical reduction, and other kinds of gaseous reactions. These species are subsequently transported and condensed onto the surface of a solid substrate placed in a zone with temperature lower than that of the source material. With proper control over the supersaturation factor, one could easily obtain 1D nanostructures in moderately large quantities. For example, Zhu and co-workers have synthesized Si_3N_4, SiC, Ga_2O_3, and ZnO nanowires by heating the commercial powders of these materials to elevated temperatures.[118]

In addition to nanowires with a circular or square cross-section, Wang and co-workers also observed the formation of nanobelts (or nanoribbons) with a rectangular cross-section by simply evaporating commercial metal oxide powders at elevated temperatures.[119] The as-synthesized nanobelts were structurally uniform, and highly pure in elemental and phase compositions. Most of them were single crystals, and free from defects and dislocations. They had a typical width in the range of 30–300 nm, width-to-thickness ratios of 5–10, and lengths of up to several millimeters. Subsequent studies by Wang and co-workers and several other groups indicate that the belt-like morphology is a distinctive and common structural characteristic for the family of semiconducting oxides with cations of different valence states and materials of distinct crystallographic structures (Fig. 13).[120] This new type of 1D nanostructure could provide a class of ideal candidates for fully understanding dimensionally confined transport phenomena in functional oxides and building functional devices along individual nanobelts.
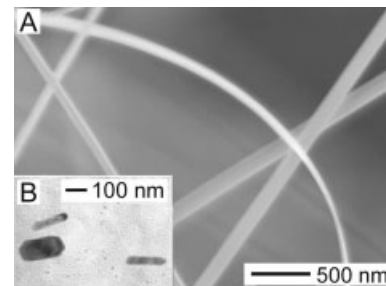
5.1.2. Indirect Vapor-Phase Methods

Although most vapor-phase methods look simple experimentally, their detailed mechanism might involve the formation of intermediates or precursors because of the use of relatively high temperatures. In many cases, decomposition and other types of side reactions also need to be taken into consideration. For example, Lieber and co-workers reported the synthesis of MgO nanowires via a carbonthermal reduction process,[121] in which Mg vapor was first generated in situ through the reduction of MgO by carbon, transported in a flow reactor to the growth zone, and finally oxidized to form MgO again. Hydrogen gas and water instead of carbon could be used as the reducing agent, and this method could also be extended to other binary oxides such as Al_2O_3, ZnO, and SnO_2.[122] In all of these syntheses, the formation of metal oxide through a two-step process might help to keep the supersaturation of the system at relatively low levels.

In a recent study, Lee and co-workers observed that Si nanowires could be obtained with relatively high yields when a mixture of Si and SiO_2 powders (rather than pure Si powders) was used as the target material for laser ablation.[123] The vapor-phase Si_xO ($x > 1$) generated by laser ablation (or thermal evaporation) seemed to be the key intermediate in this oxide-assisted process. The formation of silicon was believed to occur through the following two steps:

$$Si_xO \longrightarrow Si_{x-1} + SiO \quad (x > 1) \tag{3}$$

$$2SiO \longrightarrow Si + SiO_2 \tag{4}$$

Their TEM observations suggested that these decomposition reactions first led to the precipitation of Si nanoparticles encapsulated in shells of silicon oxide. Some of these particles might be piled up on the surface of the silicon oxide matrix, and served as seeds for the growth of nanowires in the following steps. Particles that stood separately with their growth directions perpendicular to the matrix surface would undergo fast growth. Although the exact growth mechanism for this process still needs more investigation, the authors suggested a

ADVANCED MATERIALS

number of factors that determined the wire growth kinetics. For example, the Si_xO ($x > 1$) layer at the tip of each nanowire seemed to have a catalytic effect. This layer might be in or near a molten state and thus capable of enhancing atomic absorption, diffusion, and deposition. The SiO_2 component (from the decomposition of SiO) in the shell might help to retard the lateral growth of each nanowire. The precipitation, nucleation, and growth of Si nanowires always occurred in the region closest to the cold finger, which suggested that the temperature gradient provided an external driving force for the nanowire growth. The Lee group also extended this mechanism to synthesize GaAs nanowires via laser ablation of a mixture of GaAs and Ga_2O_3.[124] The GaAs nanowires had a diameter in the range of 10 to 120 nm, and lengths up to tens of micrometers. Each one of them had a thin oxide layer covering a crystalline GaAs core with a [111] growth direction. The major advantage of these oxide-assisted methods is that no metal catalyst is required, and contamination of the resultant nanowires by the metal atoms is inherently eliminated.

In several related studies, Yang and co-workers synthesized Cu_2S nanowires by oxidizing copper into Cu_2O with O_2 gas and then sulfidizing this oxide intermediate into Cu_2S with H_2S gas under ambient conditions.[125] Xia and co-workers demonstrated the synthesis of CuO nanowires by heating copper substrates (foils, grids, and wires) in air.[126] Figure 14A and B show the SEM and HRTEM images, respectively, of a typical example that was formed on the surface of a millimeter-sized copper wire. Both electron diffraction and HRTEM studies implied that each CuO nanowire was a bi-

crystal divided by a (111) twin plane in the middle along its longitudinal axis. Two reactions were involved in this synthesis: the oxidation of Cu to form Cu_2O intermediate, and a second oxidation step to generate CuO vapor (from which uniform CuO nanowires were grown). In some cases, the involvement of an intermediate could even lead to a reduction in the temperature required for the growth of nanowires. Moreover, it is also possible to greatly reduce the synthesis temperature by using an appropriate precursor to form the desired material. For example, Xia and co-workers demonstrated that uniform nanowires of MgO could be synthesized in the temperature range of 800–900 °C by generating MgO in situ from the oxidation of MgB_2.[127] Figure 14D and E show SEM and TEM images, respectively, of a typical example of MgO nanowires that were synthesized by heating MgB_2 powders at 900 °C in a mixture of H_2/Ar. In comparison, synthesis of MgO nanowires from the direct evaporation of MgO powders required a temperature as high as 1200 °C.[121] In principle, one should be able to modify any chemical vapor deposition (CVD) method (e.g., by diluting the precursor gas to control supersaturation in the reaction chamber) to direct the growth of the deposited material into wire-like morphologies. This concept has recently been demonstrated by Buhro and co-workers with the synthesis of crystalline boron nanowires as an example.[128]

5.2. Vapor–Liquid–Solid Methods

Among all vapor-based methods, the VLS process seems to be the most successful for generating nanowires with single-crystalline structures and in relatively large quantities. This process was originally developed by Wagner and co-workers to produce micrometer-sized whiskers in 1960s,[129] and recently re-examined by Lieber, Yang, and many other research groups to generate nanowires and nanorods from a rich variety of inorganic materials.[130–134] A typical VLS process starts with the dissolution of gaseous reactants into nanosized liquid droplets of a catalyst metal, followed by nucleation and growth of single-crystalline rods and then wires. The 1D growth is mainly induced and dictated by the liquid droplets, the sizes of which remain essentially unchanged during the entire process of wire growth. In this sense, each liquid droplet serves as a soft template to strictly limit the lateral growth of an individual wire. As a major requirement, there should exist a good solvent capable of forming liquid alloy with the target material, ideally they should be able to form eutectic compounds. All major steps involved in a VLS process are schematically illustrated in Figure 15A, with the growth of Ge nanorods as an example. Based on the Ge–Au binary phase diagram (Fig. 15B), Ge (from the decomposition of GeI_2 or other precursors) and Au form liquid alloys when the temperature is raised above the eutectic point (361 °C). Once the liquid droplet is supersaturated with Ge, nanowire growth will start to occur at the solid–liquid interface. The vapor pressure of Ge in the system has to be kept sufficiently low that sec-
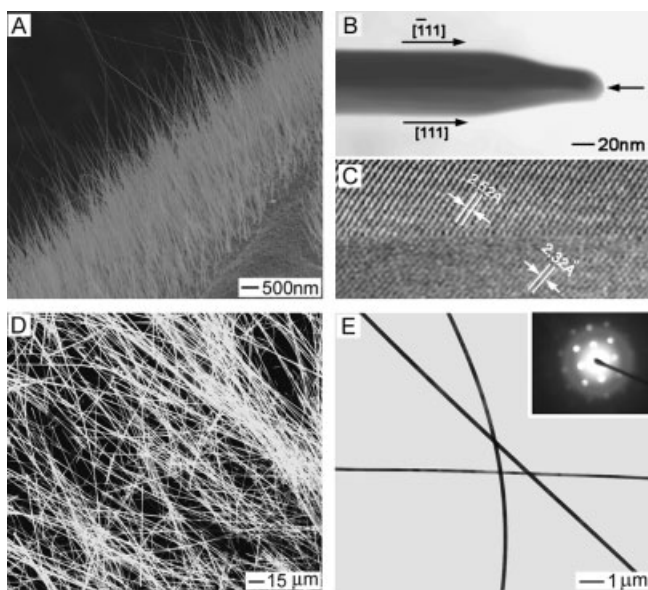
Fig. 14. A) SEM and B) TEM images of CuO nanowires synthesized by heating a copper wire (0.1 mm in diameter) in air to a temperature of 500 °C for 4 h. Each CuO nanowire was a bicrystal as shown by its electron diffraction pattern and high-resolution TEM characterization (C) [126]. D) SEM and E) TEM images of uniform MgO nanowires (~150 nm in diameter) that were synthesized by heating MgB_2 powders in a flow of H_2/Ar mixture (1:10 by volume) to a temperature of ~900 °C. The inset in (E) shows an electron diffraction pattern [127].

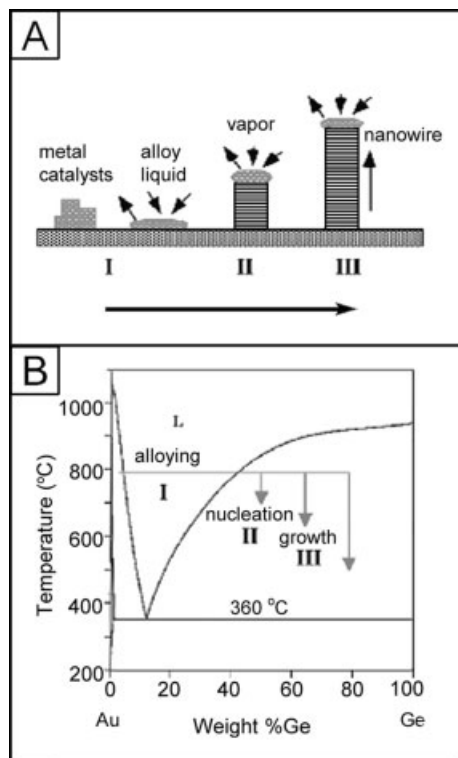Fig. 15. A) Schematic illustration showing the growth of a nanowire via the vapor–liquid–solid mechanism. B) The binary phase diagram between Au and Ge, with an indication of the compositional zones responsible for alloying, nucleation, and growth.
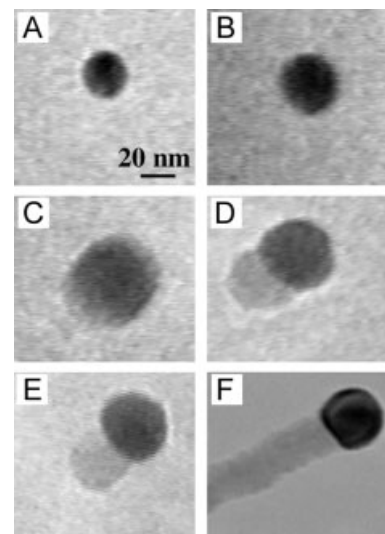

Fig. 16. The birth of a Ge nanowire on a Au nanocluster, as observed using in-situ TEM. It is clearly seen that the Au nanocluster started to melt after the formation of Ge–Au alloy, and this was followed by an increase in the liquid droplet size during the Ge vapor condensation process. When the droplet was supersaturated with the Ge component, a Ge nanowire grew out of this droplet of Au–Ge alloy and became longer as time elapsed [135].

ondary nucleation events will be completely suppressed. Both physical methods (laser ablation, thermal evaporation, and arc discharge) and chemical methods (chemical vapor transport and deposition) have been employed to generate the vapor species required for the growth of nanowires, and no significant difference was found in the quality of nanowires produced by these methods.

Yang and co-workers have confirmed this mechanism by observing the in-situ growth of Ge nanorods within the chamber of a TEM equipped with a temperature-controllable stage.[135] They used GeI$_2$ as the vapor source for Ge, and Au as the catalyst. The vapor transport was achieved by heating the system to a temperature in the range of 700 to 900 °C. Figure 16 shows a set of TEM images sequentially recorded during the growth of a Ge nanorod. These images clearly show all steps illustrated in Figure 15: the formation of Au–Ge alloy, the nucleation of Ge nanocrystal in the droplet of Au–Ge alloy, and the growth of a Ge nanorod by pushing the liquid–solid interface forward. Based on this mechanism, one can control the growth process from different aspects. To the first order of approximation, the diameter of each nanowire is largely determined by the size of the catalyst, and smaller catalysts should yield thinner nanowires. Lieber and co-workers and Yang and co-workers have demonstrated that Si and GaP nanowires of any specific size could be obtained by controlling the diameter of monodispersed gold colloids (or clusters) serving as the catalyst.[136]

The VLS process has now become a widely used method for generating 1D nanostructures from a rich variety of inorganic materials that include elemental semiconductors (Si, Ge, and B),[131] III–V semiconductors (GaN, GaAs, GaP, InP, InAs),[132] II–VI semiconductors (ZnS, ZnSe, CdS, CdSe),[133] and oxides (ZnO, MgO, SiO$_2$).[134] Among these materials, compound semiconductors such as GaAs, GaN, ZnO, and CdSe are especially intriguing targets since their direct bandgaps enable optical and optoelectronic applications that are of considerable importance to basic science and technology. The nanowires produced using the VLS approach are remarkable for the uniformity of their diameter, which is usually of the order of 10 nm over a length scale of >1 μm. Figure 17 shows SEM, TEM, and HRTEM images of a typical sample of Ge nanowires that was prepared using the vapor-transport procedure. Characterization based on electron diffraction and HRTEM indicates that each nanowire is essentially a single crystal. Once the growth has been terminated, the presence of a catalyst nanoparticle at one of the ends of the nanowire (inset of Fig. 17B) is a clear evidence supporting the VLS mechanism.

One of the challenges faced by the VLS process is the selection of an appropriate catalyst that will work with the solid material to be processed into 1D nanostructures. Currently, this is done by analyzing the equilibrium phase diagrams. It has also been shown that the analysis of catalyst and growth conditions can be substantially simplified by considering the pseudo-binary phase diagram between the metal catalyst and the solid material of interest. For instance, the pseudo-binary phase diagram of GaAs with Au exhibits a large GaAs-rich region in which liquid Au-GaAs co-exists with solid GaAs. Using this information, one should be able to obtain single-
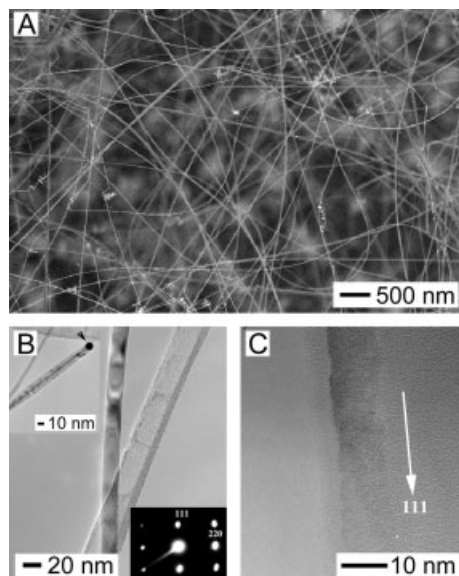
Fig. 17. A) SEM and B) TEM images of Ge nanowires prepared using the chemical vapor-transport method. Insets in (B) show the Au tip of a Ge nanowire and the electron diffraction from an individual Ge nanowires. C) The atomically resolved TEM image of a Ge nanowire [131a].

crystalline nanowires of GaAs with diameters as small as a few nanometers by setting the Au:GaAs composition ratio and growth temperature in the proper ranges. As a major limitation, it seems to be impossible to apply the VLS method to metals. The necessary use of a metal as the catalyst may also contaminate the semiconductor nanowires and thus potentially change their properties.

5.3. Solution–Liquid–Solid Methods

Based on an analogy to the VLS process, Buhro and co-workers developed a solution–liquid–solid (SLS) method for the synthesis of highly crystalline nanowires of III–V semiconductors at relatively low temperatures (Fig. 18).[137] In a typical procedure, a metal (e.g., In, Sn, or Bi) with a low melting point was used as the catalyst, and the desired material was generated through the decomposition of organometallic precursors. The product was essentially single-crystalline whiskers or filaments with lateral dimensions of 10–150 nm and lengths up to several micrometers. In principle, one could reduce the operation temperature to a value below the boiling points of commonly used aromatic solvents. For example,
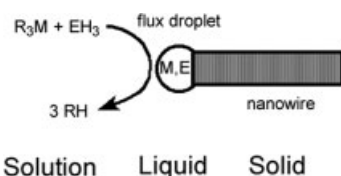

Fig. 18. Schematic illustration showing the growth of a nanowire through the solution–liquid–solid mechanism [136], which shares many similarities with the vapor–liquid–solid process depicted in Figure 15.

methanolysis of $\{tert\text{-}Bu_2In[\mu\text{-}P(SiMe_3)_2]\}_2$ in an aromatic solvent could yield polycrystalline InP fibers 10–100 nm thick and up to 1000 nm long at temperatures in the range of 111–203 °C.[138] The key component of this synthesis was a molecular component whose constituent groups could be eliminated to generate a non-molecular unit, from which the InP crystal lattices were assembled. Detailed studies indicated that the decomposition of this organometallic precursor proceeds through a sequence of isolated and fully characterized intermediates to yield complex $[tert\text{-}Bu_2In(\mu\text{-}PH_2)]_3$; this complex subsequently underwent alkane elimination to generate the building blocks—$(InP)_n$ fragments. In the following steps, the $(InP)_n$ fragments dissolved into a dispersion of droplets formed by molten indium, and recrystallized as InP fibers. This demonstration suggests that the SLS process could be modified to operate at temperatures well below those required by conventional VLS processes. This synthetic route has been further extended to many other highly covalent semiconductors (both binary and ternary), as well as their alloys.[139]

In a related work, Korgel and co-workers have successfully grown defect-free Si nanowires with nearly uniform diameters of 4–5 nm and lengths up to several micrometers by employing a supercritical fluid as the solvent for the SLS process.[140] The key strategy of their synthesis was the use of monodispersed, alkanethiol-capped Au nanocrystals that could serve as seeds to direct and confine the growth of Si into nanowires having a narrow size distribution. In a typical procedure, the sterically stabilized Au nanocrystals and a precursor to Si, diphenylsilane, were co-dispersed in hexane that was heated and pressurized above its critical point. Under these conditions, the diphenylsilane could decompose to form Si atoms. The phase diagram between Si and Au indicates that Si and Au can form an alloy phase in equilibrium with pure solid Si when the Si concentration with respect to Au is greater than 18.6 mol-% and the temperature is above 363 °C. As a result, the Si atoms were dissolved into the sterically stabilized Au nanocrystals until a supersaturation was reached, at which point they were expelled from the Au–Si alloy particle in the form of a uniform nanowire. This growth mechanism shares some similarities with the one proposed by Buhro for the SLS process. The supercritical fluid medium provides the extreme conditions necessary to promote the dissolution and crystallization of Si. More interestingly, the orientation of the Si nanowires could be controlled by varying the reaction pressure. Electron microscopic characterization indicated that the Si nanowires prepared using this method were essentially single crystals.

5.4. Solvothermal Methods

Solvothermal synthesis utilizes a solvent under pressures and temperatures above its critical point to increase the solubility of a solid and to speed up reactions between solids. It provides another commonly used methodology for generating 1D nanostructures. In a typical procedure, a precursor and

ADVANCED MATERIALS

possibly a reagent (such as amines) capable of regulating or templating the crystal growth are added into a solvent with appropriate ratios. This mixture is then placed in an autoclave to allow the reaction and nanowire growth to proceed at elevated temperatures and pressures. The major advantage of this approach is that most materials can be made soluble in a proper solvent by heating and pressurizing the system close to its critical point. As a result, this approach should be well suited for use with any solid material. Heath and co-workers pioneered the use of solvothermal synthesis for generating semiconductor nanowires.[141] They demonstrated that Ge nanowires could be synthesized (at relatively low yields) by reducing GeCl$_4$ or phenyl-GeCl$_3$ with sodium in an alkane solvent heated and pressurized to 275 °C and 100 atm (just above the critical point). Single-crystalline nanowires of 7–30 nm in diameter and up to 10 μm in length could be obtained. This method was later exploited extensively by Qian, Xie, and Li, and co-workers to process a rich variety of materials into wires,[142] tubes,[143] and whiskers.[144] Although this method seems to be versatile in generating 1D nanostructures (as judged from the diversity of materials that have been explored for use with this method), the products were often characterized by low yield, low purity, and poor uniformity in size or morphology. The aromatic solvents involved in many syntheses were not environmentally friendly either. The solvothermal process itself is inherently complex, and a systematic study of the growth mechanism is largely hindered by the use of autoclaves. In this regard, a fundamental understanding on the reaction and nanowire growth mechanism under solvothermal conditions is highly desirble, in order to advance the research in this area.

5.5. Solution-Phase Methods Based on Capping Reagents

The shape of a crystal is determined by the relative specific surface energies associated with the facets of this crystal. At equilibrium, a crystal has to be bounded by facets giving a minimum total surface energy, an argument that is known as the Wulff facets theorem.[145] Confined by this requirement, the shape of a single-crystalline nanostructure often reflects the intrinsic symmetry of the corresponding lattice (for most metals, it is a cube rather than a rod). The shape of a crystal can also be considered in terms of growth kinetics, by which the fastest growing planes should disappear to leave behind the slowest growing planes as the facets of the product.[146] This argument implies that one can control the final shape of a crystal by introducing appropriate capping reagent(s) to change the free energies of the various crystallographic surfaces and thus to alter their growth rates. In the past, a range of compounds have been evaluated as capping reagents (or the so-called surface-modifiers) to control the shape of colloidal particles synthesized using solution-phase methods.[147] Here, we only discuss two of these capping reagents that have been demonstrated for use in the synthesis of semiconductor nanorods and metal nanowires.

5.5.1. Semiconductor and Metal Nanorods

Alivisatos, Peng, and co-workers pioneered the use of mixed surfactants to control the shape of CdSe nanocrystals.[148] They found that CdSe quantum rods with aspect ratios as high as 10 could be obtained in large quantities by adding hexylphosphonic acid (HPA) to trioctylphosphine oxide (TOPO), a stabilizer commonly used in the synthesis of CdSe quantum dots. In the initial stage of a typical growth process, CdSe nanocrystals rapidly grew primarily along the *c*-axis of the wurtzite structure to form nanorods with a broad distribution in aspect ratio. As the concentration of CdSe precursor became depleted in the solution, the short axis grew significantly and the aspect ratio eventually decreased to nearly one. In their follow-up studies,[149] Peng and co-workers optimized the growth conditions to obtain CdSe nanorods as monodispersed samples and with well-controlled aspect ratios. They discovered that the growth of CdSe nanorods is a diffusion-controlled process, and cannot be explained using the Wulff reconstruction theorem. They have also shown that a strong cadmium ligand was required to maintain a relatively high precursor concentration in the solution. This argument seems to be a general one, and can also be extended to explain the formation of many other types of nanostructures in the solution phase.[150]

5.5.2. Metal Nanowires

Xia and co-workers recently demonstrated a polyol method that generated silver nanowires by reducing silver nitrate with ethylene glycol in the presence of poly(vinyl pyrrolidone) (PVP).[151] The key to the formation of 1D nanostructures is the use of PVP as a polymeric capping reagent and the introduction of a seeding step. Figure 19 shows a plausible mechanism for this process. When silver nitrate is reduced in the
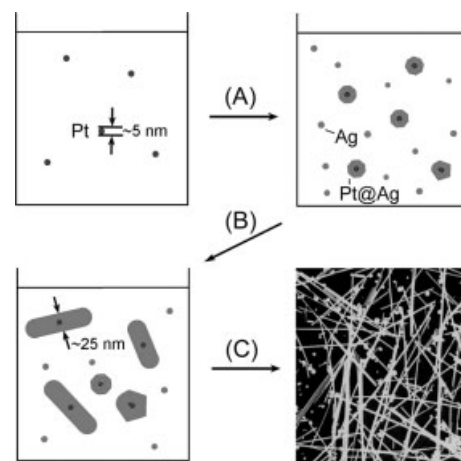
Fig. 19. Schematic illustration of major experimental steps involved in the preparation of silver nanowires through a polyol process with Pt nanoparticles as the seeds: A) Formation of bimodal silver nanoparticles through heterogeneous nucleation on Pt seeds and homogeneous nucleation; B) evolution of rod-shaped Ag nanostructures as directed by the capping reagent, poly(vinyl pyrrolidone); and C) growth of the Ag nanorods into wires at the expense of small Ag nanoparticles [151].

presence of seeds (Pt or Ag nanoparticles of a few nanometers across), silver nanoparticles with a bimodal size distribution are produced via heterogeneous and homogeneous nucleation processes, respectively. In the following step, silver nanoparticles with larger sizes will grow at the expense of smaller ones through the Ostwald ripening process. In the presence of PVP, most silver particles can be confined and directed to grow into nanowires with uniform diameters. The silver nanostructures involved in each step have been confirmed by electron microscopic and spectroscopic (based on surface plasmon resonance) studies. In this synthesis, the cubic symmetry associated with silver is reduced to a lower one when two single-crystalline seeds were fused together to form a twinned nanocrystallite.

The capability and feasibility of this polyol process has been demonstrated by generating bicrystalline nanowires of silver with diameters in the range of 30–60 nm and lengths up to ~50 μm. The product of a typical synthesis contained both nanowires and colloidal particles of silver. Such a mixture could be readily separated into pure components through centrifugation, with acetone added as the co-solvent. Figure 20A shows an SEM image of the purified silver nanowires, clearly indicating the removal of silver particles via centrifugation. Statistical evaluation suggested that these uniform nanowires had a mean diameter of 40 ± 5 nm. XRD studies indicate that these silver nanowires were crystallized purely in the fcc phase. Figure 20B gives a TEM image of several such nanowires, indicating the level of uniformity and perfection that

could be routinely achieved using this solution-phase approach. The crystallinity and structure of these nanowires were further studied using HRTEM and electron diffraction (Fig. 20C). Previous work suggested a low threshold for twinning along {111} planes of a fcc metal such as silver and gold, especially when the nanostructures have relatively high aspect ratios.[152] The HRTEM image and electron diffraction pattern both indicate that each individual silver nanowire contains a twin plane parallel to its longitudinal axis, with the mirror being positioned parallel to {111} planes. It was also possible to control the dimensions of silver nanowires by varying the experimental conditions. Figure 20D shows an SEM image of some silver nanowires that were synthesized at 185 °C (with other conditions similar to those used for A–C). These nanowires had a mean diameter of 39 ± 3 nm, and an average length of 1.9 ± 0.4 μm. Note that the average length of these nanowires had been greatly reduced (by as much as 90 %) in comparison with those grown at 160 °C (Fig. 21A–C). In other demonstrations, it was found that the diameters of the silver nanowires could be slightly reduced from 40 to 30 nm by increasing the concentration of the seeding solution.

It is believed this synthesis could be scaled up to produce silver nanowires on the gram-scale. This work on silver, together with previous studies on gold and other metals, makes it clear that most metals can be processed as nanowires through solution-phase methods by finding a chemical reagent capable of selectively forming coordination bonds with various surfaces of a metal. The availability of metal nanowires in large quantities should have a great impact on their use in electronic industry. For instance, the loading of metals in polymer composites could be greatly reduced by replacing currently used particles with nanowires with much higher aspect ratios.[153] The reduction in metal loading could decrease the consumption of metals, as well as the weight of an electronic device. In addition, these metal nanowires are immediately useful as nanoelectrodes for electrochemical analysis and detection; they are also required (as interconnects or electrodes) in fabricating nanoelectronic devices through self-assembly approaches.

6. Other Potentially Useful Approaches

A number of radically different approaches have also been demonstrated as alternative routes to the fabrication of 1D nanostructures. Most of these techniques are still in their early stages of development, and many issues remain to be addressed before they will become the method of choice for generating 1D nanostructures.
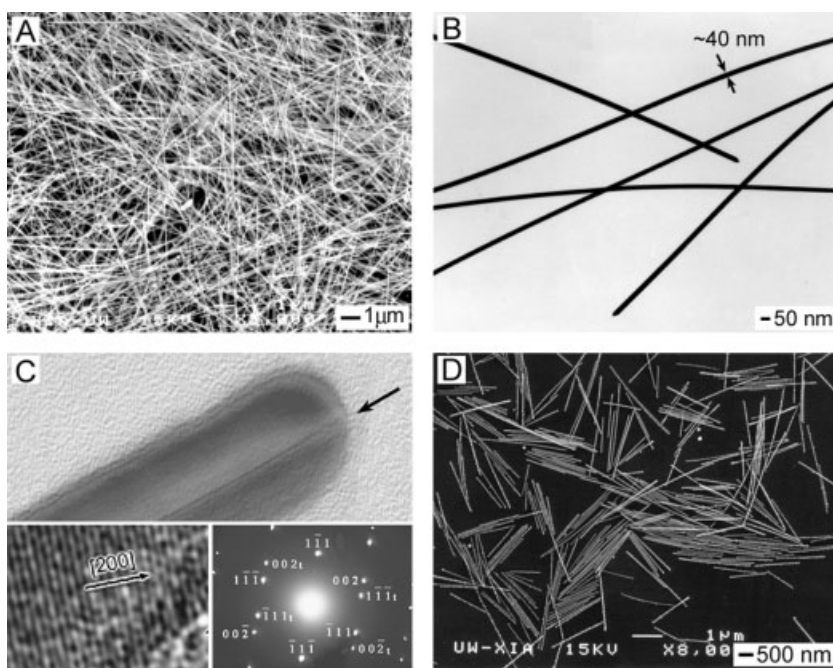
Fig. 20. A) SEM and B) TEM images of silver nanowires (after purification via centrifugation) that were synthesized at 160 °C. C) High-resolution TEM image of the end of an individual nanowire, with the arrow indicating a twin plane parallel to its long axis. The inset also shows the corresponding convergent-beam electron diffraction pattern. Indices without subscript refer to the left side of the nanowire shown in (C), and indices with subscript "t" refer to the right side. These two patterns have a reflection symmetry about the {111}-type planes. D) An SEM image of silver nanorods synthesized when the solution was heated at 185 °C, with other conditions kept the same as those for (A–C) [151].

For example, some of these techniques have only been demonstrated at relatively large scales and still need to be pushed down to the nanoscale. Some of them were mainly demonstrated as techniques for surface patterning and are yet to be adapted for generating 1D nanostructures. Here we only discuss two of these methods that are based on the self-assembly of nanoparticles and size reduction, respectively.

6.1. Self-Assembly of Nanoparticles

Self-assembly has been extensively explored as a bottom–up approach for generating complex nanostructures on various scales.[154] In particular, monodispersed colloids have been pursued as building blocks for the formation of wire-like structures through self- or externally manipulated assembly. It has been demonstrated by Schmid and co-workers that insulated 1D nanostructures could be formed by filling the pores in an alumina or polymer membrane with gold nanoparticles or clusters.[155] Rudimentary nanowires of gold were also obtained by sintering the nanoparticles confined within the pores of an alumina membrane at 300 °C for several hours. In addition, Korgel and co-workers found that ellipsoidal silver nanoparticles self-assembled into chains that were subsequently fused into bundles extending unbroken up to hundreds of nanometers in length in the solution phase.[156] More recent work by Schmid and co-workers further demonstrated that gold clusters such as $Au_{55}(PPh_3)_{12}Cl_6$ assembled into chains at the water–dichloromethane interface as induced by poly(*p*-phenyleneethynylene) dissolved in the liquid phase.[157] If PVP was present in the solution phase, 2D networks of cluster-loaded polymer chains were observed at the liquid–air interface when surface compression was applied using a Langmuir–Blodgett trough.[158] In this case, the gold clusters were mainly trapped and organized by the intersections between entangled polymer chains. Lopes and co-workers have studied the non-equilibrium self-assembly of metal nanoparticles on the surfaces of thin films formed from diblock copolymers.[159] They demonstrated that gold nanoparticles tended to aggregate into chains inside the polystyrene block (one of the blocks of the polystyrene-*block*-poly(methyl methacrylate) block copolymer) with a selectivity approaching 100 %. Alivisatos, Mirkin, and co-workers have examined biopolymers as templates to guide the assembly of gold nanoparticles into chains or lattices, typical examples include DNA strands modified with appropriate side or end functional groups.[160] In addition to molecule-based templates, patterned structures with mesoscale dimensions have also been explored as templates to direct the assembly of nanoparticles into structures with linear and more complex morphologies. For example, Xia and co-workers have recently demonstrated that it was possible to assemble spherical colloids into a number of complex structures by templating against relief structures patterned in the surfaces of solid substrates.[161] Figure 21 shows SEM images of several typical examples, including chains of spherical colloids that were characterized by a linear or helical

conformation. Note that it has been difficult to generate 1D nanostructures with the spiral morphology shown in Figure 21D using any other method. This approach can be potentially applied to building blocks with dimensions below 100 nm, as long as one can fabricate templates with feature sizes on the same scale.
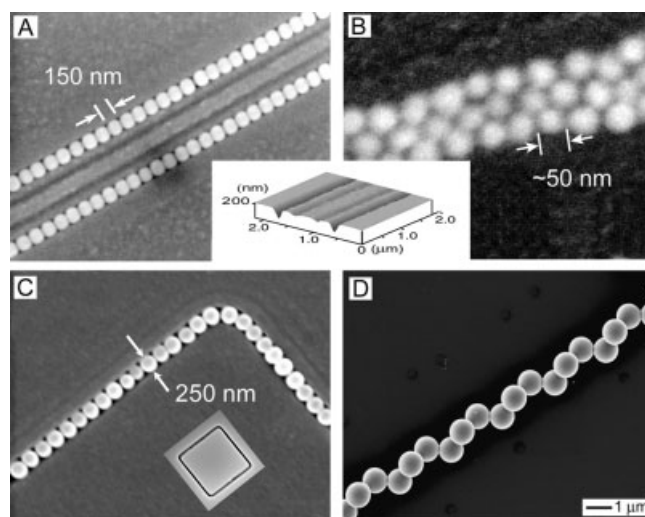

Fig. 21. A,B) Structures that were assembled from 150 nm polystyrene beads (A), and 50 nm Au colloids (B), by templating against 120 nm-wide channels patterned in a thin photoresist film (see the inset) [161a]. C) An L-shaped chain of Au@SiO$_2$ spheres assembled against a template (see the inset) patterned in a thin photoresist film [161c]. D) A spiral chain of polystyrene beads that were assembled by templating against a V-groove etched in the surface of a Si(100) wafer [161d].

In addition to self-assembly, external manipulation with a field or a mechanical probe has also been explored to induce or direct the organization of nanoparticles into arrayed structures. For example, Velev and co-workers have shown that metallic nanoparticles suspended in a liquid medium assembled into microwires up to 5 nm in length under dielectrophoresis.[162] In this approach, the mobility of and attractive interaction between nanoparticles were induced by an alternating electric field. In another demonstration, linear chains, circular rings, and pyramidal lattices have been fabricated by manipulating the positions of individual gold nanoparticles with the probe of a scanning force microscope.[163] Linear chains of gold nanoparticles have also been fabricated using a similar method and subsequently explored as templates to form continuous gold nanowires supported on the surface of a SiO$_2$/Si substrate via the hydroxylamine seeding process.[164] In addition to their use as a precursor to conductive nanowires, linear chains consisting of equally spaced gold (or silver) colloids can serve as nanoscale plasmonic waveguides.[165] Other external forces that have been explored to direct the assembly of nanoparticles include lateral capillary forces,[166] optical tweezers,[167] magnetic fields,[168] and electrostatic interactions.[169] Recent work by Kotov and co-workers demonstrated the use of dipole–dipole interactions to drive the self-assembly of monodisperse CdTe nanoparticles into highly crystalline nanowires with uniform sizes.[170]

Although the capability and feasibility of nanoscale self-assembly has been demonstrated to a certain extent, its development into a practical route to well-controlled 1D nanostructures still requires a significant number of additional studies. For example, the manipulation method based on scanning probes is a serial process and its slow speed will limit its application to only very small-scale production. The self-assembly approaches do not have this limitation, but, at the current stage of development, all of them seem to lack control over the dimensions and morphology of the resulting nanostructures. In many cases, it is necessary to accomplish a tighter confinement through the use of physical templates the dimensions of which match the sizes of the building blocks.

6.2. Size Reduction

A number of procedures have also been developed to reduce the size of 1D structures that can be routinely fabricated using conventional microfabrication techniques. These procedures may provide a cost-effective strategy for fabricating certain types of 1D structures that are expensive or difficult to directly generate at the nanometer scale. Here, we only focus on three of the most promising methods for size reduction that involve the use of isotropic deformation of a polycrystalline or amorphous material, anisotropic etching of a single crystal, and near-field optical lithography with a phase-shift mask. In all these demonstrations, it was possible to reduce the lateral dimensions of 1D structures from 1–10 μm to the regime ≤ 100 nm.

When a solid is uniaxially elongated, size reduction in two directions can be achieved at the expense of dimensional increase in the third direction. Such a deformation can also be made reversible by employing an elastomer. This reversibility adds another attractive feature to this approach in that the lateral dimension of the 1D nanostructures can be continuously reduced and iteratively adjusted by controlling the extent of mechanical deformation. The deficiency of this approach is that it depends on the uniform distortion in a solid material; the level of uniformity necessary at the < 100 nm scale may not be so easy to achieve. The first successful example of this approach can be traced back to the production of metal microwires pioneered by Taylor in the 1920s.[171] In his original demonstration, a metal wire (~2 nm thick) was encapsulated within a glass capillary and reduced to many filaments of < 1 μm in diameter by drawing this system in a gas flame whose temperature was sufficiently high to melt the metal and soften the glass tube. By cascading this process, metal filaments as thin as ~10 nm in diameter have been fabricated by Lewis and co-workers, who also explored their use as nanoelectrodes.[172] In principle, this method can be applied to many other solid materials, as long as they can be encapsulated by an appropriate glassy material.[173] In a related demonstration, Tonucci and co-workers successfully fabricated glass membranes with hexagonal arrays of cylindrical holes as small as ~30 nm in diameter by repeatedly drawing a bundle

of glass fibers > 1 μm in size.[174] Each of their glass fibers consisted of an etchable glass core surrounded by a thin sheath of a different, etch-resistant glass. In a third demonstration, Xia and co-workers have generated structures (e.g., parallel arrays of metallic lines) of 100–200 nm width by mechanically manipulating the elastomeric stamp (or mold) involved in microcontact printing or replica molding.[175] Although this method for size reduction may lack the characteristics required for registration in nanodevice fabrication, it provides easy access to 1D nanostructures that are directly useful in making sensors, arrays of nanoelectrodes, and optical diffraction gratings.

In the anisotropic etching of a single-crystalline substrate whose surface has been patterned with an array of trenches, the width of the trenches decreases in a controlled fashion as etching proceeds because the etching rates along various crystallographic directions are different.[176] For example, V-shaped grooves with well-defined cross-sections could be routinely generated in the surface of a Si(100) wafer by etching with an aqueous KOH solution.[177] This technique enables the feature size to be continuously reduced from several micrometers to less than 100 nm by controlling the etching time. When combined with other tools, this technique provides a simple and convenient approach to the fabrication of supported 1D nanostructures in the form of parallel arrays. For example, tungsten nanowires as thin as 20 nm have been fabricated by sputtering this metal onto patterned V-grooves from an oblique angle;[59] metal or polymer lines of ~200 nm in width have been generated by microcontact printing or photolithography with elastomer stamps cast from V-shaped grooves anisotropically etched in the surface of a Si(100) substrate.[178]

A third method for size reduction is based on near-field optical lithography that uses masks constructed from an elastomeric polymer such as poly(dimethylsiloxane) (PDMS).[179] Such a soft mask can non-destructively come into conformal contact with a layer of photoresist over an area as large as several hundred square centimeters without the need for external force. When a light passes through this phase-shift mask, its intensity can be modulated in the near-field such that an array of nulls or peaks in the intensity are formed at the edges of the relief structures patterned on the PDMS mask. As a result, nanoscale features can be generated in the thin film of photoresist that is placed underneath the PDMS mask. The features patterned in the photoresist film can be subsequently transferred into the underlying substrate using a reactive-ion-etching (RIE) or wet-etching process. Whitesides and co-workers have demonstrated the use of a polychromatic, incoherent light source and a conventional photoresist to produce parallel lines of ~90 nm in width over large areas on flat surfaces and on the surfaces of cylindrical lenses.[180] By optimizing the design of the mask, it was also possible to generate lines as narrow as 50 nm.[181] Since the exposure of the top surface of the resist film happens directly in the near-field of the mask, it is believed that features smaller than 50 nm will be possible. It is likely that the resolution can be further improved by reducing the wavelength of the light source, the thickness of the resist film, the thickness of the modulating

component (i.e., the surface relief of the binary masks) by increasing the index of refraction of the resist, by using surface sensitive resists, or with a combination of these approaches.

With the use of simple binary PDMS masks only, it has been possible to fabricate a variety of patterns that consist of lines with fixed width. Xia and co-workers have extended the use of this technique to generate nanostructures of single-crystalline silicon with controllable dimensions and geometric shapes.[182] They defined the nanostructures in a thin film of positive-tone photoresist using near-field optical lithography, and then transferred the pattern into the underlying substrate—silicon-on-insulator (SOI) wafer—through RIE. They were able to routinely generate parallel arrays of Si nanowires that were ~130 nm in width and separated by ~1 μm (Fig. 22A). The diameters of these wires could be further reduced to the scale of ~40 nm by using stress-limited oxidation
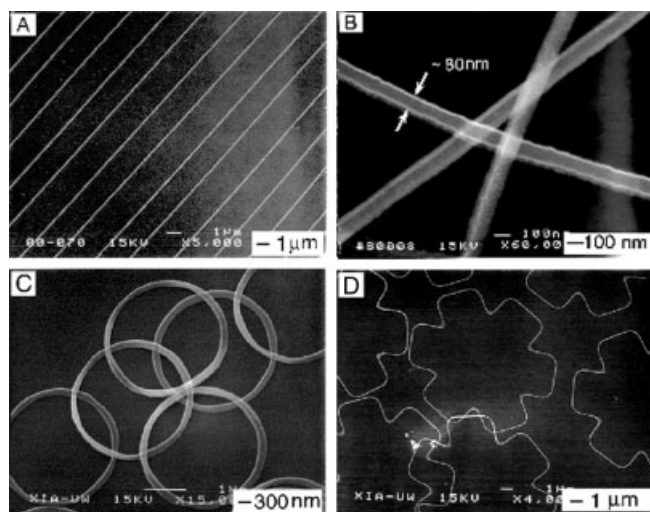

Fig. 22. A) The scanning electron diffraction image of a 2D parallel array of nanobelts (130 nm wide and 100 nm thick) that were fabricated from single-crystalline silicon using near-field optical lithography. B) An SEM image of these silicon nanobelts after they had been oxidized in air at 850 °C for ~1 h, and then lifted-off in HF solution. These nanowires had lateral dimensions of ~80 nm and lengths up to ~2 cm. C) An SEM image of rings (~2 μm in diameter) that were made of single-crystalline Si wires with lateral dimensions of ~110 nm. D) The SEM image of a more complex structure that contained connecting triangles of Si wires with widths varying from 80 to 120 nm [182].

in air at elevated temperatures. In addition to nanowires, they have also demonstrated the fabrication of free-standing nanorods, rings, and interconnected triangles made of single-crystalline silicon. Figure 22 shows several typical SEM images of these nanostructures. Even without further improvement, this technique is valuable for a range of applications that require the generation of 1D nanostructures rapidly and at low costs.

7. Heterostructured Nanowires

The success of semiconductor integrated circuits has largely hinged upon the ability to form heterostructures through carefully controlled doping and interfacing. As a matter of fact, the 2D semiconductor interface is ubiquitous in optoelectronic devices such as LEDs, laser diodes, quantum cascade lasers, and transistors.[183] For 1D nanostructures, the capability of forming heterostructures should be equally important for their potential applications as efficient light-emitting sources and thermoelectric devices. While there are a number of well-developed techniques (e.g., MBE) for generating heterostructures and superlattices in thin films, a generic scheme for forming heterojunctions and superlattices in 1D nanostructures with well-defined, coherent interfaces was not demonstrated until very recently. Previous studies on semiconductor nanowires and CNTs have mainly dealt with homogeneous systems with a few exceptions that involved heterostructures. Notable examples include heterojunctions formed between CNTs and SiC nanowires,[184] and p–n junctions on individual CNTs or GaAs/Ga$_{1-x}$In$_x$As nanowires.[185] A sequential electrochemical method was recently demonstrated by Keating and co-workers for fabricating striped metal nanorods.[84] This method, however, could only yield polycrystalline products with less than ideal interfaces. Yang and co-workers have recently demonstrated the use of a hybrid pulsed laser ablation/chemical vapor deposition (PLA–CVD) process for generating semiconductor nanowires with periodic longitudinal heterostructures.[186] In this process, Si and Ge vapor sources were independently controlled and alternately delivered into the VLS nanowire growth system. As a result, single-crystalline nanowires with a Si/SiGe superlattice structure were obtained.

Figure 23A shows a scanning transmission electron microscopy (STEM) image of two such nanowires in the bright-field mode. Along the longitudinal axis of each wire, dark stripes appear periodically, reflecting the alternating deposition of the SiGe alloy and Si segments. Since the electron scattering cross-section of Ge atoms is larger than that of Si atoms, the SiGe alloy block appeared to be darker than the pure Si
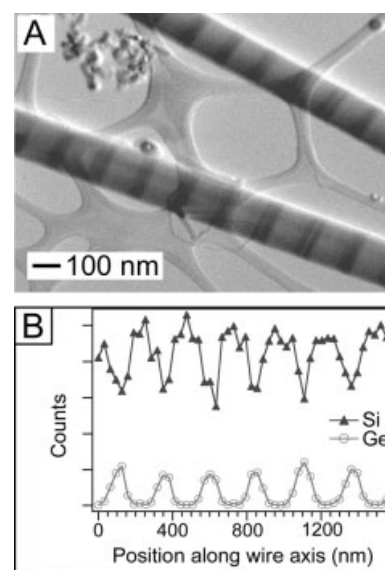

Fig. 23. A) A TEM image of two typical Si/SiGe superlattice nanowires. B) Compositional profiles showing the spatial modulation in Si and Ge contents along the longitudinal axis of a nanowire [186].

block. The chemical composition of the dark region was also examined using EDX spectroscopy, showing a strong Si peak and apparent Ge doping (~ 12 wt.-% Ge). The periodic modulation of Ge doping was further confirmed by scanning a focused electron beam along the nanowire growth axis and tracking the change in X-ray signal from Si and Ge atoms in the wire (Fig. 23B). Both Si and Ge X-ray signals showed periodic modulation, with their intensities anticorrelated: wherever the X-ray signal from Ge showed a maximum, the signal from Si showed a minimum. This observation also supported the formation of a Si/SiGe superlattice along the wire axis.

Using a similar approach, Lieber and co-workers and Samuelson and co-workers have also successfully prepared GaAs/GaP and InAs/InP heterostructured nanowires, respectively.[187] Since the supply of vapor sources can be readily programmed, it is believed that this VLS process with modulated source can be easily extended to prepare various other heterostructures on individual nanowires in a "custom-designed" fashion. It will also enable the creation of various functional devices (e.g., p–n junctions, coupled quantum dot structures, and heterostructured bipolar transistors) on individual nanowires. These heterostructured nanowires can be further used as important building blocks to construct nanoscale electronic circuits and light emitting devices. A recent work by Yang, Majumdar, and co-workers also demonstrated that superlattice nanowires with reduced phonon transport and high electron mobilities are promising candidates for improving the efficiency of thermoelectric devices.[188]

8. Properties and Applications

Compared with bulk materials, low-dimensional nanoscale materials, with their large surface areas and possible quantum-confinement effects, exhibit distinct electronic, optical, chemical and thermal properties. In many cases, 1D nanostructures are superior to their counterparts with larger dimensions. For instance, cyclic voltammetric detection limits for electroactive species at an array of cylindrical gold nanoelectrodes (10 nm in diameter) could be three orders of magnitude lower than those observed at a conventional disk microelectrode made of gold.[189] Greatly enhanced coercivities as high as 680 Oersteds (cf. only tens of Oersteds for bulk Ni) and remnant magnetization up to 90 % have also been observed for arrayed Ni nanowires of 30 nm diameter.[190] It is obvious that 1D nanostructures with well-controlled dimensions, composition, and crystallinity represent a new class of intriguing system for investigating structure–property relationships and related applications. The objective of this section is to briefly summarize all these studies, with an emphasis on examples demonstrated by Yang and co-workers at UC Berkeley.

8.1. Thermal Stability

The thermal stability of 1D nanostructures is of critical importance for their implementation as building blocks in nano-

scale electronic and photonic devices. It is well documented that the melting point of a solid material will be greatly reduced when it is processed as nanostructures.[191] In a series of studies, El-Sayed and co-workers used spectroscopic methods to investigate the photothermal melting and shape transformation of gold nanorods dispersed in micellar solutions.[192] They found that the nanorods were melted and transformed into spherical particles when they were exposed to femtosecond laser pulses at moderate energies. At higher energies (for fs pulses) or when exposed to nanosecond laser pulses, these nanorods were fragmented and then transformed into spherical particles with smaller dimensions. They also determined that an average energy of ~ 60 fJ was required to melt a single gold nanorod (with an aspect ratio of ~ 4.1) dispersed in an aqueous medium.[192b]

Yang and co-workers used in-situ high-temperature TEM to investigate the melting and recrystallization of Ge nanowires encapsulated by carbon sheaths.[193] The Ge nanowires (10–100 nm in diameter) were prepared using the VLS process, and subsequently coated with carbon sheaths 1–5 nm thick to confine the molten Ge and prevent the formation of liquid droplets at elevated temperatures. Two distinct features were observed in the melting–recrystallization cycle: One was the significant lowering of the melting point, which was found to be inversely proportional to the diameter of the nanowire. The other was the large hysteresis loop associated with the melting–recrystallization cycle. For example, a Ge nanowire of 55 nm in diameter and ~ 1 μm in length started to melt from both ends at ~ 650 °C (the melting point of bulk Ge is 930 °C). The melting then moved towards the center of this wire, and the entire wire was molten at ~ 848 °C. Upon cooling, the recrystallization process occurred at a temperature (558 °C) much lower than the initial melting temperature. By taking advantage of the relatively low melting points of nanowires encapsulated in carbon sheaths, Yang and co-workers also demonstrated the capability to manipulate individual nanowires using techniques such as cutting, interconnecting, and welding. Figure 24 shows a set of TEM snapshots clearly demonstrating the welding of two Ge nanowires encapsulated within a carbon sheath.[193] In this case, the two Ge nanowires melted, and the liquid fronts moved towards each other as the temperature was increased. They were eventually welded to form a single-crystalline nanowire after recrystallization.

In two related studies, Wang, Lee, and co-workers observed that silicon nanostructures with various morphologies were formed at different temperatures when a Si/SiO$_2$ mixture was thermally evaporated in an alumina tube.[194] In addition to Si nanowires, they also obtained many other types of Si nanostructures (e.g., those in the shape of an octopus, pin, tadpole, and linear chain) with significant yields. These nanostructures were believed to evolve from Si nanowires through spheroidization, a process that involved material transport along individual nanowires. They also found that both formation and annealing temperatures played important roles in determining the relative ratios of these nanostructures in the products. It was possible to achieve a tight control over the morphology
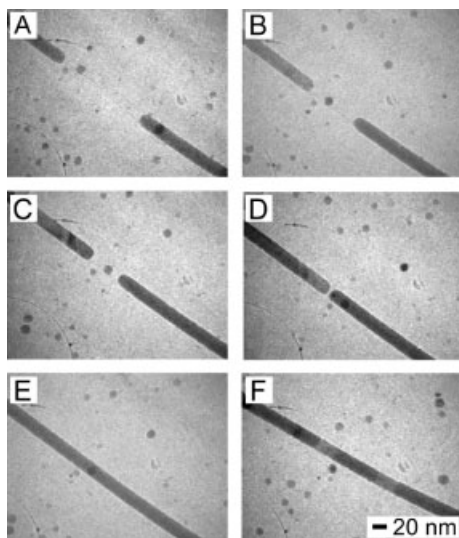
Fig. 24. A set of TEM snapshots that clearly shows the melting, flowing, and welding of two Ge nanowires (encapsulated by a carbon sheath) into a single nanowire [193].

and crystallinity of these Si nanostructures by simply varying the temperature. These results represent an important step toward design and controlled synthesis of nanostructures using the knowledge of their thermal stability.

The remarkable reduction in melting point associated with a nanowire has several important implications. First, the annealing temperature necessary for the synthesis of defect-free nanowires might only be a small fraction of the annealing temperature required for the bulk material. It is thus possible to perform zone-refining to purify nanowires at a modest temperature. Second, a reduction in melting point enables one to cut, interconnect, and weld nanowires at relatively mild temperatures. This capability may provide a new tool to integrate these 1D nanostructures into functional devices and circuitry. Third, as the thickness of nanowires is reduced to a smaller and smaller length scale, their stabilities may become extremely sensitive to environmental changes such as temperature fluctuation and residual stress variation. As driven by Rayleigh instability,[195] nanowires may spontaneously undergo a spheroidization process to break up into shorter segments at room temperature to reduce the relatively high free energy associated with a 1D system, when their diameters are sufficiently thin or the bonding between constituent atoms are too weak.

8.2. Mechanical Properties

Understanding the mechanical properties of nanostructures is essential for the atomic-scale manipulation and modification of these materials, which have been known to behave qualitatively different when the dimensions are reduced from micro- to nanoscale. For example, the hardness and yield stress of a polycrystalline material typically increase with decreasing grain size on the micrometer scale, a phenomenon known as the Hall–Petch effect.[196] It can be explained in

terms of the piling up of dislocations at the grain boundaries when the crystal planes in individual grains are sheared. As the grains are downsized, the area of their boundaries increases and thereby makes the material tougher by blocking dislocations more effectively. On the nanometer scale, however, an opposite behavior was discovered by Schiøtz and co-workers in their computational simulations: samples of nanocrystalline copper and palladium became softer with decreasing the grain size.[197] This abnormal behavior was believed to mainly arise from sliding motions at grain boundaries. As a result, the strength of a polycrystalline material first increases and then decreases with decreasing grain size, and there exists a characteristic length for each solid material to achieve the toughest strength. For copper and palladium nanomaterials, this characteristic length is around 19.3 and 11.2 nm, respectively. In principle, these conclusions based on studies of 0D systems could also be refined and further extended to describe 1D systems.

As for single-crystalline 1D nanostructures, they are supposed to be significantly stronger than their counterparts that have larger dimensions. This property can be attributed to a reduction in the number of defects per unit length (as a result of decreasing lateral dimensions) ((Defects often lead to mechanical failure.) In this regard, whiskers have been extensively studied in the 1970s for the fabrication of tough composites (the so-called whisker technology).[115] Several years ago, the Lieber group pioneered the use of atomic force microscopy (AFM) in determining the mechanical properties (elasticity, strength, and toughness) of individual, structurally isolated SiC nanorods that were pinned at one end to the surface of a solid substrate.[198] The bending force was measured as a function of displacement along the unpinned lengths. Continued bending of these nanorods eventually led to fracture. Based on their measurements, a Young's modulus of 610–660 GPa was estimated for these nanorods. These results were in good agreement with the value of ~ 600 GPa that was theoretically predicted for [111] oriented SiC and the average value previously measured for micrometer-sized whiskers. The large Young's modulus associated with SiC nanorods implies that these materials are a class of promising candidates for use as reinforcing elements in generating strong composites (with ceramic, metal, or polymer serving as the matrix). Wang and co-workers demonstrated another useful method based on resonance vibration for measuring the mechanical properties of an individual 1D nanostructure.[199] They fixed one of the ends of a CNT to the surface of a TEM sample holder, and attached a nanoparticle to the free end of this nanotube. By measuring the resonance frequency, they were able to calculate the Young's modulus of this nanotube. In principle, this method can be further extended to measure the mechanical parameters of inorganic nanowires.

AFM was also used by Fernandez and co-workers to measure the change in length of Au nanowires during elongation–compression cycles.[200] The nanowires were formed between two gold structures (one of them was coated as a thin film on the AFM tip) by pushing them into physical contact. They

found that the Au nanowires elongated under stretching in quantized steps up to three integer multiples of 0.176 nm and that they spontaneously shorten in steps of 0.152 nm when relaxed. They explained these observations by assuming that the sliding of crystal planes within the Au nanowires created stacking faults and thus changed the local structure from ccp to hcp. These results provide some direct evidence for the mechanism responsible for the plastic deformation of a nanowire when it undergoes mechanical stretching or compression. This approach can be further extended to examine the atomic events occurring during the plastic failure of various metals and their alloys. In a related study, an STM supplemented with a force sensor was adopted to investigate the mechanical properties of a freely suspended chain of single Au atoms.[201] It was found that the bond strength of the nanowire is approximately twice that of a bulk metallic bond. Computational studies on this system indicate that the total effective stiffness of the nanowire had a strong dependence on the local arrangement of atoms at the chain bases (that is, the contacts between the nanowires and the pads).

8.3. Electron Transport Properties

Miniaturization in electronics through improvements in the so-called "top–down" fabrication techniques is approaching the point where fundamental issues are expected to limit the dramatic increases in computing speed. Obviously, there is also the pressing issue of fabrication cost as the feature size reaches the sub-100 nm region. As a result, CNTs and nanowires have recently been explored as building blocks to fabricate nanoscale electronic devices through self-assembly—a typical "bottom–up" approach. The prototype devices that have been demonstrated include field-effect transistors (FETs), p–n junctions, bipolar junction transistors, complementary inverters, and resonant tunneling diodes.[202] It is believed that the "bottom–up" approach to nanoelectronics has the potential to go beyond the limits of the traditional "top–down" manufacturing techniques. As the critical dimension of an individual device becomes smaller and smaller, the electron transport properties of their components become an important issue to study. Studies from a number of groups indicated that some metal nanowires might undergo a transition to become semiconducting as their diameters are reduced below certain values. For instance, two-probe measurements made by Dresselhaus and co-workers on arrays of single-crystalline Bi nanowires indicated that these nanowires underwent a metal-to-semiconductor transition at a diameter of ~52 nm.[203] Two-probe measurements performed by Choi and co-workers on individual single-crystalline Bi nanowires of ~40 nm in diameter showed that these nanowires were semiconductors or insulators because their resistances increased with decreasing temperature.[204] As a result of quantum confinement, it was proposed that the external conduction sub-band and valence sub-band of this system moved in opposite directions to open up a bandgap. In this particular

material, the carrier mobility is also suppressed by carrier confinement along the long axis of a wire and by surface imperfection. Gold represents another metal whose electron-transport properties have been extensively studied in the form of short nanowires as thin as a single, linear chain of atoms.[205] Because these wires are extremely short in length (usually a few atoms across, sometimes also referred to as point contacts), their conductance has been shown to be in the ballistic regime with the transverse momentum of electrons becoming discrete. The transport phenomena (e.g., conductance quantization in units of $2e^2 h^{-1}$) observed in this kind of 1D system are found to be independent of material.[206] As for semiconductors, recent measurements on a set of nanoscale electronic devices (Fig. 25) indicated that GaN nanowires as thin as 17.6 nm could still function properly as a semiconductor.[207]
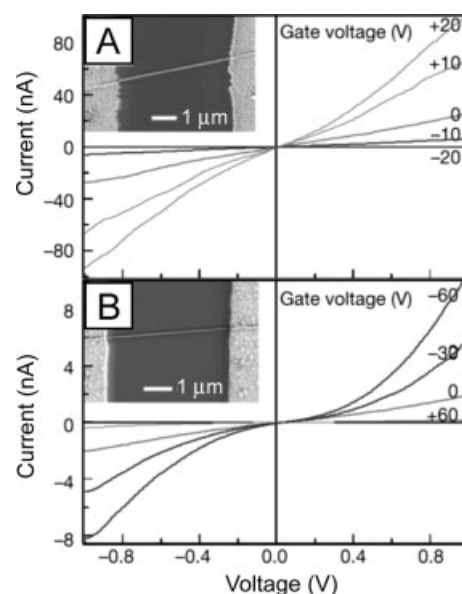
Fig. 25. Room-temperature I–V behavior for a Te-doped (A) and Zn-doped (B) InP nanowire at various gate potentials (courtesy of Professor Charles Lieber at Harvard University). The inset shows the nanowire sitting across two electrodes. The diameter of the nanowire was 47 and 45 nm, respectively [202a].

In a related study, transport measurements by Heath and co-workers suggested that Si nanowires with a thickness of ~15 nm had become insulating.[208]

Another issue related to the electronic applications of chemically synthesized nanowires is the assembly of these building blocks into various device architectures. To this end, a number of groups have demonstrated methods capable of directing the assembly of 1D nanostructures into a variety of functional devices. For example, Mallouk and co-workers have synthesized nanorods containing diode junctions, and then assembled them into arrayed systems.[209] It is worth noting that the Lieber group has been able to assemble semiconductor nanowires into cross-bar p–n junctions and junction arrays with controllable electrical characteristics with yields as high as 95 %.[210] These junctions have been further used to create integrated nanoscale FET arrays (Fig. 26) with nano-
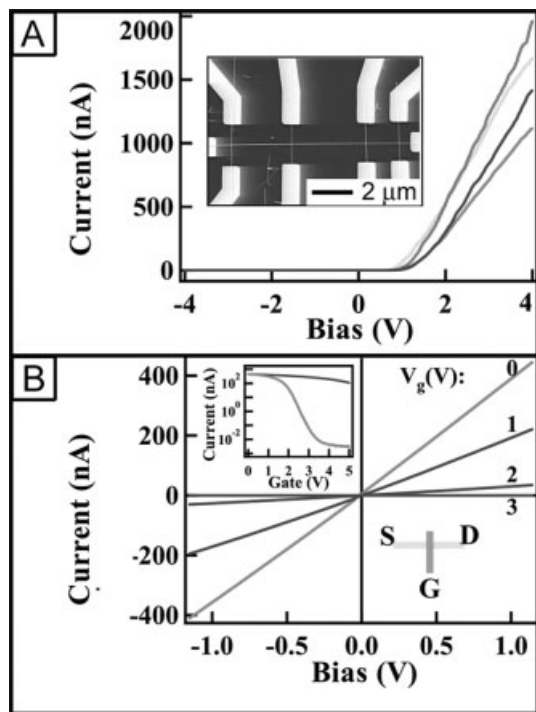
Fig. 26. A) *I–V* behavior for a multiple-junction array formed between four p-type Si nanowires and one n-type GaN nanowire. The four curves represent the *I–V* response for each of the four junctions. Inset is a scanning electron microscopy image of the multiple-junction device. B) Gate-dependent *I–V* characteristics of a crossed nanowire field-effect transistor. The gate voltage (0, 1, 2, and 3 V) for each *I–V* curve is indicated. The inset (top left) shows *I* vs V_{gate} for n-type GaN nanowire (bottom trace) and global back (top trace) gates when the bias is set at 1 V. The transconductance for this device was 80 and 280 nS (V_{sd} = 1 V) when a global back gate and nanowire gate was used, respectively. The inset (bottom right) shows the measurement configuration (courtesy of Prof. Charles Lieber at Harvard University) [202b].

wires as both the conducting channel and gate electrode. In addition, OR, AND, and NOR logic-gate structures with substantial gain have been configured and tested to implement some basic computation. In another example, doped silicon nanowires have been used to fabricate passive diodes, bipolar transistors, and complementary inverters using self-assembly.

There are several appealing features for this "bottom–up" approach to nanoelectronics. First, the size of the nanowire building blocks can be readily tuned to sub-100 nm and smaller, which should lead to a high density of devices on a chip. Second, the material systems for the nanowires are essentially unlimited, which should give researchers great flexibility to select the right materials for the desired device functionality. For example, the Lieber group has recently demonstrated several GaN nanowire based nanodevices which would be of interest for their high-power/high-temperature electrical applications. It is obvious that great progress has been made along the direction of using nanowire building blocks for various device applications. Nevertheless, one has to admit that ultimately achieving the goal of "bottom–up" manufacturing in the future will still require substantial work, including, for example, the development of 3D hierarchical assembly processes, as well as the improvement of material synthesis.

8.4. Phonon-Transport Properties

In contrast to the extensive studies on electron transport, investigation of phonon transport in 1D nanostructures was not reported until very recently. As the dimension of a 1D nanostructure is reduced to the range of phonon mean free paths (MFPs), the thermal conductivity will be reduced due to scattering by boundaries. Theoretical studies suggested that as the diameter of a silicon nanowire became smaller than 20 nm, the phonon dispersion relation might be modified (as a result of the phonon confinement) such that the phonon group velocities would be significantly less than the bulk value.[211] Molecular dynamics (MD) simulations also showed that the thermal conductivities of Si nanowires could be two orders of magnitude smaller than that of bulk silicon in the temperature range from 200 K to 500 K.[212] The reduced thermal conductivity is desirable in applications such as thermoelectric cooling and power generation, but is not preferable for other applications such as electronics and photonics.

Dresselhaus and co-workers have theoretically predicted that the thermoelectric figure of merit could be substantially enhanced for thin nanowires by carefully tailoring their diameters, compositions, and carrier concentrations.[213] This prediction still needs to be validated experimentally by measuring the thermal conductivities, Seebeck coefficients, carrier mobilities, and electrical conductivities of different nanowire systems. Good thermoelectrical systems include nanowires made of Bi, BiSb alloy, and Bi_2Te_3.[214] The Si/SiGe superlattice nanowires recently developed by Yang and co-workers will add another interesting twist to this direction of work, noting the possible interfacial phonon scattering within such highly complex 1D nanostructures.[186]

8.5. Optical Properties

As for quantum dots, size-confinement also plays an important role in determining the energy levels of a nanowire once its diameter has been reduced below a critical value (the Bohr radius). Korgel and co-workers found that the absorption edge of Si nanowires (synthesized with hexane supercritical fluid as the solvent) was significantly blue-shifted as compared with the indirect bandgap (~1.1 eV) of bulk silicon.[140] They also observed sharp, discrete features in the absorption spectra and relatively strong "band-edge" photoluminescence (PL). These optical features most likely originated from quantum-confinement effects, although surface states might also make additional contributions.[215] In addition, the variation in growth direction for these Si nanowires led to different optical signatures. For example, the <100> oriented nanowires displayed a strong feature reminiscent of the L ⟶ L critical point in the Si band structure with a slowly rising phonon-assisted optical transition, whereas the <110> oriented Si nanowires exhibited distinctly molecular-type transitions. The <100> oriented wires also exhibited a significantly higher exciton energy relative to the <110> oriented ones.

In contrast to that from quantum dots, light emitted from nanowires is highly polarized along their longitudinal axes. As shown by Lieber and co-workers,[216] there exists a striking anisotropy in the PL intensities recorded in the direction parallel and perpendicular to the long axis of an individual, isolated indium phosphide (InP) nanowire (Fig. 27). The magnitude of polarization anisotropy could be quantitatively explained in
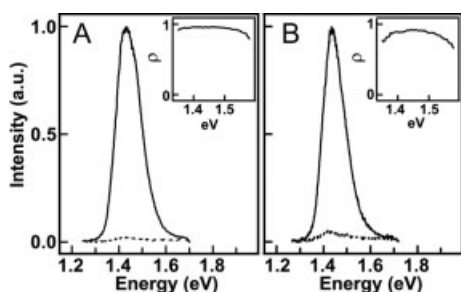

Fig. 27. A) Excitation and B) emission spectra recorded from an individual InP nanowire of 15 nm diameter (courtesy of Prof. Charles Lieber at Harvard University). The polarization of the exciting laser was aligned parallel (solid line) and perpendicular (dashed line) to the long axis of this nanowire, respectively. The inset plots the polarization ratio as a function of energy [216].

terms of the large dielectric contrast between the nanowire and the surrounding environment, as opposed to quantum mechanical effects such as mixing of valence bands. Lieber and co-workers further demonstrated the use of this large polarization response to fabricate polarization-sensitive nanoscale photodetectors that may find use in integrated photonic circuits, optical switches and interconnects, near-field imaging, and high-resolution detection.

In a recent publication, Alivisatos and co-workers demonstrated how semiconductor nanorods could be used to enhance the processibility and efficiency of solar cells.[217] They fabricated thin-film photovoltaic devices by blending CdSe nanorods with polythiophenes to obtain hybrid materials. The intrinsic features and thus performance of such a device could be tuned by controlling the aspect ratios of the nanorods. They also found that nanorods were superior to quantum dots in photovoltaic applications, because they could provide a direct path for electrical transport at much lower loadings. Under Air Mass (AM) 1.5 Global solar conditions, a power conversion efficiency of as high as 1.7 % has been achieved.

For nanorods made of noble metals such as Au and Ag, their surface plasmon resonance (SPR) properties have been extensively studied by El-Sayed and co-workers and other research groups.[93] Different from their 0D counterparts (i.e., spherical colloids), the 1D nanostructures exhibit two SPR modes, corresponding to the transverse and longitudinal excitations. While the wavelength of transverse mode is essentially fixed around 520 nm for Au and 410 nm for Ag, their longitudinal modes can be easily tuned to the span across the spectral region from visible to near-infrared (NIR) by controlling their aspect ratios. It was also demonstrated that gold nanorods with an aspect ratio of 2.0–5.4 could fluoresce with a quantum yield more than one million times that of the metal.[218] These properties, coupled with biological inertness,

make Au and Ag nanorods ideal candidates for use as colorimetric markers or sensors, and contrast-enhancing reagents for in-vivo optical imaging.[219]

8.6. Lasing in Semiconductor Nanowires

Nanowires with flat ends can also be exploited as optical resonance cavities to generate coherent light on the nanoscale. To this end, Yang and co-workers have observed room-temperature UV-lasing from arrays of ZnO nanorods grown on sapphire substrates using the VLS method.[220] ZnO is a wide bandgap (3.37 eV) compound semiconductor that is suitable for blue optoelectronic applications with ultraviolet lasing action already been reported in disordered particles and thin films.[221] In addition, ZnO has an exciton binding energy as high as 60 meV, which is significantly larger than that of ZnSe (22 meV) and GaN (25 meV). This information indicates that the excitons in ZnO are thermally stable at room temperature.

In a typical set-up for lasing experiments (Fig. 28A), one end of the nanowire was terminated in the epitaxial interface

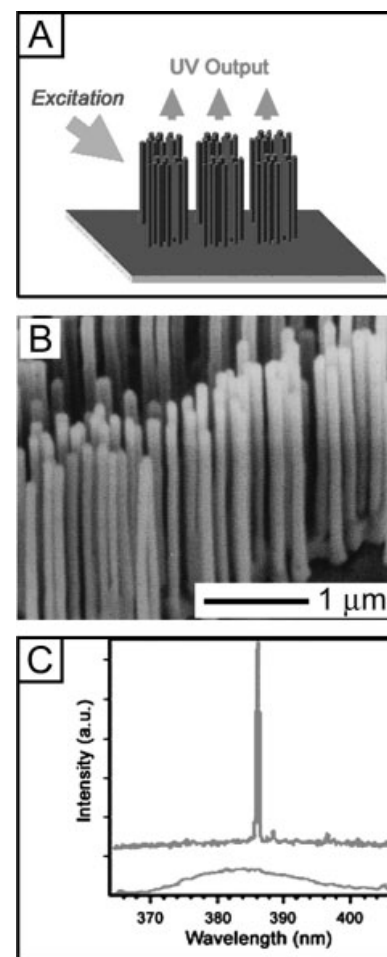Fig. 28. A) Schematic illustration of the excitation and detection configuration used for the lasing study. B) SEM image of a 2D array of ZnO nanowires grown as uniaxial crystals on the surface of a sapphire substrate. C) The power-dependent emission spectra recorded from a 2D array of ZnO nanowires, with the excitation energy being below (bottom trace) and above (top trace) the threshold [220].

between the sapphire and ZnO and the other end in the flat (0001) plane of hexagonal ZnO (Fig. 28B). Considering the refractive indices of sapphire (1.8), ZnO (2.5), and air (1.0), both ends of each nanowire can serve as good mirrors to construct an optical cavity. Such a natural cavity/waveguide configuration suggests a simple approach to the fabrication of nanoscale optical resonance cavities without cleavage and etching. In a typical experiment, the nanowires were optically pumped by the fourth harmonic of a Nd:YAG (YAG: ytrium–aluminium–garnet) laser with various intensities. Light emission was collected in the direction either normal to the end-surface plane or along the longitudinal axis of the nanowire. Figure 28C shows the emission spectra recorded at different pumping powers. When the excitation power was below the threshold, the spectrum (Fig. 28C, bottom trace) consisted of a broad, spontaneous emission peak with a full width at half maximum (FWHM) of ~17 nm. This spontaneous emission mainly originated from the recombination of excitons through an exciton–exciton collision process, in which one of the excitons radiatively recombines to generate a photon. The emission peak was narrowed as the excitation power was increased, owing to the preferential amplification of frequencies close to the maximum of the gain spectrum. Once the power had exceeded the threshold (~40 kW cm^{-2}), a sharp peak emerged in the emission spectrum (Fig. 28C, top trace). The line width of this peak could be more than 50 times smaller than that of the spontaneous emission peak. Above the threshold, the integrated emission intensity also increased rapidly with the pumping power. The narrowing of line width and rapid increase in intensity both suggest that stimulated emission was supported by these arrayed nanorods.

The observation of lasing action in arrayed ZnO nanowires without requiring fabrication of mirrors suggests that single-crystalline, well-facetted nanowires can indeed function as effective resonance cavities. This concept of using well-cleaved nanowires as natural optical cavities may be extendable to many other different semiconductor systems. In a more recent study, Yang and co-workers also observed lasing effects in GaN nanowires.[222] By creating p–n junctions in these individual nanowires, it might be possible to test the possibility of making electrically pumped UV and blue lasers out of individual nanowires. The chemical flexibility as well as the one-dimensionality of these nanowires should make them ideal candidates for fabricating miniaturized laser light sources. These miniaturized nanolasers will find applications in nanophotonics and microanalysis.

The lasing effect in nanowires was also confirmed by the optically characterizing individual ZnO nanowires using near-field scanning microscopy (NSOM).[223] Figure 29 shows a typical example where the nanowires were excited with short pulses (<1 ps) of 4.35 eV photons (285 nm) in order to observe PL and lasing. The emission from an individual nanowire was collected using a chemically etched fiber optic probe held in the constant-gap mode. Both topographic (based on the shear-force feedback signal) and optical information could be collected simultaneously during forward and reverse scans.
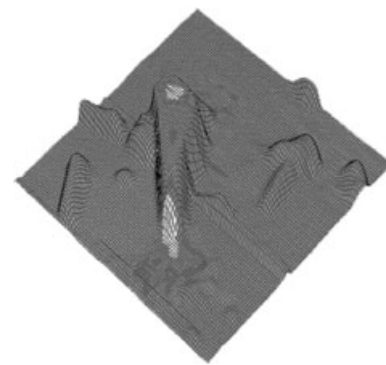

Fig. 29. Near-field optical image of an individual lasing ZnO nanowire. Note that the lasing emission is only seen at the two ends of this nanowire [223].

As shown in Figure 29, lasing was clearly observed from a nanowire that was situated at an angle to the quartz substrate. The intense signal collected near the ends of the nanowire demonstrates the waveguiding and confinement of the emitted photons to a cone-shaped region near the end of the nanowire. In a related study, Dickson, Lyon, and co-workers also demonstrated that silver nanowires could serve as waveguides to direct the propagation of photons through surface plasmon coupling.[224]

8.7. Nonlinear Optical Properties

In addition to their interesting PL and lasing properties described in previous two sections, recent work by Yang, Saykally, and co-workers suggests that semiconductor nanowires might also find use as frequency converters or logic/routing elements in nanoscale optoelectronic circuitry.[225] Coherent NLO phenomena, such as second- and third-harmonic generations (SHG and THG, respectively), depend explicitly on the crystallographic structure of a medium, as well as the polarization scheme. The temporal response of non-resonant harmonic generation is similar to the pulse width of the incident laser (in some cases, as short as 20 fs), while incoherent processes are at least 2–4 orders of magnitude slower. Moreover, non-resonant SHG is essentially independent of wavelength below the energy bandgap of a semiconductor, most often including the 1.3–1.5 μm wavelength region typically used in optical-fiber communications. Zinc oxide is a material of particular interest. Studies of microcrystalline ZnO thin films have revealed a large second-order nonlinearity, $\chi^{(2)}$, a parameter that determines the efficiency of a material as a nonlinear optical converter at optical frequencies.

An NSOM operated in the oblique collection mode was used to measure the NLO properties of individual ZnO nanowires.[225] In this setup, the sample is illuminated in the far-field, as it is preferred for nonlinear near-field imaging because of its suitability for high incident pulse intensity experiments. Figure 30 depicts two SHG images, showing the dependence of SHG signal intensity on the polarization of input pulse and the orientation of ZnO nanowire. The dependence arises from two
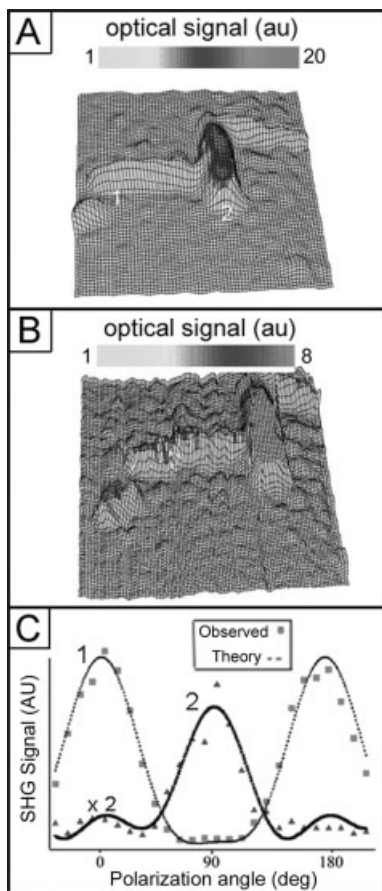
Fig. 30. Dependence of nanowire single-harmonic generation (SHG) signals on the polarization: A) A combined topographical and SHG image of two wires at angle of approximately 90°. The image size is ~ 13×13 μm^2 and the maximum topographic height is 130 nm. The beam is s-polarized, and incident from the right. B) An SHG image recorded from same region as in (A) with a p-polarized incident beam. C) Polarization-dependent SHG data and theoretical predictions taken from the wires labeled in (A). The theoretical curves are calculated for the SHG signal and $\chi_{\mathrm{eff}}^{(2)}$ for a hexagonal crystal [225].

independent, non-vanishing components of $\chi^{(2)}$ observed in SHG for ZnO, $\chi_{zzz}^{(2)}$ and $\chi_{zxx}^{(2)}$. In this case, two wires were situated approximately normal to each other, with an s- and p-polarized incident beam in Figure 30A and Figure 30B, respectively. The polarization ratio, $\mathrm{SHG_{s\text{-}inc}}/(\mathrm{SHG_{p\text{-}inc}} + \mathrm{SHG_{s\text{-}inc}})$, was 0.90 for wire No. 1. The wire No. 2 had an average signal that was 2.5 times that from wire No.1. The SHG polarization effect was also quantitatively analyzed by taking polarization traces from several wires. In doing so, the near-field probe was maintained above each wire, and the input polarization was rotated as the SHG signal was monitored (Fig. 30C). The theoretical traces were computed to fit the polarization data. Nearly all the wires tested (80–100 nm in diameter) exhibited a ratio $\chi_{zzz}^{(2)}/\chi_{zxx}^{(2)}$ of approximately 2.0–2.3, while one larger wire (~ 125 nm in diameter) yielded $\chi_{zzz}^{(2)}/\chi_{zxx}^{(2)} = 4.2$. These ratios were comparable to the value (3.0) for a ZnO bulk crystal, and as much as 6.0 times higher than that of polycrystalline thin films.

Using a reference material, Yang, Saykally and co-workers also measured the absolute magnitude of each component of $\chi^{(2)}$ for individual ZnO nanowires. In this case, $\chi_{zxx}^{(2)}$ and $\chi_{zzz}^{(2)}$ were determined by measuring the nanowire SHG with respect to a ZnSe disk (at 1.4 μm excitation). Relative to the ZnSe reference (78 pm V^{-1}), the $\chi_{zzz}^{(2)}$ for an individual ZnO wire was 5.5 pm V^{-1} and the $\chi_{zxx}^{(2)}$ was 2.5 pm V^{-1}. The $\chi_{zzz}^{(2)}$ value was considerably lower than the reported value (18 pm V^{-1}) for the bulk crystal, but in relatively good agreement with values reported for ZnO thin films (4–10 pm V^{-1}). In addition, the SHG signal collected from an individual nanowire was found to be essentially wavelength-independent ($\lambda_{\mathrm{SHG}} > 400$ nm) and relatively efficient, with a $\chi_{\mathrm{eff}}^{(2)}$ (≥ 5.5 pm V^{-1}) larger than that of β-barium borate (BBO, $\chi_{\mathrm{eff}}^{(2)}$ ≈ 2.0 pm V^{-1}), the most commonly used NLO crystal for frequency doubling in the UV-region. These NLO measurements indicate that ZnO nanowires are potentially useful as an effective frequency converter in the UV region. They might also find use as logic components in nanoscale optoelectronics.

8.8. Photoconductivity and Optical Switching Properties

Among all nanoscale devices, switches are critical for important applications like memory and logic. Electrical switching on the nanometer and molecular scales has been predominantly achieved through the application of a gate potential, as exemplified by nanotube transistors.[226] Recent work from several groups demonstrated that it is also possible to create highly sensitive electrical switches by controlling the photoconductance of individual semiconductor nanowires. For example, Yang and co-workers found that the conductance of ZnO nanowire was extremely sensitive to ultraviolet light exposure.[227] The light-induced insulator-to-conductor transition enabled them to reversibly switch a nanowire between OFF and ON states. In a typical experiment, four-probe measurements on individual ZnO nanowires indicated that they were essentially insulating in the dark, with a resistivity > 3.5 MΩ cm^{-1}. When these nanowires were exposed to a UV-light source with wavelengths below 400 nm, their resistivity was instantly reduced by 4 to 6 orders in magnitude. In addition to their high sensitivities, these photoconductive nanowires exhibited an excellent wavelength selectivity. Figure 31A shows the evolution of photocurrent when a ZnO nanowire was exposed first to very intense visible light at 532 nm (Nd:YAG, the second harmonic) for 200 s and then to UV light at 365 nm. There is no photoresponse at all to the green light, while exposure to the less intense UV light led to the typical change in conductivity by 4 orders of magnitude. Measurements on the spectral response show that the ZnO nanowires indeed have a cut-off wavelength at 385 nm, a value that agreed well with the bandgap of ZnO.

It has been unambiguously established that oxygen chemisorption plays a profound role in enhancing the photosensitivity of bulk or thin-film ZnO. It is believed that a similar photoresponse mechanism could be applied to the nanowire system with additional consideration of high surface areas associated with nanowires, which could further enhance the sen-
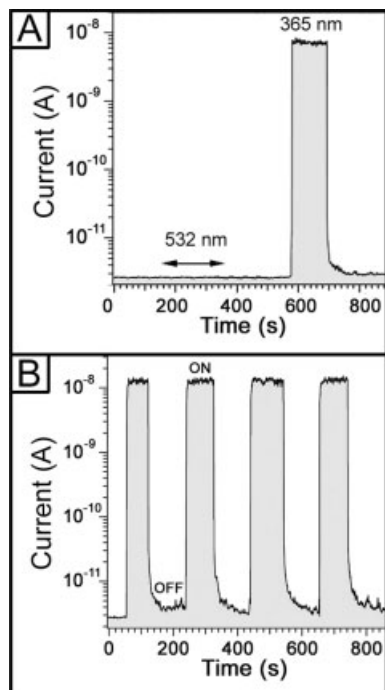
Fig. 31. A) The photoresponse (change in current under a constant bias) of a ZnO nanowire to light exposure at two different wavelengths: 532 and 365 nm. B) Reversible switching of a ZnO nanowire between its low and high conductivity states [227].

sitivity of the device. It is generally accepted that the photoresponse of ZnO consists of two parts: a solid-state process where an electron and a hole are created ($h\nu \longrightarrow h^+ + e^-$) and a two-step process involving oxygen species adsorbed on the surface. In the dark, oxygen molecules adsorb on the oxide surface as negatively charged ions by capturing free electrons of the n-type oxide semiconductor ($O_{2(g)} + e^- \longrightarrow O^-_{2(ad)}$) thereby creating a depletion layer with low conductivity in the vicinity of the nanowire surface. Upon exposure to UV light, photogenerated holes migrate to the surface and discharge the adsorbed oxygen ions through surface electron–hole recombination ($h^+ + O^-_{2(ad)} \longrightarrow O_{2(g)}$). At the same time, photogenerated electrons destroy the depletion layer, and thus significantly increase the conductivity of the nanowire.

Encouraged by their observations on the photoconductive characteristics of ZnO nanowires, Yang and co-workers further evaluated the potential of these nanowires as candidates for optoelectronic switches, with the insulating state as "OFF" in the dark, and the conducting state as "ON" when exposed to UV light. Figure 31B plots the photoresponse of a ZnO nanowire as a function of time while the UV-lamp was switched on and off. It is evident that this nanowire could be reversibly and rapidly switched between the low- and high-conductivity states. With some further optimization on the nanowire composition (e.g., through proper doping), the photocurrent decay time (or the response time) could be reduced to the microsecond scale. Their demonstrations suggested that these highly sensitive photoconducting nanowires could serve as very sensitive UV-light detectors in many appli-

cations such as microanalysis and missile-plume detection, and as fast-switching devices for nanoscale optoelectronics applications where ON and OFF states can be addressed optically.

8.9. Sensing Applications

Another major application for 1D nanostructures is likely related to the sensing of important molecules, either for medical, environmental, or security-checking purposes. The extremely high surface-to-volume ratios associated with these nanostructures make their electrical properties extremely sensitive to species adsorbed on surfaces. For example, Tao and co-workers have demonstrated this concept using arrays of Cu nanowires that contained nanoscale gaps generated through an automated electrochemical process.[228] Upon adsorption of organic molecules onto these Cu nanowires, the quantized conductance was reduced to a fractional value as a result of scattering of conduction electrons by the absorbates. In another demonstration, Penner and co-workers fabricated hydrogen sensors with Pd nanowires supported on the surface of a polymeric thin film.[229] Since each nanowire contained many break junctions along their longitudinal axis that could be reduced as hydrogen gas was absorbed into the crystal lattice, the resistance of these nanowires exhibited a strong dependence on the concentration of hydrogen gas. The response time could be as short as 75 ms. In addition to metal nanowires, semiconductor ones have also been explored for use in chemical and biochemical sensing. For example, Lieber and co-workers have modified the surfaces of semiconductor nanowires and implemented them as highly sensitive, real-time sensors for pH and biological species.[230] The mechanism could be understood in terms of the change in surface charge as caused by protonation and deprotonation. The small dimensions and high sensitivities associated with these sensors suggest that they are good candidates for exploration in use related to array-based screening and in-vivo diagnostics.

More recently, Yang and co-workers fabricated the first room-temperature photochemical NO$_2$ sensors based on individual single-crystalline oxide nanowires and nanoribbons.[231] They demonstrated the concept with SnO$_2$ nanowires as a typical example. Tin dioxide is a wide bandgap (3.6 eV) semiconductor. For n-type SnO$_2$ single crystals, the intrinsic carrier concentration is determined by deviations from the stoichiometry in the form of equilibrium oxygen vacancies, which are predominantly atomic defects. The electrical conductivity of nanocrystalline SnO$_2$ depends strongly on surface states produced by molecular adsorption that often lead to space-charge-layer changes and band modulation. Nitrogen dioxide, a combustion product that plays the key role in tropospheric ozone and smog formation, acts as an electron-trapping adsorbate on SnO$_2$ crystal surfaces and can be detected by monitoring the electrical conductance of the material. Because NO$_2$ chemisorbs strongly on SnO$_2$ surfaces, commercial sensors based on particulate or thin-film SnO$_2$ have to be operated at 300–500 °C to enhance the surface

molecular desorption kinetics and continuously "clean" the sensors. The high-temperature operation of these oxide sensors is not favorable in many cases, particularly in an explosive environment.

Yang and co-workers found that the strong photoconductive nature of individual single-crystalline SnO_2 nanobelts makes it possible to achieve equally favorable adsorption–desorption behavior at room temperature by illuminating the devices with UV light of energy near the SnO_2 bandgap. They analyzed the optoelectronic response of these nanowire devices in air and NO_2 environments in order to evaluate their chemical sensing capabilities. Figure 32 shows the conductance response of one nanosensor cycled between
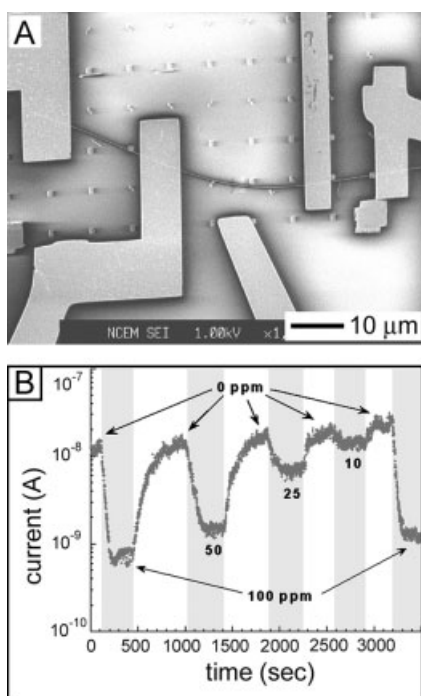

Fig 32. A) SEM image showing a SnO_2 nanobelt spanning across four electrodes of a transport measurement device. B) Cycling a nanosensor near its resolution limit under 365 nm light with a bias of 0.5 V. The concentrations of NO_2 are indicated. The horizontal bars represent averaged signals. The difference in average signals for these three cycles was 16 % [231].

pure air and 3 ppm NO_2. The resolution limit achieved by these oxide nanobelts fell between 2–10 ppm. Even with a low signal/noise ratio, current steps could be clearly distinguished as the NO_2 source was turned on and off. This behavior was stable for > 20 cycles without noticeable drift and the response times could be kept shorter than 1 min. These measurements indicated that individual oxide nanobelts are small, fast, and sensitive devices for detecting ppm-level NO_2 at room temperature with the exposure of UV light. The advantages of low-temperature, potentially drift-free operation make these oxide nanobelts good candidates for miniaturized, ultra-sensitive gas sensors in many applications.

8.10. Field-Emission Properties

It is well known that nanotubes and nanowires with sharp tips are promising candidates for applications related to cold cathode, field emission of electrons. Lee and co-workers have investigated the field-emission characteristics of Si and SiC nanorods using current–voltage measurements.[232] Both nanorods exhibited well-behaved and robust field emission. The turn-on field for Si and SiC nanorods was 15 and 20 V µm^{-1}, respectively, and the current density of 0.01 mA cm^{-2} was comparable with those observed for other field emitters made of CNTs and diamond. The SiC nanorods exhibited a particularly high electron field emission, as well as good stability. In a recent publication, Lee and co-workers also studied the field-emission properties of well-aligned ZnO nanorods grown using a low-temperature CVD method.[233] The turn-on field was 6 V µm^{-1}, which corresponded to a current density of 0.1 µA cm^{-2}. The current reached mA cm^{-2} when the applied field was increased to 11 V µm^{-1}. Considering their ease of preparation, these nanorods might find use as active components in fabricating field-emission display devices.

9. Concluding Remarks

This article provides an overview on a variety of chemical methods that have been developed for generating nanostructures with 1D morphologies (wires, rods, belts, and tubes). We broadly divided these methods into three categories, in which i) anisotropic growth is dictated by the linear, crystallographic structure of a solid material; ii) anisotropic growth is directed or confined by a template; and iii) anisotropic growth is kinetically achieved by controlling the supersaturation or through the use of an appropriate capping reagent. We also briefly discussed a number of methods for generating 1D nanostructures that are based on the self-assembly of nanoscale building blocks and size reduction of microscale structures. Each method has its specific merits and inevitable weaknesses. For example, the methods based on structural confinement are able to provide thin nanowires (a few nanometers in diameter) with an extremely uniform cross-section over a length scale of several hundred micrometers. These methods, however, only work well for a limited set of solid materials that contain highly anisotropic structures. The template-directed methods, on the other hand, provide a good control over the uniformity and dimensions. The use of a template, however, greatly limits the scale of nanowires that one can prepare in each round of synthesis. Removal of the template through a post-synthesis process may also cause damage to the nanowire product. In addition, most nanowires synthesized using template-directed methods are polycrystalline in structure, an unwanted feature that may limit their use in device fabrication and fundamental studies. The methods involving the use of capping reagents are able to generate nanowires with highly crystalline struc-

tures and well-controlled compositions, albeit it is a non-trivial task to select the appropriate capping reagent for use with each metal or semiconductor, nor is it easy to achieve precise control over the longitudinal dimension and monodispersity of resultant nanowires. The vapor-phase methods based on the control of supersaturation are able to produce nanowires and nanobelts of various materials, but only in moderately large quantities. It is also not easy to control the dimensions and uniformity of the nanostructures. In terms of feasibility, methods based on the VLS process seem to be most versatile in generating 1D nanostructures with controllable sizes and compositions. These methods, however, are not suitable for use with metals, and the requirement of gold (or other metals) as the catalyst may also cause contamination for the resultant nanowires. Preliminary work from many research groups suggest that the ultimate use of 1D nanostructures is strongly dependent upon our ability to precisely control or fine tune their dimensions, chemical compositions, surface properties, phase purity, and crystal structure. Judged against these metrics, all the methods described in this review still need to be greatly improved before they will find widespread use in commercial applications. As the utilization of 1D nanostructures grows in importance in a broad range of areas, the demand for new (and more effective) synthetic methods will certainly increase.

This article also discussed a range of interesting properties associated with 1D nanostructures, in the context of various intriguing applications. It is obvious that the largest (but not necessarily most realizable) opportunities for 1D nanostructures are in electronics, where smaller dimensions have historically allowed the production of denser, faster circuits, and where the ability to produce nanostructures may lead to new types of devices to be operated on quantum mechanical principles. For truly nanoscale systems, the problem is not just the fabrication of individual functional devices. A number of issues related to circuit design also need to be resolved before complex, high-speed integrated circuits can be fabricated. For instance, the interactions between nanoscale devices, the dissipation of the heat that they generate, and the design of circuits incorporating large numbers of devices differing significantly and unavoidably in their performance are all problems that will also have to be managed.

There are also a range of applications for 1D nanostructures in areas outside of electronics. Examples may include, for instance, ultrasmall chemical and mechanical sensors that are based on nanoelectrodes and nanoelectromechanical systems; optical elements with nanometer dimensions for optoelectronics, near-field probing, nonlinear optical conversion, and information storage; and structures for use in cell biology that will have the ability to probe and manipulate phenomena that occur at scales smaller than organelles. These applications, together with a fundamental interest in nanoscience will continuously provide compelling motivation for research into techniques for synthesizing 1D nanostructures with better controlled dimensions and properties.

One-dimensional nanostructures and most of the applications derived from these materials are still in an early stage of

technical development. There are a number of issues that remain to be addressed before these materials can reach their potential in core industrial applications. First of all, the chemical/thermal/mechanical stability of 1D nanostructures still needs to be systematically studied and better controlled. As discussed in Section 8.1, when the dimension of nanowires is reduced to a smaller and smaller length scale, their melting point will be significantly reduced in comparison with the bulk material. Their weakened thermal stability may eventually place a limit on the conditions under which they can serve as functional components or interconnects. It is worth noting that thin nanowires tend to break into shorter segments even at room temperature, a phenomenon that has been known as Rayleigh instability.[195] When deposited on the surface of a solid substrate, a slight difference in the residual stresses of the nanowires and the substrate may cause the nanowires to buckle and then fracture into shorter segments. Figure 33 shows the TEM image of a 10 nm Ag nanowire that was de-
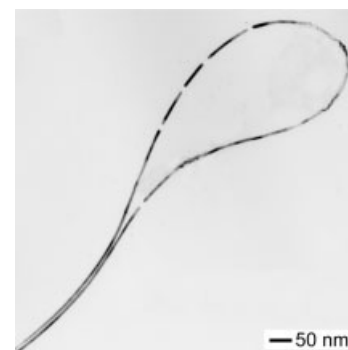

Fig. 33. The TEM image of a silver nanowire (~10 nm in diameter) that broke into short segments during sample preparation. The fragmentation might be caused by strains built up in the nanowire when carbon film on the TEM grid was slighted deformed during solvent evaporation.[234]

posited on a carbon-coated TEM grid.[234] During sample preparation, this thin nanowire broke into a number of fragments along its longitudinal axis. To enhance the stability of nanowires, it might be necessary to form nanoscale-type structures by coating the nanowires with sheaths of a tougher material.

The second challenge faced by chemically synthesized nanowires is their self-assembly into complex structures or device architectures. Recent demonstrations by Yang and co-workers and Lieber and co-workers have started to address this issue, and several promising techniques have been demonstrated to assemble nanowires into test structures such as arrayed crossbar junctions. For example, Yang and co-workers have used microfluidic channels as templates to guide the assembly of molybdenum selenide molecular wires into parallel arrays and cross-bar junctions (Fig. 34).[235] Lieber and co-workers have used a similar procedure to assemble semiconductor nanowires (synthesized by laser-ablation VLS) into functional devices such as p–n junctions and LEDs.[210] The biggest system that has been fabricated using this method contained a 3 × 4 array of crossbar junctions separated by ~1 μm
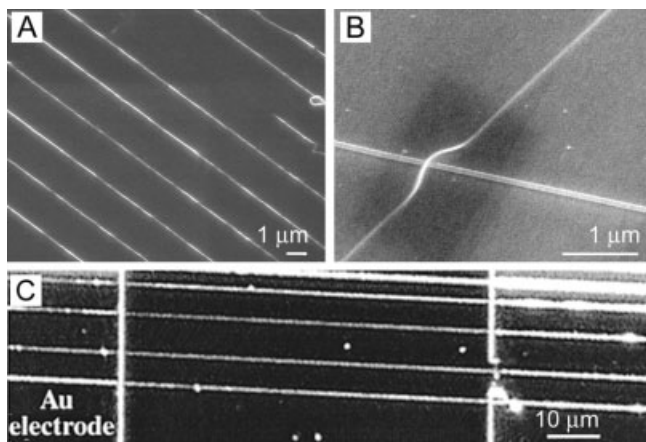
ADVANCED MATERIALS

Fig. 34. A) The SEM image of a parallel array of [Mo$_3$Se$_3^-$]$_\infty$ wires fabricated on a silicon wafer by flowing a dispersion of these wires through microchannels formed between a poly(dimethylsiloxane) (PDMS) mold and the substrate. B) The SEM image of a nanowire crossbar junction that was formed by rotating the PDMS mold by 90° and then repeating the procedure as for (A). C) The SEM image of a parallel array of [Mo$_3$Se$_3^-$]$_\infty$ wires spanning across two gold electrodes [235].

from each other. Further increase of the integration density seems to be difficult. Another potentially useful method for the assembly of nanowires is based on the Langmuir–Blodgett technique.[236] In this case, nanowires can be coated with uniform sheaths to form nanocables and then organized into a closely packed, parallel array at the liquid–air interface. Consecutive transfer of the parallel arrays onto a solid substrate will enable the fabrication of large arrays of crossbar junctions with relatively high densities (Fig. 35A). With Ag nanowires synthesized using the polyol process as an example, we have recently made progress along this direction. For example, we have successfully coated the surfaces of these Ag nanowires with uniform sheaths of amorphous silica to form Ag@SiO$_2$ coaxial nanocables (Fig. 9A).[103] The thickness of the silica coating (and thus the separation between the silver nanowires in the array) could be controlled in the range from 2–100 nm by varying the deposition time and/or the concentration of the
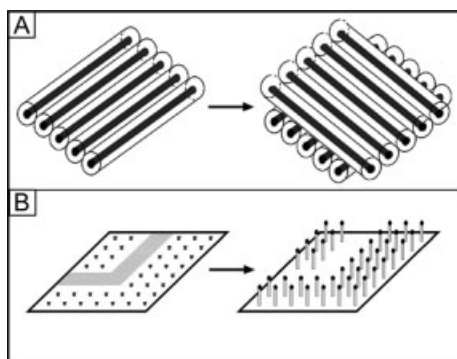

Fig. 35. Schematic illustration showing how 2D arrays of crossbar junctions can be fabricated by assembling core@sheath nanowires into a parallel array at air–liquid interface and then transferring consecutively onto a solid substrate, with the orientation of nanowires in each layer rotated by 90°. A) Schematic illustration of 2D patterning of nanowires using the CVD–VLS method. The linear defects in the patterned 2D array of catalysts are expected to be transferred into the 2D lattice of nanowires with high fidelity. Such lattices can serve as 2D photonic crystals to control the propagation of light.

sol–gel precursor. We believe that the ability to form such functional architectures represents one of the critical steps towards the fabrication of nanoelectronic devices. When stacked into multilayers with a good registration between adjacent layers, these long-range ordered lattices may also serve as photonic crystals to control the propagation of light.[237]

The third challenge is to demonstrate radically new applications for 1D nanostructures in an effort to greatly expand the scope of areas that these materials will impact on. To this end, Park and co-workers have synthesized ferroelectric BaTiO$_3$ nanowires and then demonstrated the possibility to store high-density information on individual nanowires by polarizing the domains with an SPM tip.[238] The bar-coding application demonstrated by Keating and co-workers represents another good example.[84a] In a third example proposed by Yang and co-workers, it was envisioned that semiconductor nanorods could be grown as a 2D periodic lattice on the surface of a solid substrate and subsequently used as a photonic crystal (Fig. 35B). In a typical procedure, an array of catalyst will be patterned on the surface of a solid substrate using nanolithographic techniques such as e-beam writing and soft lithography. Such an array of catalyst will serve as a template to grow an spatially ordered array of nanorods with controllable dimensions and lattice constants using the VLS method. The periodic structures fabricated using this method can function as 2D photonic crystals, with their bandgaps determined by the periodicity and contrast in refractive index. By introducing lattice defects (both point and linear) and light sources (e.g., nanorods containing light-emitting junctions) into these regular dielectric arrays, it might be possible to fabricate miniaturized, coherent light sources (in the visible and near infrared regimes) characterized by extremely low thresholds and essentially no energy loss.

There are almost unlimited research opportunities that are being, and will be explored by many laboratories around the world in this general area of 1D nanostructures. The scientific and technical potentials of these nanostructures are for sure great, and the future of this sub-field of nanoscience is certainly bright. However, one should also realize that some potential environmental and health issues might arise when more and more such 1D nanostructures are produced in labs. Based on previous studies on asbestos and chrysolite, we expect many of these 1D nanostructures might be environmentally and health harzadous. Researchers who are dealing with these types of nanostructures or planning to get into the field should take great caution when handling these 1D nanostructures. In this regard, a systematical evaluation on how these nanostructure will impact our environment and health is urgently needed!

[1] See, for example, a) *Handbook of Nanostructured Materials and Nanotechnology* (Ed: H. S. Nalwa), Academic Press, New York **2000**. b) *Nanostructured Materials: Clusters, Composites, and Thin Films* (Eds: V. M. Shalaev, M. Moskovits), American Chemical Society, Washington, DC **1997**. c) *Nanomaterials: Synthesis, Properties, and Applications* (Eds: A. S. Edelstein, R. C. Cammarata), Institute of Physics, Philadelphia, PA **1996**.

[2] See, for example, a) A special issue on nanoscale materials, *Acc. Chem. Res.* **1999**, *32*. b) P. Alivisatos, P. F. Barbara, A. W. Castleman, J. Chang, D. A. Dixon, M. L. Kline, G. L. McLendon, J. S. Miller, M. A. Ratner, P. J. Rossky, S. I. Stupp, M. I. Thompson, *Adv. Mater.* **1998**, *10*, 1297. c) Special issue on nanostructured materials, *Chem. Mater.* **1996**, *8*, 1569. d) G. A. Ozin, *Adv. Mater.* **1992**, *4*, 612.

[3] a) R. Dagani, *C&EN News* **2000**, *October*, 27. b) W. Schulz, *C&EN News* **2000**, *May*, 41. c) A. Thiaville, J. Miltat, *Science* **1999**, *284*, 1939.

[4] a) *Future Trends in Microelectronics: The Nano Millennium* (Eds: S. Luryi, J. Xu, A. Zaslavsky), Wiley-Interscience, New York **2002**. b) Special issue of *Nature*, **2000**, *406*, 1021.

[5] C. Ross, *Annu. Rev. Mater. Sci.* **2001**, *31*, 203.

[6] a) C. B. Murray, C. R. Kagan, M. G. Bawendi, *Annu. Rev. Mater. Sci.* **2000**, *30*, 545. b) A. P. Alivisatos, *Science* **1996**, *271*, 933. c) L. Brus, *J. Phys. Chem.* **1994**, *98*, 3575. d) M. G. Bawendi, M. L. Steigerwald, L. E. Brus, *Annu. Rev. Phys. Chem.* **1990**, *41*, 477.

[7] a) J. M. Krans, J. M. van Rutenbeek, V. V. Fisun, I. K. Yanson, L. J. de Jongh, *Nature* **1995**, *375*, 767. b) B. L. Al'tshuler, P. A. Lee, *Phys. Today* **1988**, *December*, 36.

[8] a) K. K. Likharev, T. Claeson, *Sci. Am.* **1992**, *June*, 80. b) K. K. K. Likharev, *IBM J. Res. Dev.* **1988**, *32*, 144.

[9] G. Markovich, C. P. Collier, S. E. Henrichs, F. Remacle, R. D. Levine, J. R. Heath, *Acc. Chem. Res.* **1999** *32*, 415.

[10] *Physics of Quantum Well Devices* (Ed: B. R. Nag), Kluwer, Dordrecht, The Netherlands **2000**.

[11] *Molecular Beam Epitaxy: Fundamentals and Current Status* (Eds: M. A. Herman, H. Sitter), Springer, Berlin **1996**.

[12] a) P. Alivisatos, *Pure Appl. Chem.* **2000**, *72*, 3. b) A special issue on semiconductor quantum dots, *MRS Bull.* **1998**, *2*, 15.

[13] a) R. Notzel, K. H. Ploog, *Adv. Mater.* **1993**, *5*, 22. b) H. Weller, *Adv. Mater.* **1993**, *5*, 88. c) J. H. Fendler, *Chem. Rev.* **1987**, *87*, 877.

[14] M. Nirmal, L. Brus, *Acc. Chem. Res.* **1999**, *32*, 407.

[15] V. I. Klimov, A. A. Mikhailovsky, S. Xu, A. Malko, J. A. Hollingsworth, C. A. Leatherdale, H. J. Eisler, M. G. Bawendi, *Science* **2000**, *314*, 290.

[16] D. L. Klein, R. Roth, A. K. L. Lim, A. P. Alivisatos, P. L. McEuen, *Nature* **1997**, *389*, 699.

[17] H. Pettersson, L. Baath, N. Carlsson, W. Seifert, L. Samuelson, *Appl. Phys. Lett.* **2001**, *79*, 78.

[18] A. N. Shipway, E. Katz, I. Willner, *ChemPhysChem* **2000**, *1*, 18.

[19] J. Phillips, *J. Appl. Phys.* **2002**, *91*, 4590.

[20] a) S. Coe, W. K. Woo, M. Bawendi, V. Bulovic, *Nature* **2002**, *420*, 800. b) V. L. Colvin, M. C. Schlamp, A. P. Alivisatos, *Nature* **1994**, *370*, 354.

[21] a) Z. L. Wang, *Adv. Mater.* **2000**, *12*, 1295. b) J. Hu, T. W. Odom, C. M. Lieber, *Acc. Chem. Res.* **1999**, *32*, 435. c) A special issue in *MRS Bull.* **1999**, *24*, pp. 20–49.

[22] F. Cerrina, C. Marrian, *MRS Bull.* **1996**, *December*, 56.

[23] a) J. M. Gibson, *Phys. Today* **1997**, *October*, 56. b) S. Matsui, Y. Ochiai, *Nanotechnology* **1996**, *7*, 247.

[24] a) S. H. Hong, J. Zhu, C. A. Mirkin, *Science* **1999**, *286*, 523. b) J. A. Dagata, *Science* **1995**, *270*, 1625.

[25] a) M. D. Levenson, *Solid State Technol.* **1995**, *September*, 81. b) P. N. Dunn, *Solid State Technol.* **1994**, *June*, 49.

[26] Y. Xia, J. A. Rogers, K. E. Paul, G. M. Whitesides, *Chem. Rev.* **1999**, *99*, 1823.

[27] A special issue on carbon nanotubes *Acc. Chem. Res.* **2002**, *36*, 997.

[28] E. I. Givargizov, *Highly Anisotropic Crystals* (Eds: M. Senechal, S. College), Reidel, Dordrecht, The Netherlands **1987**.

[29] a) J. J. Stejny, R. W. Trinder, J. Dlugosz, *J. Mater. Sci.* **1981**, *16*, 3161. b) J. Stejny, J. Dlugosz, A. Keller, *J. Mater. Sci.* **1979**, *14*, 1291.

[30] W. Noll, *Z. Anorg. Chem.* **1950**, *261*, 1.

[31] K. H. Meyer, H. Mark, *Helv. Chim. Acta* **1937**, *61*, 1932.

[32] L. Stryer, *Biochemistry*, 3rd ed., W. H. Freeman and Company, New York **1988**, p. 261.

[33] a) J. M. Tarascon, F. J. DiSalvo, C. H. Chen, P. J. Carrol, M. Walsh, L. Rupp, *J. Solid State Chem.* **1985**, *58*, 290. b) P. Davidson, J. C. Gabriel, A. M. Levelut, P. Batail, *Europhys. Lett.* **1993**, *21*, 317.

[34] a) J. H. Golden, F. J. DiSalvo, J. M. J. Fréchet, J. Silcox, M. Thomas, J. Elman, *Science* **1996**, *273*, 782. b) J. H. Golden, H. Deng, F. J. DiSalvo, J. M. J. Fréchet, P. M. Thompson, *Science* **1995**, *268*, 1463.

[35] L. Venkataraman, C. M. Lieber, *Phys. Rev. Lett.* **1999**, *83*, 5334.

[36] a) B. Messer, J. H. Song, M. Huang, Y. Wu, F. Kim, P. Yang, *Adv. Mater.* **2000**, *12*, 1526. b) J. Song, B. Messer, Y. Wu, H. Kind, P. Yang, *J. Am. Chem. Soc.* **2001**, *123*, 9714.

[37] a) K. W. Bagnal, *The Chemistry of Selenium, Tellurium, and Polonium*, Elsevier, New York **1966**. b) A. A. Kudryavtsev, *The Chemistry & Technology of Selenium and Tellurium*, Collet's, London **1974**, pp. 1–8.

[38] a) L. I. Berger, *Semiconductor Materials*, CRC Press, Boca Raton, FL **1997**, pp. 86–88. b) *Tellurium* (Ed: W. C. Cooper), Van Nostrand Reinhold Co., New York **1971**.

[39] a) A. A. Kudryavtsev, *The Chemistry & Technology of Selenium and Tellurium*, Collet's, London **1974**, pp. 227–237. b) T. C. Carter, *Thermoelectric and Thermomagnetic Effects and Applications*, McGraw-Hill, New York **1967**. c) H. T. Regensburger, *J. Appl. Phys.* **1963**, *34*, 1730.

[40] a) B. Gates, B. Mayers, B. Cattle, Y. Xia, *Adv. Funct. Mater.* **2002**, *12*, 219. b) B. Gates, Y. Yin, Y. Xia, *J. Am. Chem. Soc.* **2000**, *122*, 12 582.

[41] a) H. R. Kruyt, A. E. van Arkel, *Kolloid-Z.* **1928**, *32*, 29. b) A. Gutbier, *Z. Anorg. Allgen. Chem.* **1902**, *32*, 106.

[42] a) A. R. Roosen, W. C. Carter, *Physica A (Amsterdam)* **1998**, *261*, 232. b) E. Matijevic, *Chem. Mater.* **1993**, *5*, 412.

[43] B. Gates, B. Mayers, A. Grossman, Y. Xia, *Adv. Mater.* **2002**, *14*, 1749.

[44] K. S. Suslick, *Science* **1990**, *247*, 1439.

[45] a) N. Furuta, Y. Ohasi, H. Itinose, Y. Igarashi, *Jpn. J. Appl. Phys.* **1975**, *14*, 929. b) N. Furuta, H. Itinose, N. Maruyama, Y. Ohasi, *Jpn. J. Appl. Phys.* **1972**, *11*, 1113.

[46] B. Mayers, Y. Xia, *J. Mater. Chem.* **2002**, *12*, 1875.

[47] F. Fiévet, J. P. Lagier, M. Figlartz, *MRS Bull.* **1989**, *December*, 29.

[48] B. Mayers, Y. Xia, *Adv. Mater.* **2002**, *14*, 279.

[49] M. Mo, J. Zeng, X. Liu, W. Yu, S. Zhang, Y. Qian, *Adv. Mater.* **2002**, *14*, 1658.

[50] B. Mayers, B. Gates, Y. Yin, Y. Xia, *Adv. Mater.* **2001**, *13*, 1380.

[51] A. A. Kudryavtsev, *The Chemistry and Technology of Selenium and Tellurium*, Collet's, London **1974**, p. 53.

[52] a) A. K. Cheetham, P. Day, *Solid State Chemistry (Compounds)*, Clarendon Press, Oxford **1992**, p. 31. b) *Extended Linear Chain Compounds* (Ed: J. S. Miller), Plenum Press, New York **1982**. c) *Chemistry and Physics of One-Dimensional Metals* (Ed: H. J. Keller), Plenum Press, New York **1977**.

[53] a) C. Wang, K. Tang, Q. Yang, B. Hai, G. Shen, C. An, W. Yu, Y. Qian, *Inorg. Chem. Comm.* **2001**, *4*, 339. b) E. I. Gerzanich, V. A. Lyakhovitskaya, V. M. Fridkin, B. A. Popovkin, in *Current Topics in Materials Science*, Vol. 10 (Ed: E. Kaldis), North-Holland Publishing Company, Amsterdam **1982**, pp. 55–190.

[54] J. S. Miller, A. J. Epstein, *Prog. Inorg. Chem.* **1976**, *20*, 1.

[55] a) A. Prodan, V. Marinkovic, N. Jug, H. J. P. van Midden, H. Böhm, F. W. Boswell, J. C. Bennet, *Surf. Sci.* **2001**, *482*, 1368. b) C. Felser, E. W. Finckh, H. Kleinke, F. Rocker, W. Tremel, *J. Mater. Chem.* **1998**, *8*, 1787. c) F. Lévy, H. Berger, *J. Cryst. Growth* **1983**, *61*, 61.

[56] a) M. Hanack, M. Lang, *Adv. Mater.* **1994**, *6*, 819. b) H. S. Nalwa, *Appl. Organomet. Chem.* **1990**, *4*, 91. c) T. J. Marks, *Angew. Chem. Int. Ed. Engl.* **1990**, *29*, 857.

[57] M. Madou, *Fundamentals of Microfabrication*, CRC Press, Boca Raton, FL **1997**.

[58] a) E. T. T. Jones, O. M. Chyan, M. S. Wrighton, *J. Am. Chem. Soc.* **1987**, *109*, 5526. b) D. J. Bishop, J. C. Licini, G. J. Dolan, *Appl. Phys. Lett.* **1985**, *46*, 1000. c) G. J. Dolan, *Appl. Phys. Lett.* **1977**, *31*, 337.

[59] a) J. Jorritsma, M. A. M. Gijs, J. M. Kerkhof, J. G. H. Stienen, *Nanotechnology* **1996**, *7*, 263. b) E. Olson, G. C. Spalding, A. M. Goldman, M. J. Rooks, *Appl. Phys. Lett.* **1994**, *65*, 2740.

[60] a) E. Kapon, K. Kash, E. M. Clausen Jr., D. M. Hwang, E. Colas, *Phys. Phys. Lett.* **1992**, *60*, 477. b) M. Walther, E. Kaplon, J. Christen, D. M. Hwang, R. Bhat, *Appl. Phys. Lett.* **1992**, *60*, 521.

[61] T. Müller, K.-H. Heinig, B. Schmidt, *Nucl. Instrum. Methods Phys. Res.* **2001**, *175*, 468.

[62] A. Sugawara, T. Coyle, G. G. Hembree, M. R. Scheinfein, *Appl. Phys. Lett.* **1997**, *70*, 1043.

[63] A. Y. Cho, *MRS Bull.* **1995**, *April*, 21.

[64] G. Fasol, *Science*, **1998**, *280*, 545.

[65] Y. C. Chang, L. L. Chang, L. Esaki, *Appl. Phys. Lett.* **1985**, *47*, 1324.

[66] W. Wegscheider, P. Leiffer, K. West, R. E. Leibenguth, *Appl. Phys. Lett.* **1994**, *65*, 2512.

[67] J. L. Vossen, W. Kern, *Thin Film Processes*, Academic Press, New York **1978**.

[68] a) R. M. Penner, *J. Phys. Chem. B* **2002**, *106*, 3339. b) E. C. Walter, B. J. Murray, F. Favier, G. Kaltenpoth, M. Grunze, R. M. Penner, *J. Phys. Chem. B* **2002**, *106*, 11 407. c) M. P. Zach, K. H. Ng, R. M. Penner, *Science* **2000**, *290*, 2120.

[69] a) H. H. Song, K. M. Jones, A. A. Baski, *J. Vac. Sci. Technol. A* **1999**, *17*, 1696. b) T. M. Jung, S. M Prokes, R. Kaplan, *J. Vac. Sci. Technol. A* **1994**, *12*, 1838.

[70] a) J. C. Hulteen, C. R. Martin, *J. Mater. Chem.* **1997**, *7*, 1075. b) C. R. Martin, *Acc. Chem. Res.* **1995**, *28*, 61. c) C. R. Martin, *Science* **1994**, *266*, 1994.

[71] R. L. Fleisher, P. B. Price, R. M. Walker, *Nuclear Tracks in Solids*, University of California Press, Berkeley, CA **1975**.

[72] A. Despic, V. P. Parkhutik, in *Modern Aspects of Electrochemistry* (Eds: J. O. Bockris, R. E. White, B. E. Conway), Vol. 20, Plenum Press, New York **1989**, Ch. 6.

[73] Metals: a) T. Gao, G. Meng, J. Zhang, S. Sun, L. Zhang, *Appl. Phys. A* **2002**, *74*, 403. b) V. M. Fedosyuk, O. I. Kasyutich, W. Schwarzacher, *J. Magn. Magn. Mater.* **1999**, *198–199*, 246. c) H. Masuda, K. Fukuda, *Science* **1995**, *268*, 1466. d) C. J. Brumlik, V. P. Menon, C. R. Martin, *J. Mater. Res.* **1994**, *9*, 1174. e) C. A. Huber, T. E. Huber, M. Sadoqi, J. A. Lubin, S. Manalis, C. B. Prater, *Science* **1994**, *263*, 800. f) V. M. Cepak, C. R. Martin, *J. Phys. Chem. B* **1998**, *102*, 9985. g) T. M. Whitney, J. S. Jiang, P. C. Searson, C. L. Chien, *Science* **1993**, *261*, 1316.

[74] Metals: a) H. Cao, Y. Xu, J. Hong, H. Liu, G. Yin, B. Li, C. Tie, Z. Xu, *Adv. Mater.* **2001**, *13*, 1393. b) X. Zhang, L. Zhang, G. Meng, G. Li, N. Jin-Phillipp, F. Phillipp, *Adv. Mater.* **2001**, *13*, 1238. c) G. S. Cheng, L. D. Zhang, Y. Zhu, G. T. Fei, L. Li, C. M. Mo, Y. Q. Mao, *Appl. Phys. Lett.* **1999**, *75*, 2455.

[75] Ceramics: a) M. Zheng, L. Zhang, X. Zhang, J. Zhang, G. Li, *Chem. Phys. Lett.* **2001**, *334*, 298. b) Y. Lei, L. D. Zhang, G. W. Meng, G. H. Li, X. Y. Zhang, C. H. Liang, W. Chen, S. X. Wang, *Appl. Phys. Lett.* **2001**, *78*, 1125. d) Y. Li, G. W. Meng, L. D. Zhang, *Appl. Phys. Lett.* **2000**, *76*, 2011. e) P. Hoyer, *Langmuir* **1996**, *12*, 1411.

[76] Polymers: a) S. A. Sapp, D. T. Mitchell, C. R. Martin, *Chem. Mater.* **1999**, *11*, 1183. b) R. P. Burford, T. Tongtam, *J. Mater. Sci.* **1991**, *26*, 3264. c) Z. Cai, C. R. Martin, *J. Am. Chem. Soc.* **1989**, *111*, 4138.

[77] a) Z. Zhang, D. Gekhtman, M. S. Dresselhaus, J. Y. Ying, *Chem. Mater.* **1999**, *11*, 1659. b) Z. Zhang, J. Y. Ying, M. S. Dresselhaus, *J. Mater. Res.* **1998**, *13*, 1745.

[78] a) S. J. Limmer, S. Seraji, Y. Wu, T. P. Chou, C. Nguyen, G. Cao, *Adv. Funct. Mater.* **2002**, *12*, 59. b) S. J. Limmer, S. Seraji, M. J. Forbess, Y. Wu, T. P. Chou, C. Nguyen, G. Cao, *Adv. Mater.* **2001**, *13*, 1269.

[79] a) V. M. Cepak, C. R. Martin, *Chem. Mater.* **1999**, *11*, 1363. b) V. M. M. Cepak, J. C. Hulteen, G. Che, K. B. Jirage, D. D. Lakshmi, E. R. Fisher, C. R. Martin, *Chem. Mater.* **1997**, *9*, 1065. c) C. R. Martin, R. V. Parthasarathy, *Adv. Mater.* **1995**, *7*, 487. d) P. Hoyer, *Adv. Mater.* **1996**, *8*, 857. e) M. Nishizawa, V. P. Menon, C. R. Martin, *Science* **1995**, *268*, 700. f) R. V. Parthasarathy, K. L. N. Phani, C. R. Martin, *Adv. Mater.* **1995**, *7*, 896. g) P. Hoyer, N. Baba, H. Masuda, *Appl. Phys. Lett.* **1995**, *66*, 2700.

[80] M. Barbic, J. J. Mock, D. R. Smith, S. Schultz, *J. Appl. Phys.* **2002**, *91*, 9341.

[81] M. E. T. Molares, V. Buschmann, D. Dobrev, R. Neumann, R. Scholz, I. U. Schuchert, J. Vetter, *Adv. Mater.* **2001**, *13*, 62.

[82] G. Yi, W. Schwarzacher, *Appl. Phys. Lett.* **1999**, *74*, 1747.

[83] Z. Miao, D. Xu, J. Ouyang, G. Guo, X. Zhao, Y. Tang, *Nano Lett.* **2002**, *2*, 717.

[84] a) S. R. Nicewarner-Pena, R. G. Freeman, B. D. Reiss, L. He, D. J. Pena, I. D. Walton, R. Cromer, C. D. Keating, M. J. Natan, *Science* **2001**, *294*, 137. b) B. R. Martin, D. J. Dermody, B. D. Reiss, M. Fang, L. A. Lyon, M. J. Natan, T. E. Mallouk, *Adv. Mater.* **1999**, *11*, 1021.

[85] a) C.-M. Yang, H.-S. Sheu, K. J. Chao, *Adv. Funct. Mater.* **2002**, *12*, 143. b) K.-B. Lee, S.-M. Lee, J. Cheon, *Adv. Mater.* **2001**, *13*, 517. c) B. H. Hong, S. C. Bae, C. Lee, S. Jeong, K. S. Kim, *Science* **2001**, *294*, 348. d) M. H. Huang, A. Choudrey, P. Yang, *Chem. Commun.* **2000**, 1063. e) Y.-J. Han, J. M. Kim, G. D. Stucky, *Chem. Mater.* **2000**, *12*, 2068. f) S. Bhattacharyya, S. K. Saha, D. Chakravorty, *Appl. Phys. Lett.* **2000**, *77*, 3770. g) H. Kang, Y.-W. Jun, J.-I. Park, K.-B. Lee, J. Cheon, *Chem. Mater.* **2000**, *12*, 3530.

[86] a) D. Ugarte, A. Chatelain, W. A. de Heer, *Science* **1996**, *274*, 1897. b) E. Dujardin, T. W. Ebbesen, H. Hiura, K. Tanigaki, *Science* **1994**, *265*, 1850. c) P. M. Ajayan, S. Iijima, *Nature* **1993**, *361*, 333.

[87] a) A. Govindaraj, B. C. Satishkumar, M. Nath, C. N. R. Rao, *Chem. Mater.* **2000**, *12*, 202. b) Z. L. Zhang, B. Li, Z. J. Shi, Z. N. Gu, Z. Q. Xue, L.-M. Peng, *J. Mater. Res.* **2000**, *15*, 2658. c) W. K. Hsu, J. Li, H. Terrones, M. Terrones, N. Grobert, Y. Q. Zhu, S. Trasobares, J. P. Hare, C. J. Pickett, H. W. Kroto, D. R. M. Walton, *Chem. Phys. Lett.* **1999**, *301*, 159.

[88] J. Sloan, J. Hammer, M. Zwiefka-Sibley, M. L. H. Green, *Chem. Commun.* **1998**, 347.

[89] J. Sloan, D. M. Wright, H.-G. Woo, S. Bailey, G. Brown, A. P. E. York, K. S. Coleman, J. L. Hutchison, M. L. H. Green, *Chem. Commun.* **1999**, 699.

[90] H. Ringsdorf, B. Schlarb, J. Venzmer, *Angew. Chem. Int. Ed. Engl.* **1988**, *27*, 113.

[91] a) M. Li, H. Schnablegger, S. Mann, *Nature* **1999**, *10*, 1358. b) S. Kwan, F. Kim, J. Arkana, P. Yang, *Chem. Commun.* **2001**, 447.

[92] Y.-Y. Yu, S. S. Chang, C.-L. Lee, C. R. C. Wang, *J. Phys. Chem. B* **1997**, *101*, 6661.

[93] M. A. El-Sayed, *Acc. Chem. Res.* **2001**, *34*, 257.

[94] a) F. Kim, J. Song, P. Yang, *J. Am. Chem. Soc.* **2002**, *124*, 14 316. b) A. Kameo, A. Suzuki, K. Torigoe, K. Esumi, *J. Colloid Interface Sci.* **2001**, *241*, 289. c) K. Esumi, K. Matsuhisa, K. Torigoe, *Langmuir* **1995**, *11*, 3285.

[95] a) C. J. Murphy, N. R. Jana, *Adv. Mater.* **2002**, *14*, 80. b) C. J. Johnson, E. Dujardin, S. A. Davis, C. J. Murphy, S. Mann, *J. Mater. Chem.* **2002**, *12*, 1765. c) P. L. Gai, M. A. Harmer, *Nano Lett.* **2002**, *2*, 771. d) N. R. Jana, L. Gearheart, C. J. Murphy, *Adv. Mater.* **2001**, *13*, 1389. e) N. R. Jana, L. Gearheart, C. J. Murphy, *Chem. Commun.* **2001**, 617. f) N. R. Jana, L. Gearheart, C. J. Murphy, *J. Phys. Chem. B* **2001**, *105*, 4065.

[96] L. Huang, H. Wang, Z. Wang, A. Mitra, K. N. Bozhilov, Y. Yan, *Adv. Mater.* **2002**, *14*, 61.

[97] Y. Li, X. Li, Z.-X. Deng, B. Zhou, S. Fan, J. Wang, X. Sun, *Angew. Chem. Int. Ed.* **2002**, *41*, 333.

[98] F. S. Bates, G. H. Fredrickson, *Phys. Today* **1999**, *52*, 32.

[99] a) D. Zhang, L. Qi, J. Ma, H. Cheng, *Chem. Mater.* **2001**, *13*, 2753. b) J. Zhan, X. Yang, D. Wang, S. Li, Y. Xia, Y. Qian, *Adv. Mater.* **2000**, *12*, 1348. c) Y. Xie, Z. Qiao, M. Chen, X. Liu, Y. Qian, *Adv. Mater.* **1999**, *11*, 1512.

[100] J. J. L. M. Cornelissen, R. van Heerbeek, P. C. J. Kamer, J. N. H. Reek, N. A. M. Sommerdijk, R. J. M. Nolte, *Adv. Mater.* **2002**, *14*, 489.

[101] S. O. Obare, N. R. Jana, C. J. Murphy, *Nano Lett.* **2001**, *1*, 601.

[102] K. S. Mayya, D. I. Gittins, A. M. Dibaj, F. Caruso, *Nano Lett.* **2001**, *1*, 727.

[103] Y. Yin, Y. Lu, Y. Sun, Y. Xia, *Nano Lett.* **2002**, *2*, 427.

[104] R. R. He, M. Law, R. Fan, F. Kim, P. Yang, *Nano Lett.* **2002**, *2*, 1109.

[105] L. J. Lauhon, M. S. Gudiksen, D. Wang, C. M. Lieber, *Nature* **2002**, *420*, 57.

[106] a) Y. Zhang, H. Dai, *Appl. Phys. Lett.* **2000**, *77*, 3015. b) Y. Zhang, N. W. Franklin, R. J. Chen, H. Dai, *Chem. Phys. Lett.* **2000**, *331*, 35. c) P. M. Ajayan, O. Stephan, P. Redlich, C. Colliex, *Nature* **1995**, *375*, 564.

[107] a) K. Keren, M. Krueger, R. Gilad, G. Ben-Yoseph, U. Sivan, E. Braun, *Science* **2002**, *297*, 72. b) E. Braun, Y. Eichen, U. Sivan, G. Ben-Yoseph, *Nature* **1998**, *391*, 775. c) W. E. Ford, O. Harnack, A. Yasuda, J. M. Wessels, *Adv. Mater.* **2001**, *13*, 1793.

[108] H. Dai, E. W. Wong, Y. Z. Lu, S. Fan, C. M. Lieber, *Nature* **1995**, *375*, 769.

[109] a) C. Tang, S. Fan, M. L. de la Chapelle, H. Dang, P. Li, *Adv. Mater.* **2000**, *12*, 1346. b) J. Zhu, S. Fan, *J. Mater. Res.* **1999**, *14*, 1175. c) C. Tang, S. Fan, M. L. de la Chapelle, H. Dong, P. Li, *Adv. Mater.* **2000**, *12*, 1346.

[110] Y. Wu, B. Messer, P. Yang, *Adv. Mater.* **2001**, *13*, 1487.

[111] J. H. Song, Y. Wu, B. Messer, H. Kind, P. Yang, *J. Am. Chem. Soc.* **2001**, *123*, 10 397.

[112] a) Y. Sun, B. T. Mayers, Y. Xia, *Nano Lett.* **2002**, *2*, 481. b) X. Wen, S. Yang, *Nano Lett.* **2002**, *2*, 451. c) Y. Sun, B. T. Mayers, *Adv. Mater.* **2003**, in press.

[113] a) B. Gates, Y. Wu, Y. Yin, P. Yang, Y. Xia, *J. Am. Chem. Soc.* **2001**, *123*, 11 500. b) B. Gates, B. Mayers, Y. Wu, Y. Sun, B. Cattle, P. Yang, Y. Xia, *Adv. Funct. Mater.* **2002**, *12*, 679.

[114] H. Liu, D. K. Biegelsen, N. M. Johnson, F. A. Pnoce, R. F. W. Pease, *J. Vac. Sci. Technol. B* **1993**, *11*, 2532.

[115] *Whisker Technology* (Ed: A. P. Levitt), Wiley-Interscience, New York **1970**.

[116] M. Volmer, I. Estermann, *Z. Phys.* **1921**, *7*, 13.

[117] a) G. W. Sears, *Acta Metall.* **1955**, *3*, 367. b) G. W. Sears, *Acta Metall.* **1955**, *3*, 361. c) G. W. Sears, *Acta Metall.* **1953**, *1*, 457.

[118] Y. Zhang, N. Wang, S. Gao, R. He, S. Miao, J. Liu, J. Zhu, X. Zhang, *Chem. Mater.* **2002**, *14*, 3564.

[119] Z. W. Pan, Z. R. Dai, Z. L. Wang, *Science* **2001**, *291*, 1947.

[120] a) Z. R. Dai, J. L. Gole, J. D. Stout, Z. L. Wang, *J. Phys. Chem. B* **2002**, *106*, 1274. b) Z. R. Dai, Z. W. Pan, Z. L. Wang, *J. Phys. Chem. B* **2002**, *106*, 902. c) H. Zhang, A. C. Dohnalkova, C. Wang, J. S. Young, E. C. Buck, L. Wang, *Nano Lett.* **2002**, *2*, 105.

[121] a) P. Yang, C. M. Lieber, *J. Mater. Res.* **1997**, *12*, 2981. b) Y. S. Yuan, M. S. Wong, S. S. Wang, *J. Mater. Res.* **1996**, *11*, 8. c) P. Yang, C. M. Lieber, *Science* **1996**, *273*, 1836.

[122] a) S. Hayashi, H. Saito, *J. Cryst. Growth*, **1974**, *24/25*, 345. b) E. G. Wolfe, T. D. Coskren, *J. Am. Ceram. Soc.* **1965**, *48*, 279.

[123] W.-S. Shi, H.-Y. Peng, Y.-F. Zheng, N. Wang, N.-G. Shang, Z.-W. Pan, C.-S. Lee, S.-T. Lee, *Adv. Mater.* **2000**, *12*, 1343.

[124] W.-S. Shi, Y.-F. Zheng, N. Wang, C.-S. Lee, S.-T. Lee, *Adv. Mater.* **2001**, *13*, 591.

[125] S. Wang, S. Yang, *Chem. Mater.* **2001**, *13*, 4794.

[126] X. Jiang, T. Herricks, Y. Xia, *Nano Lett.* **2002**, *2*, 1333.

[127] Y. Yin, G. Zhang, Y. Xia, *Adv. Funct. Mater.* **2002**, *12*, 293.

[128] E. J. Otten, O. R. Louire, M.-F Yu, J. M. Cowley, M. J. Dyer, R. S. Ruoff, W. E. Buhro, *J. Am. Chem. Soc.* **2002**, *124*, 4564.

[129] R. S. Wagner, W. C. Ellis, *Appl. Phys. Lett.* **1964**, *4*, 89.

[130] a) X. F. Duan, C. M. Lieber, *Adv. Mater.* **2000**, *12*, 298. b) X. F. Duan, C. M. Lieber, *J. Am. Chem. Soc.* **2000**, *122*, 188. c) A. M. Morales, C. M. Lieber, *Science* **1998**, *279*, 208.

[131] Elemental semiconductors: a) Y. Wu, P. Yang, *Chem. Mater.* **2000**, *12*, 605. b) Y. J. Zhang, Q. Zhang, N. L. Wang, Y. J. Yan, H. H. Zhou, J. Zhu, *J. Cryst. Growth* **2001**, *226*, 185. c) J. Westwater, D. P. Gosain, S. Tomiya, S. Usui, *J. Vac. Sci. Technol.* **1997**, *B15*, 554.

[132] III–V semiconductors: a) C. C. Chen, C. C. Yeh, C. H. Chen, M. Y. Yu, H. L. Liu, J. J. Wu, K. H. Chen, L. C. Chen, J. Y. Peng, Y. F. Chen, *J. Am. Chem. Soc.* **2001**, *123*, 2791. b) J. Zhang, X. S. Peng, X. F. Wang, Y. W. Wang, L. D. Zhang, *Chem. Phys. Lett.* **2001**, *345*, 372. c) M. Q. He, P. Z. Zhou, S. N. Mohammad, G. L. Harris, J. B. Halpern, R. Jacobs, W. L. Sarney, L. Salamanca-Riba, *J. Cryst. Growth* **2001**, *231*, 357. d) W. S. Shi, Y. F. Zheng, N. Wang, C. S. Lee, S. T. Lee, *J. Vac. Sci. Tech. B* **2001**, *19*, 1115. e) C. C. Chen, C. C. Yeh, *Adv. Mater.* **2000**, *12*, 738. f) T. Shimada, K. Hiruma, M. Shirai, M. Yazawa, K. Haraguchi, T. Sato, M. Katsuyama, *Superlattices Microstruct.* **1998**, *24*, 453. g) K. Hiruma, M. Yazawa, T. Katsuyama, K. Ogawa, K. Haraguchi, M. Koguchi, H. Kakibayashi, *J. Appl. Phys.* **1995**, *77*, 447. h) M. Yazawa, M. Kohuchi, A. Muto, K. Hiruma, *Adv. Mater.* **1993**, *5*, 577.

[133] II–VI semiconductors: a) Y. W. Wang, L. D. Zhang, C. H. Liang, G. Z. Wang, X. S. Peng, *Chem. Phys. Lett.* **2002**, *357*, 314. b) Y. W. Wang, G. W. Meng, L. D. Zhang, C. H. Liang, J. Zhang, *Chem. Mater.* **2002**, *14*, 1773. c) X. Duan, C. M. Lieber, *Adv. Mater.* **2000**, *12*, 298. d) M. Lopez-Lopez, A. Guillen-Cervantes, Z. Rivera-Alvarez, I. Hernandez-Calderon, *J. Cryst. Growth* **1998**, *193*, 528.

[134] Oxides: a) Y. J. Chen, J. B. Li, Y. S. Han, X. Z. Yang, J. H. Dai, *J. Cryst. Growth* **2002**, *245*, 163. b) X. C. Wu, W. H. Song, K. Y. Wang, T. Hu, B. Zhao, Y. P. Sun, J. J. Du, *Chem. Phys. Lett.* **2001**, *336*, 53. c) M. H. Huang, Y. Wu, H. Feick, E. Webber, P. Yang, *Adv. Mater.* **2000**, *13*, 113.

[135] Y. Wu, P. Yang, *J. Am. Chem. Soc.* **2001**, *123*, 3165.

[136] a) Y. Wu, H. Yan, M. Huang, B. Messer, J. Song, P. Yang, *Chem. Eur. J.* **2002**, *8*, 1260. b) M. S. Gudiksen, C. M. Lieber, *J. Am. Chem. Soc.* **2000**, *122*, 8801.

[137] T. J. Trentler, K. M. Hickman, S. C. Geol, A. M. Viano, P. C. Gibbons, W. E. Buhro, *Science* **1995**, *270*, 1791.

[138] a) S. D. Dingman, N. P. Rath, P. D. Markowitz, P. C. Gibbons, W. E. Buhro, *Angew. Chem. Int. Ed.* **2000**, *39*, 1470. b) T. J. Trentler, S. C. Goel, K. M. Hickman, A. M. Viano, M. Y. Chiang, A. M. Beatty, P. C. Gibbons, W. E. Buhro, *J. Am. Chem. Soc.* **1997**, *119*, 2172.

[139] a) P. D. Markowitz, M. P. Zach, P. C. Gibbons, R. M. Penner, W. E. Buhro, *J. Am. Chem. Soc.* **2001**, *123*, 4502. b) O. R. Lourie, C. R. Jones, B. M. Bartlett, P. C. Gibbons, R. S. Ruoff, W. E. Buhro, *Chem. Mater.* **2000**, *12*, 1808. c) T. J. Trentler, S. C. Goel, K. M. Hickman, A. M. Viano, M. Y. Chiang, A. M. Beatty, P. C. Gibbons, W. E. Buhro, *J. Am. Chem. Soc.* **1997**, *119*, 2172.

[140] a) X. Lu, T. Hanrath, K. P. Johnston, B. A. Korgel, *Nano Lett.* **2003**, *3*, 93. b) T. T. Hanrath, B. A. Korgel, *J. Am. Chem. Soc.* **2001**, *124*, 1424. c) J. D. Holmes, K. P. Johnston, R. C. Doty, B. A. Korgel, *Science* **2000**, *287*, 1471.

[141] J. R. Heath, F. K. LeGoues, *Chem. Phys. Lett.* **1993**, *208*, 263.

[142] X. Wang, Y. Li, *J. Am. Chem. Soc.* **2002**, *124*, 2880.

[143] a) Q. Lu, F. Gao, D. Zhao, *Nano Lett.* **2002**, *2*, 725. b) Q. Zhang, L. Gao, J. Sun, S. Zheng, *Chem. Lett.* **2002**, 226. c) T. Kasuga, M. Hiramatsu, A. Hoson, T. Sekino, K. Niihara, *Langmuir* **1998**, *14*, 3160.

[144] a) Y. Li, M. Sui, Y. Ding, G. Zhang, J. Zhuang, C. Wang, *Adv. Mater.* **2000**, *12*, 818. b) Y. Xie, P. Yan, J. Lu, W. Wang, Y. Qian, *Chem. Mater.* **1999**, *11*, 2619. c) P. Yan, Y. Xie, W. Wang, F. Liu, Y. Qian, *J. Am. Chem. Soc.* **1999**, *121*, 4062.

[145] A. Venables, *Introduction to Surface and Thin Film Processes*, Cambridge University Press, Cambridge **2000**, p. 4.

[146] Z. L. Wang, *J. Phys. Chem. B* **2000**, *104*, 1153.

[147] a) Y. Sun, Y. Xia, *Science* **2002**, *298*, 2176. b) A. C. Curtis, D. G. Duff, P. P. Edwards, D. A. Jefferson, B. F. G. Johnson, A. I. Kirkland, A. S. Wallace, *Angew. Chem. Int. Ed. Engl.* **1988**, *27*, 1531. c) J. S. Bradley, B. Tesche, W. Busser, M. Maase, M. T. Reetz, *J. Am. Chem. Soc.* **2000**, *122*, 4631. d) T. S. Ahmadi, Z. L. Wang, T. C. Green, A. Henglein, M. A. El-Sayed, *Science* **1996**, *272*, 1924.

[148] a) X. G. Peng, L. Manna, W. D. Yang, J. Wickham, E. Scher, A. Kadavanich, A. P. Alivisatos, *Nature* **2000**, *404*, 59. b) L. Manna, E. C. Scher, A. P. Alivisatos, *J. Am. Chem. Soc.* **2000**, *122*, 12 700.

[149] a) Z. A. Peng, X. G. Peng, *J. Am. Chem. Soc.* **2001**, *123*, 1389. b) Z. A. Peng, X. G. Peng, *J. Am. Chem. Soc.* **2002**, *124*, 3343.

[150] a) V. F. Puntes, K. M. Krishnan, A. P. Alivisatos, *Science* **2001**, *291*, 2115. b) N. Cordente, M. Respaud, F. Senocq, M.-J. Casanove, C. Amiens, B. Chaudret, *Nano Lett.* **2001**, *1*, 565. c) S. Park, S. Kim, S. Lee, Z. G. Khim, K. Char, T. Hyeon, *J. Am. Chem. Soc.* **2000**, *122*, 8581.

[151] a) Y. Sun, B. Gates, B. Mayers, Y. Xia, *Nano Lett.* **2002**, *2*, 165. b) Y. Sun, Y. Xia, *Adv. Mater.* **2002**, *14*, 833. c) Y. Sun, Y. Yin, B. T. Mayers, T. Herricks, Y. Xia, *Chem. Mater.* **2002**, *14*, 4736.

[152] a) S. Link, Z. L. Wang, M. A. El-Sayed, *J. Phys. Chem. B* **2000**, *104*, 7867. b) Z. L. Wang, M. B. Mohamed, S. Link, M. A. El-Sayed, *Surf. Sci.* **1999**, *440*, L809. c) G. Bögels, H. Meekes, P. Bennema, D. Bollen, *J. Phys. Chem. B* **1999**, *103*, 7577.

[153] F. Carmona, F. Barreau, P. Delhaes, R. Canet, *J. Phys. Lett.* **1980**, *41*, L531.

[154] L. Isaacs, D. N. Chin, N. Bowden, Y. Xia, G. M. Whitesides, in *Supramolecular Technology* (Ed: D. N. Reinhoudt), John Wiley & Sons, New York **1999**, pp. 1–46.

[155] G. Hornyak, M. Kröll, R. Pugin, T. Sawitowski, G. Schmid, J.-O. Bovin, G. Karsson, H. Hofmeister, S. Hopfe, *Chem. Eur. J.* **1997**, *3*, 1951.

[156] B. A. Korgel, D. Fitzmaurice, *Adv. Mater.* **1998**, *10*, 661.

[157] D. Wyrwa, N. Beyer, G. Schmid, *Nano Lett.* **2002**, *2*, 419.

[158] T. Reuter, O. Vidoni, V. Torma, G. Schmid, L. Nan, M. Gleiche, L. Chi, H. Fuchs, *Nano Lett.* **2002**, *2*, 709.

[159] W. A. Lopes, *Phys. Rev. E* **2002**, *65*, 031 606.

[160] a) A. P. Alivisatos, K. P. Johnsson, X. G. Peng, T. E. Wilson, C. J. Loweth, M. P. Bruchez Jr., P. G. Schultz, *Nature* **1996**, *382*, 609. b) C. A. Mirkin, R. L. Letsinger, R. C. Mucic, J. J. Storhoff, *Nature* **1996**, *382*, 607.

[161] a) Y. Yin, Y. Lu, B. Gates, Y. Xia, *J. Am. Chem. Soc.* **2001**, *123*, 8718. b) Y. Yin, Y. Lu, Y. Xia, *J. Mater. Chem.* **2001**, *11*, 987. c) Y. Lu, Y. Yin, Z.-Y. Li, Y. Xia, Y. *Nano Lett.* **2002**, *2*, 785. d) Yin, Y. Xia, *J. Am. Chem. Soc.* **2003**, *125*, in press.

[162] K. D. Hermanson, S. O. Lumsdon, J. P. Williams, E. W. Kaler, O. D. Velev, *Science* **2001**, *294*, 1082.

[163] a) R. Resch, C. Baur, A. Bugacov, B. E. Keol, P. M. Echternach, A. Madhukar, N. Montoya, A. A. G. Requicha, P. Will, *J. Phys. Chem. B* **1999**, *103*, 3647. b) R. Resch, C. Baur, A. Bugacov, B. E. Keol, A. Madhukar, A. A. G. Requicha, P. Will, *Langmuir* **1998**, *14*, 6613.

[164] S. Meltzer, R. Resch, B. E. Keol, M. E. Thompson, A. Madhukar, A. A. G. Requicha, P. Will, *Langmuir* **2001**, *17*, 1713.

[165] S. A. Maier, M. L. Brongersma, P. G. Kik, S. Meltzer, A. A. G. Requicha, H. A. Atwater, *Adv. Mater.* **2001**, *13*, 1501.

[166] a) N. D. Denkov, O. D. Velev, P. A. Kralchevsky, I. B. Ivanov, H. Yoshimura, K. Nagayama, *Langmuir* **1992**, *8*, 3183. b) O. D. Velev, N. D. Denkov, V. N. Paunov, P. A. Kralchevsky, K. Nagayama, *Langmuir* **1993**, *9*, 3702. c) A. S. Dimitrov, T. Miwa, K. Nagayama, *Langmuir* **1999**, *15*, 5257.

[167] M. M. Burns, J.-M. Fournier, J. A. Golovchenko, *Science* **1990**, *249*, 749.

[168] M. Tanase, L. A. Bauer, A. Hultgren, D. M. Silevitch, L. Sun, D. H. Reich, P. C. Searson, G. J. Meyer, *Nano Lett.* **2001**, *1*, 155.

[169] a) M. Trau, D. A. Saville, I. A. Aksay, *Langmuir* **1997**, *13*, 6375. b) M. Trau, S. A. Sankaran, D. A. Saville, I. A. Aksay, *Nature* **1995**, *374*, 437. c) T. B. Jones, *Electromechanics of Particles*, Cambridge University Press, Cambridge, UK **1995**.

[170] Z. Tang, N. A. Kotov, M. Giersig, *Science* **2002**, *297*, 237.

[171] G. F. Taylor, *Phys. Rev.* **1924**, *23*, 655.

[172] R. M. Penner, M. J. Heben, T. L. Longin, N. S. Lewis, *Science* **1990**, *250*, 1118.

[173] I. W. Donald, *J. Mater. Sci.* **1987**, *22*, 2661.

[174] R. J. Tunucci, B. L. Justus, A. J. Campilo, C. E. Ford, *Science* **1992**, *258*, 783.

[175] Y. Xia, E. Kim, X.-M. Zhao, J. A. Rogers, M. Prentiss, G. M. Whitesides, *Science* **1996**, *273*, 347.

[176] *Silicon Chemical Etching* (Ed: J. Grabmaier), Springer-Verlag, Berlin **1982**.

[177] K. E. Petersen, *Proc. IEEE* **1982**, *70*, 420.

[178] a) J. L. Wilbur, E. Kim, Y. Xia, G. M. Whitesides, *Adv. Mater.* **1997**, *7*, 649. b) Q. Qin, Y. Xia, A. Black, G. M. Whitesides, *J. Vac. Sci. Technol. B* **1998**, *16*, 98.

[179] a) J. A. Rogers, K. E. Paul, R. J. Jackman, G. M. Whitesides, *Appl. Phys. Lett.* **1997**, *70*, 2658. b) J. A. Rogers, K. E. Paul, R. J. Jackman, G. M. Whitesides, *J. Vac. Sci. Technol. B* **1998**, *16*, 59. c) H. Schmid, H. Biebuyck, B. Michel, O. J. F. Martin, *Appl. Phys. Lett.* **1998**, *72*, 2379.

[180] J. Aizenberg, J. A. Rogers, K. E. Paul, G. M. Whitesides, *Appl. Opt.* **1998**, *37*, 2145.

[181] Z.-Y. Li, Y. Yin, Y. Xia, *Appl. Phys. Lett.* **2001**, *78*, 2431.

[182] Y. Yin, B. Gates, Y. Xia, *Adv. Mater.* **2000**, *12*, 1426.

[183] C. Weisbuch, B. Vinter, *Quantum Semiconductor Structures*, Academic Press, Boston **1991**.

[184] a) Y. Cui, X. F. Duan, J. T. Hu, C. M. Lieber, *J. Phys. Chem. B* **2000**, *104*, 5213. b) J. Hu, M. Ouyang, P. Yang, C. M. Lieber, *Nature* **1999**, *399*, 48.

[185] S. W. Chung, J. Y. Yu, J. R. Heath, *Appl. Phys. Lett.* **2000**, *76*, 2068.

[186] Y. Wu, R. Fang, P. Yang, *Nano Lett.* **2002**, *2*, 83.

[187] a) M. S. Gudiksen, L. J. Lauhon, J. Wang, D. C. Smith, C. M. Lieber, *Nature* **2002**, *415*, 617. b) M. T. Bjork, B. J. Ohlsson, T. Sass, A. I. Persson, C. Thelander, M. H. Magnusson, K. Deppert, L. R. Wallenberg, L. Samuelson, *Nano Lett.* **2002**, *2*, 87.

[188] D. Li, Y. Wu, P. Kim, L. Shi, N. Mingo, L. Yang, P. Yang, A. Majumdar, **2003**, unpublished.

[189] V. P. Menon, C. R. Martin, *Anal. Chem.* **1995**, *67*, 1920.

[190] D. J. Sellmyer, M. Zheng, R. Skomski, *J. Phys. Condens. Mater.* **2001**, *13*, R433.

 0935-9648/03/0503-0388 $ 17.50+.50/0

[191] P. Buffat, J.-P. Borel, *Phys. Rev.* **1976**, *13*, 2287.

[192] S. Link, C. Burda, M. B. Mohamed, B. Nikoobakht, M. A. El-Sayed, *Phys. Rev.* **2000**, *61*, 6086.

[193] a) Y. Wu, P. Yang, *Adv. Mater.* **2001**, *13*, 520. b) Y. Y. Wu, P. D. Yang, *Appl. Phys. Lett.* **2000**, *77*, 43.

[194] a) Z. W. Pan, Z. R. Dai, L. Xu, S. T. Lee, Z. L. Wang, *J. Phys. Chem. B* **2001**, *105*, 2507. b) H. Y. Peng, Z. W. Pan, L. Xu, X. H. Fan, N. Wang, C. S. Lee, S. T. Lee, *Adv. Mater.* **2001**, *13*, 317.

[195] D. Quere, J.-M. D. Meglio, F. Brochard-Wyart, *Science* **1990**, *249*, 1256.

[196] a) E. O. Hall, *Proc. Phys. Soc. London B* **1951**, *64*, 747. b) N. J. Petch, *J. Iron Steel Inst.* **1953**, *174*, 25.

[197] J. Schiøtz, F. D. Di Tolla, K. W. Jacobsen, *Nature* **1998**, *391*, 561.

[198] E. W. Wong, P. E. Sheehan, C. M. Lieber, *Science* **1997**, *277*, 1971.

[199] P. Poncharal, Z. L. Wang, D. Ugarte, W. A. de Heer, *Science* **1999**, *283*, 1513.

[200] P. E. Marszalek, W. J. Greenleaf, H. Li, A. F. Oberhauser, J. M. Fernandez, *PNAS* **2000**, *97*, 6282.

[201] G. Rubio-Bollinger, S. R. Bahn, N. Agraït, K. W. Jacobsen, S. Vieira, *Phys. Rev. Lett.* **2001**, *87*, 026 101.

[202] a) X. Duan, Y. Huang, Y. Cui, J. Wang, C. M. Lieber, *Nature* **2001**, *409*, 66. b) Y. Huang, X. Duan, Y. Cui, L. J. Lauhon, K.-H. Kim, C. M. Lieber, *Science* **2001**, *294*, 1313. c) D. H. Cobden, *Nature* **2001**, *409*, 32. d) G. Y. Tseng, J. C. Ellenbogen, *Science* **2001**, *294*, 1293. e) R. F. Service, *Science* **2001**, *293*, 782.

[203] Z. Zhang, X. Sun, M. S. Dresselhaus, J. Y. Ying, *Phys. Rev. B* **2000**, *61*, 4850.

[204] S. H. Choi, K. L. Wang, M. S. Leung, G. W. Stupian, N. Presser, B. A. Morgan, R. E. Robertson, M. Abraham, S. W. Chung, J. R. Heath, S. L. Cho, J. B. Ketterson, *J. Vac. Sci. Technol. A* **2000**, *18*, 1326.

[205] A. I. Yanson, G. R. Bollinger, H. E. van den Brom, N. Agrait, J. M. van Ruitenbeek, *Nature* **1998**, *395*, 783.

[206] H. van Houten, C. Beenakker, *Phys. Today* **1996**, July, 22.

[207] a) Y. Wang, X. Duan, Y. Cui, C. M. Lieber, *Nano Lett.* **2002**, *2*, 101. b) Y. Cui, C. M. Lieber, *Science* **2001**, *291*, 851.

[208] S. W. Chung, J. Y. Yu, J. R. Heath, *Appl. Phys. Lett.* **2000**, *76*, 2068.

[209] a) N. I. Kovtyukhova, B. R. Martin, J. K. N. Mbindyo, T. E. Mallouk, M. Cabassi, T. S. Mayer, *Mater. Sci. Eng. C* **2002**, *19*, 255. b) N. I. Kovtyukhova, B. R. Martin, J. K. N. Mbindyo, P. A. Smith, B. Razavi, T. S. Mayer, T. E. Mallouk, *J. Phys. Chem. B* **2001**, *105*, 8762.

[210] Y. Huang, X. Duan, Q. Wei, C. M. Lieber, *Science* **2001**, *291*, 630.

[211] a) K. Schwab, E. A. Henriksen, J. M. Worlock, M. L. Roukes, *Nature* **2000**, *404*, 974. b) A. Buldum, S. Ciraci, C. Y. Fong, *J. Phys. Condens. Mater.* **2000**, *12*, 3349.

[212] S. G. Volz, G. Chen, *Appl. Phys. Lett.* **1999**, *75*, 2056.

[213] a) J. Heremans, C. M. Thrush, *Phys. Rev. B* **1999**, *59*, 12 579. b) G. Dresselhaus, M. S. Dresselhaus, Z. Zhang, X. Sun, *Int. Conf. on Thermoelectrics, Nagoya, Japan, 1998*, IEEE, Piscataway, NJ **1998**, p. 43.

[214] a) R. Venkatasubramanian, E. Silvola, T. Colpitts, B. O'Quinn, *Nature* **2001**, *413*, 597. b) C. B. Vining, *Nature* **2001**, *413*, 577.

[215] M. V. Wolkin, J. Jorne, P. M. Fauchet, G. Allan, C. Delerue, *Phys. Rev. Lett.* **1999**, *82*, 197.

[216] J. F. Wang, M. S. Gudiksen, X. F. Duan, Y. Cui, C. M. Lieber, *Science* **2001**, *293*, 1455.

[217] W. U. Huynh, J. J. Dittmer, A. P. Alivisatos, *Science* **2002**, *295*, 2425.

[218] M. B. Mohamed, V. Volkov, S. Link, M. A. El-Sayed, *Chem. Phys. Lett.* **2000**, *317*, 517.

[219] Y. Sun, Y. Xia, *Anal. Chem.* **2002**, *74*, 5297.

[220] M. Huang, S. Mao, H. Feick, H. Yan, Y. Wu, H. Kind, E. Weber, R. Russo, P. Yang, *Science* **2001**, *292*, 1897.

[221] Z. K. Tang, G. L. Wong, P. Yu, M. Kawasaki, A. Ohtomo, H. Koinuma, Y. Segawa, *Appl. Phys. Lett.* **1998**, *72*, 3270.

[222] J. Johnson, H. J. Choi, K. P. Knutsen, R. D. Schaller, R. J. Saykally, P. Yang, *Nature Mater.* **2002**, *1*, 101.

[223] J. C. Johnson, H. Yan, R. D. Schaller, L. Haber, R. J. Saykally, P. Yang, *J. Phys. Chem. B* **2001**, *105*, 11 387.

[224] R. M. Dickson, L. A. Lyon, *J. Phys. Chem. B* **2000**, *104*, 6095.

[225] J. C. Johnson, H. Yan, R. D. Schaller, P. B. Peterson, P. Yang, R. J. Saykally, *Nano Lett.* **2002**, *2*, 279.

[226] C. Dekker, *Phys. Today* **1999**, May, 22.

[227] H. Kind, H. Yan, M. Law, B. Messer, P. Yang, *Adv. Mater.* **2002**, *14*, 158.

[228] C. Z. Li, H. X. He, A. Bogozi, J. S. Bunch, N. J. Tao, *Appl. Phys. Lett.* **2000**, *76*, 1333.

[229] a) E. C. Walter, F. Faview, R. M. Penner, *Anal. Chem.* **2002**, *74*, 1546. b) F. Favier, E. C. Walter, M. P. Zach, T. Benter, R. M. Penner, *Science* **2001**, *293*, 2227.

[230] Y. Cui, Q. Wei, H. Park, C. M. Lieber, *Science* **2001**, *293*, 1289.

[231] M. Law, H. Kind, F. Kim, B. Messer, P. Yang, *Angew. Chem. Int. Ed.* **2002**, *41*, 2405.

[232] X. T. Zhou, H. L. Lai, H. Y. Peng, F. C. K. Au, L. S. Liao, N. Wang, I. Bello, C. S. Lee, S. T. Lee, *Chem. Phys. Lett.* **2000**, *318*, 58.

[233] C. J. Lee, T. J. Lee, S. C. Lyu, Y. Zhang, H. Ruh, H. J. Lee, *Appl. Phys. Lett.* **2002**, *81*, 3648.

[234] Y. Sun, B. Mayers, Y. Xia, **2003**, unpublished.

[235] B. Messer, J. H. Song, P. Yang, *J. Am. Chem. Soc.* **2000**, *122*, 10 232.

[236] F. Kim, S. Kwan, J. Arkana, P. Yang, *J. Am. Chem. Soc.* **2001**, *123*, 4360.

[237] K. M. M. Ho, C. T. Chan, C. M. Soukoulis, R. Biswas, M. Sigalas, *Solid State Commun.* **1994**, *89*, 413.

[238] W. S. Yun, J. J. Urban, Q. Gu, H. Park, *Nano Lett.* **2002**, *2*, 447.

————————————————————